TURUN
YLIOPISTO
Matemaattis-luonnontieteellinen
tiedekunta

# Reactive components of Finnish aggregates causing alkali-silica reaction in concrete and evaluation of petrographical examination and accelerated mortar bar test as assessment methods

Leevi Grönlund

Geologia
Pro gradu -tutkielma
Laajuus: 30 op

17.6.2024
Turku

Pro gradu -tutkielma

**Pääaine**: Kallioperägeologia
**Tekijä**: Leevi Grönlund
**Otsikko**: Suomalaisen kiviaineksen alkali-silikareaktiota aiheuttavat reaktiiviset komponentit ja petrografisen menetelmän sekä kiihdytetyn laastiprismakokeen soveltuvuus testausmenetelminä
**Ohjaaja**: Esa Heilimo
**Sivumäärä**: 74 sivua + liitteet 38 sivua
**Päivämäärä**: 17.6.2024

---

Alkali-silikareaktio on alkali-kiviainesreaktiotyypeistä yleisemmin tavattu sekä laajemmin tutkittu muoto. Alkali-silikareaktio on betonirakenteissa havaittava vaurioitumismekanismi, joka liittyy kiviaineksen metastabiilin silikan sekä sementin alkalien väliseen reaktioon betonissa. Metastabiili silika liittyy tyypillisesti luonnonolosuhteissa kiviaineksessa esiintyvän kvartsin epästabiileihin polymorfeihin, mikro- ja kryptokiteisiin tai heikosti kiteytyneeseen tai häiriintyneeseen kvartsin kiderakenteeseen. Kiviaineksen alkali-silikareaktiivisuutta tutkitaan tyypillisesti ensisijaisesti petrografisella tutkimuksella tai kiihdytetyllä laastiprismakokeella, jotka ovat sekä suhteellisen nopeita että kustannukseltaan edullisia tutkimusmenetelmiä.

Tutkielman tavoitteena oli tunnistaa petrografisella menetelmällä kiviainesnäytteistä mahdolliset alkali-silikareaktiivisuuteen vaikuttavat komponentit ja arvioida niiden välisiä merkittävyyseroja reaktiossa kiihdytetyn laastiprismakokeen avulla. Molemmat testausmenetelmät seurasivat RILEMin suosituksen mukaista menettelytapaa, ja lisäksi menetelmien yhteensopivuutta arvioitiin tämän tutkimuksen tulosten perusteella. Kvartsi luokiteltiin ei-reaktiiviseen kvartsiin, jännittyneeseen kvartsiin ja mikro-/kryptokiteiseen kvartsiin optisten ominaisuuksien perusteella, ja lisäksi kvartsista määritettiin keskiarvo aaltosammumisen kulmalle. Petrografisen tutkimuksen tuloksia verrattiin kiihdytetyn laastiprismakokeen paisumistuloksiin käyttäen tilastollisia menetelmiä korrelaatioiden löytämiseksi. Näytteet perustuivat itsekerättyyn aineistoon tutkimusta varten koostuen sekä lohkare- että kalliopaljastumanäytteistä, jotka kerättiin useista paikoista ympäri Suomea.

Tutkituista näytteistä havaittiin olennaisimpina silikan metastabiileina muotoina mikrokiteinen sekä kiderakenteeltaan jännittynyt kvartsi. Mikrokiteinen kvartsi johti jännittynyttä kvartsia suhteellisesti nopeampaan ja laajempaan paisumiseen tutkituissa näytteissä perustuen kiihdytetyn laastiprismakokeen tuloksiin. Aaltosammumisen kulman mittaamisesta voi olla hyötyä reaktiivisuutta arvioidessa, mutta pelkän kulman mittaamista ei voida luotettavasti käyttää reaktiivisuuden määritykseen johtuen muista mittaustuloksiin vaikuttavista tekijöistä ohuthieessä. Tutkimusmenetelmiä voidaan pitää hyvin vertailukelpoisina, mutta perustuen laajempaan tutkimustyöhön, kiviaineksen soveltuvuutta arvioidessa menetelmiä ei suositella poissulkevina johtuen niiden taipuvaisuudesta tuottaa heikompia tuloksia kuin todellisten betonirakenteiden suorituskyky luonnossa.

Kiihdytetyn laastiprismakokeen soveltuvuutta Fennoskandian alueen kiviaineksen tutkimiseen tulisi tarkemmin arvioida yhteistyössä muiden Fennoskandian alueen tutkijoiden kanssa peilaamalla kiihdytetyn laastiprismakokeen tuloksia todellisten betonirakenteiden suorituskykyyn. Alkali-silikareaktion tutkimista Suomessa voidaan kehittää kouluttamalla asiantuntijoita tunnistamaan petrografisessa menetelmässä erityisesti tässä tutkielmassa havaittuja kvartsin reaktiivisia muotoja.

---

**Avainsanat:** alkali-kiviainesreaktio, alkali-silikareaktio, metastabiili silika, petrografinen tutkimus, kiihdytetty laastiprismakoe

Master's thesis

**Subject**: Bedrock geology
**Author**: Leevi Grönlund
**Title**: Reactive components of Finnish aggregates causing alkali-silica reaction in concrete and evaluation of petrographical examination and accelerated mortar bar test as assessment methods
**Supervisor**: Esa Heilimo
**Number of pages**: 74 pages + attachments 38 pages
**Date**: 17.6.2024

---

The alkali-silica reaction is the most common of the alkali-silica reaction types and the most widely studied. The alkali-silica reaction is a damage mechanism observed in concrete structures and is related to the reaction between metastable silica in aggregate and alkalis provided by cement in concrete. Metastable silica in nature is typically associated with unstable silica polymorphs, micro- and cryptocrystals of quartz, or quartz with poorly crystalline or disturbed crystal structure present in the aggregates. The alkali-silica reactivity of aggregates is typically investigated primarily by petrographic or accelerated mortar-bar test, which are both relatively rapid and inexpensive assessment methods.

The aim of the study was to use a petrographic method to identify the possible components affecting alkali-silica reactivity in studied rock samples and to evaluate the differences in significance between them using an accelerated mortar prism test. Both test methods followed the procedure recommended by RILEM and their compatibility was additionally evaluated based on the results of this study. Quartz was classified as non-reactive unstrained quartz, strained quartz ja micro/cryptocrystalline quartz based on optical features, and additionally, average of undulatory extinction angle of quartz was measured. The results of the petrographic examination were compared with the swelling results of the accelerated mortar prism test using statistical methods to find correlations. The samples were self-collected for the purpose of this study, consisting of both boulder and outcrop samples from several locations around Finland.

From the samples examined, the most relevant metastable forms of silica were found to be microcrystalline and strained quartz. Microcrystalline quartz resulted in relatively faster and more extensive swelling than strained quartz in the studied samples based on the results of the accelerated mortar bar test. Measuring the angle of undulatory extinction can be useful tool in assessing the reactivity but cannot be reliably used deterministically in estimating reactivity due to other factors affecting the measurement results in thin section. Applied testing methods can be considered highly comparable, but based on a larger body of research, the methods are not recommended as exclusionary when assessing the suitability of aggregates due to their tendency to produce more pessimistic results than performance of real concrete structures in nature.

Suitability of accelerated mortar bar test for assessing Fennoscandian aggregates should be further evaluated together with other researchers within Fennoscandian area by mirroring the results of accelerated mortar bar test to actual performance of real concrete structures. Assessing ASR in Finland could be developed by training researchers to distinguish reactive forms of quartz during petrographical examination, especially the ones identified in this study.

---

**Key words**: alkali-aggregate reaction, alkali-silica reaction, metastable silica, petrographical examination, accelerated mortar bar test

# Table of Contents

# 1 Introduction

Alkali-aggregate reaction (AAR) is a chemical-physical reaction in hydrated concrete, in which certain reactive aggregates interact with alkalis in the concrete pore solution in concrete structures over a period of couple to dozens of years. The reaction may result in expansion of reaction products within the concrete structure, forming cracks that can result in premature loss of concrete strength and structural disruption (Leemann et al. 2016). Cracking additionally eases access of environment to inner parts of the structure, possibly accelerating AAR and other deterioration mechanisms causing structural decay (Ferreira & Holt 2013). AAR is a complex phenomenon with recognized variations in reaction mechanisms, which has resulted in its further classification into different types. Most common of these reactions is known as alkali-silica reaction (ASR), in which deleterious reaction occurs between certain reactive phases of silica within aggregates and alkalis present in concrete pore solution (Jensen 2012).

Relation between rock types and their susceptibility to ASR has been widely investigated all over the world, and fundamentally any rock containing silica has potential to participate in reaction in right conditions that enable the reaction. Alkali reactivity of aggregates is dependent on several factors such as the mineralogical composition, geological origin, and texture of the rock (Broekmans 2004). In Finland, various compositionally acid and silica-rich rock types are found across the country and hence potentially reactive rocks are everywhere regardless geographical position (Korsman & Koistinen 1998). Many commonly used rock types used in concrete in Finland such as granite or gneiss are generally considered stable due to presumption of associated silica phase consisting of relatively inert quartz (Lahdensivu et al. 2018). However, geological nomenclature lacks sufficient specification regarding geological history of the rock which makes linkage between rock type and alkali-silica reactivity problematic (Fernandes et al. 2012). Precambrian bedrock of Finland has been affected by deformation and consequently likely changed the stability of included silica constituents which may set apparently stable or generally as none-to-low-reactive recognised rock type susceptible to ASR (Korsman & Koistinen 1998).

Since ASR causes deleterious damage in concrete that may result in structure losing its demanded properties in dedicated application for its designed life, it is essential to

investigate materials planned to use in concrete before actual production. From industrial perspective it is important to utilize testing methods that are simultaneously reliable, feasible and cost-efficient. General aggregate assessment procedure starts with visual petrographical examination either or both macro- and micro-scale, aiming to optically detect possible reactive constituents, and reactivity is estimated by their relative proportions of the whole rock composition. (Sims & Nixon 2003a)

If pointed necessary after petrographical examination, testing is typically continued by conducting mortar or concrete prism tests, in which the deleterious potential of aggregate is evaluated with practical expansion tests. Advantage of petrographical examination is its low cost and swiftness as testing is usually conducted within weeks from sample delivery to testing laboratory, whereas practical tests tend to be more costly and long-term, taking up to one year depending on test method applied. High-end equipment such as Scanning Electron Microscope (SEM)-based Mineral Liberation Analyser (MLA) are known to offer substantial advantages for qualitative and quantitative analysis, but currently these are typically utilized only for scientific purposes due to mismatching cost and benefit at commercial level (Sims & Nixon 2003a). Therefore, petrographic analysis with plain polarization microscope is by far the dominant testing method today in Finland. Even though existence of comprehensive guidance for conducting the petrographic assessment itself, supportive materials for identifying reactive aggregate constituents from innocuous are scarce, and general presumption is that examination should be carried out by experienced petrographer (Sims & Nixon 2003b). Experience, knowledge, and personal views will affect the results of assessment which naturally is unconventional from scientifical approach and may in worse case lead to missleading conclusions. To mitigate this, it is important for petrographers to have systematic testing procedures to reduce subjective influence.

This study aims to detect and evaluate the significance of different quartz microstructures observable from polarization microscope in alkali-silica reaction by quantifying and classifying quartz into unstrained, strained, and microcrystalline types and by measuring the undulatory extinction (UE) angle of quartz. For this study, a collection composed of boulder and outcrop rock samples has been gathered from several locations around Finland with target to comprise a set of aggregates with versatile quartz microstructures for the purpose of this study. The significance of

different quartz types and suitability of undulatory extinction angle measuring for assessing the aggregate alkali-silica reactivity was evaluated by comparing the results of petrographical examination to accelerated mortar bar test (AMBT) expansion results conducted for the same aggregate material. Moreover, study evaluates the mutual compatibility of petrographical examination and AMBT methods and their suitability for typical Finnish aggregate material based on aggregate assessment results and research work done by others.

# 2 Background

## 2.1 History and classification of alkali-aggregate reaction

According to Jensen (2012) AAR was introduced to literature in the 1940's by Thomas Stanton, who started to investigate cracking in concrete structures in California, USA. Alkali-reactive aggregates were initially discovered by petrographic investigations and laboratory tests, which resulted in distinguishing the first reactive rock types and associated minerals such as opal, chalcedony, volcanic glass, devitrified glass, tridymite and hydromica. During next decades, as result of new studies and investigations, list was continued with several other rock types such as argillite, phyllite and greywacke (Gillott et al. 1973). In 1970's, as understanding of the various reaction mechanisms and reactivity of different rock types evolved, AAR was suggested to be subdivided into three subgroups: 1) alkali-silica reaction (ASR), 2) alkali-carbonate reaction (ACR) and 3) alkali-silicate reaction (ASiR). Nowadays of these, alkali-silica reaction and alkali-carbonate reaction are generally recognised reaction types that differ from each other by the type of reactive mineral phases and involved reaction mechanisms (Fournier & Bérubé 2000).

Alkali-silica reaction is present in aggregates containing reactive metastable silica, and its reaction mechanisms are described in more detail in chapter 2.3. Alkali-carbonate reaction is associated with impure dolomitic limestones, and alkali-silicate reaction in rocks containing certain reactive silicates. Of these, alkali-silica reaction is by far the most common type in investigated AAR damaged structures (Jensen 2012). Alkali-carbonate reaction has first been described by Gillott (1964), who explained initiation of the reaction due to carbonates reacting with strong alkalis, producing magnesium hydroxide (brucite), calcium carbonate and alkali carbonate. Reaction and expansion

mechanism of alkali-carbonate reaction is out of the scope of this study, but it is worth to mention that the root cause of ACR is still today debated among researchers (Jensen 2012). Some studies have described expansion being solely caused by dedolomization of limestones (Lopez-Buendia et al. 2008), whereas some have suggested ACR being a misinterpretation of reaction mechanism, in which observed deleterious expansion occurs instead of as result of reaction of carbonates, solely due to ASR in hardly distinguishable disseminated microcrystalline quartz present in limestones (Katayama, 2010). This refers that at least some AAR driven expansive reactions in limestones may be due to ASR rather than ACR. Studies in the 1970's and 1980's revealed that some aggregates used to be considered more stable can also be reactive when having certain mineralogical properties. In these aggregates, crypto- and microcrystalline, strained, and grained quartz or certain feldspars were proven being prone to initiate reaction with alkalis (Jensen 2012).

After Jensen (2012), alkali-aggregate reaction has been divided into 3 subgroups: 1) very fast reactive AAR, 2) fast reactive ASR and 3) slow reactive ASR. This division, instead of basis on reaction mechanism in question, is based on reactivity rates, ruling out the controversies regarding ACR, thus making classification from this point more undisputed. Very fast reactive AAR includes rock types containing generally very unstable silica constituents and rocks which are affected by ACR, such as alkali-induced reactions in argillaceous dolomitic limestones and certain rhyolites. Minerals like fine dolomite, clay minerals, microscopic opal, quartz, and chalcedony are often associated in very fast reactive AAR, causing deleterious damage in laboratory samples within few days and less than year in actual concrete structures (Table 1). Very fast ASR differs remarkably from fast and slow ASR in reaction rate, in which the reaction takes significantly less time.

In fast reactive ASR, reaction causes deleterious damage in structures within 10 years. Typical rock types where it occurs are siliceous limestone, metamarl, opaline sandstone, rhyolite, andesite, glass- or opal-bearing basalts, porous flint, and some certain chert, as well as other rock types with mineral composition generally consisting of opal, chalcedony, opaline and chalcedonic silica, volcanic and artificial glass, and cryptocrystalline quartz (Table 1). Fast reactive ASR has been detected worldwide, is considered common and reaction mechanism has been well described. Fast reaction is generally connected to fine reactive particles and their relative proportions in rock

volume, and the reaction shows up as rapid expansion in expansion tests. Expansion of fast progressing ASR is strongly connected to rate of water uptake that swells the gel produced after reaction between alkalis and aggregate. (Jensen 2012)

Jensen (2012) specifies low reactive ASR to take over 10 years in concrete structures to form deleterious damage. Expansion in slow progressing ASR is most significantly caused by increment of crystallization pressure after reactions in reactive constituents that take long time to develop. Reactive constituents associated with slower ASR is generally cryptocrystalline, microcrystalline and highly strained quartz and also subgrained and recrystallized quartz, which are present in wide range of different rock types such as sandstones, siltstones, clay stones, phyllites, quartzites, mylonites, cataclasites, granites and gneisses.

Slow reactive ASR is the most common and worldwide extent type of alkali-silica reactions. It typically occurs in coarser aggregates, where expansion rate and extent tends to be lower due to slow progression of reaction, but may by time ultimately develop larger volumetric expansion compared to faster reactions. However, a clear distinction between fast and slow reactive ASR and associated mineral-rock types are still insufficiently documented (Jensen 2012). There are also differences and inconsistence between studies regarding whether reactive components are considered as rapidly or slowly reacting, particularly with the case of microcrystalline quartz. For example, Velasco-Torres et al. (2010) have suggested microcrystalline quartz representing rather rapidly reactive constituent that causes fast-proceeding ASR, whereas other authors such as Jensen (2012) consider microcrystalline quartz as slowly reactive.

*Table 1. List of reactive minerals typical associated rock types with respect to alkali-aggregate reaction (Jensen 2012).*

| Reaction type | Reactive minerals | Reactive rock types |
|---|---|---|
| Very fast reactive AAR | Fine dolomite crystals, expansive clay minerals, disseminated sub microscopic opal/quartz/chalcedony, certain siliceous volcanic glass (hydrated or devitrified), certain artificial glass and possibly in rare cases also cristobalite and tridymite. | Certain argillaceous dolomitic limestone (ACR), certain rhyolite, tuff and siliceous volcanic rock with volcanic siliceous glass, artificial alkali-silica rich glass and undispersed silica dust. |

| | | |
|---|---|---|
| Fast reactive ASR | Opa, opaline silica, chacedony, chalcedonic silica, certain volcanic and artificial glass and cryptocrystalline quartz. Possible alkali contribution from feldspar. | Siliceous limestone, metamarl, opaline sandstone, rhyolite, andesite, basalt with glass or opal, porous flint, certain chert and flint or any tock containing sufficient content of the reactive minerals. |
| Slow reactive ASR | Cryptocrystalline and microcrystalline quartz, highly strained quartz with sub grain development and recrystallized quartz. Possible alkali contribution from feldspar. | Sandstone, siltstone, clay stone, phyllite, argillite, quartzite, mylonite, cataclasite, metarhyolite, certain greywacke, certain hornfels, certain granite and gneiss or any rock containing sufficient amount of the reactive minerals. |

## 2.2 Relation between alkali-silica reaction and rock type

Currently the general view is that determination of rock type and determining the mineral content from the sample is insufficient to reliably detect deleterious rock from innocuous (Fernandes et al. 2012). This is due to geological nomenclature lacking specification regarding geological history of the rock, during which the mineralogical properties of solidified rock may be significantly affected by later geological processes. Transition from rock type to another is often ambiguous, complicating the nomination. Certain rock type with characteristic mineral composition may not have undergone any later transformation after initial crystallization, whereas other compositionally equivalent rock may be subsequently influenced by deformation, recrystallization and/or alteration. Despite classification as same rock type, these compositionally equivalent rocks are likely to differ concerning the susceptibility to interact with alkalis in concrete pore solution, and hence mere application of general rock nomenclature to characterize the contribution to alkali-silica reaction is inadequate (Fernandes et al. 2012). This was pointed out for instance in the study by Velasco-Torres et al. (2010), in which the reactivity of granitic aggregates was compared, resulting in distinguishing both fast and slow type of reactive components. Despite nominal uncertainties between alkali-silica reactivity and rock type, as result of great number of studies conducted all over the world, it is acknowledged that some distinct mineralogical and structural properties enhancing aggregate reactivity are

more commonly associated with certain rock types, allowing broad generalisation of reactivity based on rock type (Fernandes et al. 2012).

There are three major types of rock: igneous, sedimentary and metamorphic. Igneous rocks are formed after cooling and solidification of liquid magma or lava, and they are divided into intrusive or extrusive types depending on rock solidification occurring either below or on the bedrock surface. Intrusive rocks are often referred as plutonic rocks, and extrusive rocks as volcanic rocks. Plutonic and volcanic rocks are both widely used aggregates in concrete (Fernandes et al. 2012). Volcanic rocks have often crystallized rapidly, occasionally resulting in fine grained and glassy matrix. Volcanic rocks are typically associated to alkali-silica reactivity by poorly crystallized silica species such as chalcedony and opal, or metastable high temperature silica polymorphs cristobalite and tridymite (Katayama et al. 1989; Batic et al. 1994; Katayama 1997; Wakizaka 2000). Some volcanic rocks have been distinguished being innocuous at the time after their crystallization, but later silica alteration and devitrification of matrix glass have afterwards increased their reactivity (Katayama et al. 2004). Fernandes et al. (2012) emphasize that due to volcanic rocks being generally finer in grain size compared to plutonic rocks, identification of reactive silica phases from matrix is often more challenging. In more coarse and crystalline plutonic rocks, field structure investigations and expansion tests have shown notably greater variation in terms of ASR performance, and international consensus concerning contributing factors has yet not been achieved. Total surface area of quartz has been shown to correlate with reactivity, which indicates that general grain size, and amount of microcrystalline quartz are major influential factors. Ambiguities are mainly related to deformation-driven structural and textural characteristics presumably increasing the reactivity, including quartz lattice quality, microcracks and dynamic quartz recrystallization.

Sedimentary rocks are largely comprised of accumulated siliceous detritus from pre-existing igneous, metamorphic or sedimentary rocks that have weathered and eroded, transported and deposited by sedimentary processes before consolidated into their current form after compaction and cementation. Sedimentary rocks are versatile in grain size, texture, structure and mineralogic composition with typical main minerals consisting of quartz, clays, and carbonate. The age of rock forming minerals within sedimentary rock may also vary substantially due to different initial origins. Due to composition of detrital particles, sedimentary rocks often contain pore space between

grains thus increasing the porosity and permeability, consequently increasing the input of concrete pore fluids into aggregate interior that accelerate reactions. Some flints and cherts are known to compose largely of highly reactive micro- to cryptocrystalline quartz. High reactive contents together with high permeability make these sedimentary rocks highly prone to advance ASR to deleterious level in even at low modal contents. (Fernandes et al. 2012)

Metamorphic rocks have formed from precursors of igneous, sedimentary or metamorphic rocks submitted to temperature, pressure, deformation and fluids in different geological conditions. Current analytical methods make it possible to identify the protoliths of metamorphosed rocks and their metamorphic paths to their current state (Passchier & Trouw 1996). The naming of metamorphic rocks is generally versatile since there are several bases on nomenclature such as precursor rock type, mineralogical composition, or texture (Winkler 1979). Alkali reactivity of metamorphic rocks is typically related to fine grain size and deformation. Fine grain size creates a high surface area for alkali attack which enhances reactivity. Deformation under brittle or ductile conditions promote reactivity by affecting the stability. This raises the significance of microstructural analysis in which the texture and fabric of the rock should be described in detail (Fernandes et al. 2012).

## 2.3 Reaction and expansion mechanism of alkali-silica reaction

### 2.3.1 General

Silica ($SiO_2$) is a molecule with Si atom in the centre which is connected to four oxygen atoms around it with fixed angle of 109 degrees between O–Si–O -bonds, forming a tetrahedral molecular geometry. Silica molecules are connected through oxygen vertices called siloxane bonds (≡Si–O–Si≡), comprising a 3D network of silica units. Silicates that comprise most of the rock-forming minerals in earth's crust are fundamentally composed of silica networks and hence silica is present all over the bedrock. Network rarely consists entirely of pure silica, but instead certain elements are present as impurities such as hydrogen (H) and metallic elements Na, K and Ca. Although O–Si–O -bond angle is fixed in $SiO_2$ units, the Si–O–Si vertices between may vary from 100 to 170 degrees, allowing formation of different crystallographic

forms that can optically observed show up from macro-crystalline to amorphous (figure 1). (Rajabipour et al. 2015)

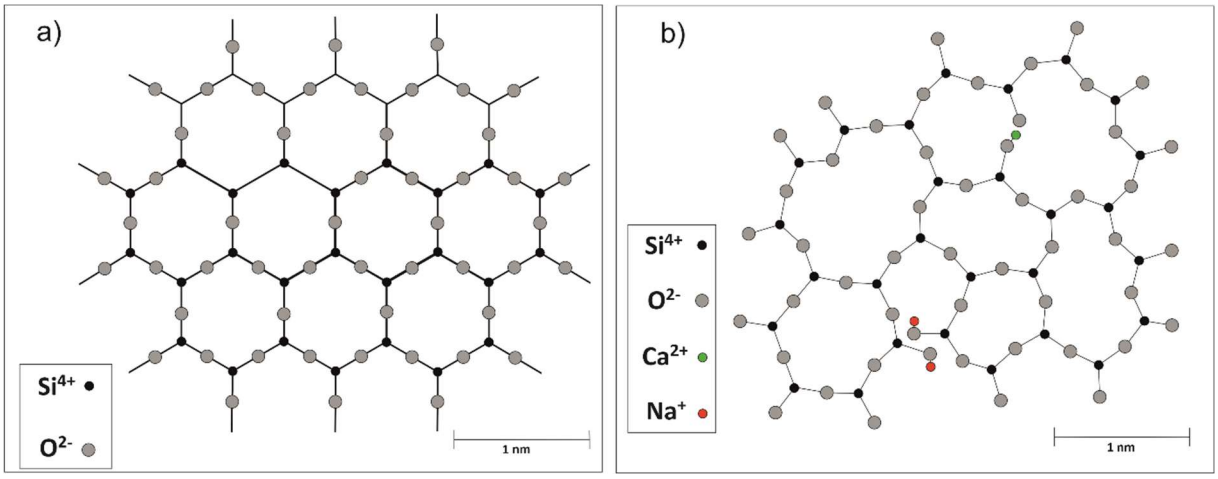


*Figure 1. a) Representation of pure crystalline solid quartz in which silica tetrahedra have uniformly sized and arranged. b) Representation of typical arrangement of silica tetrahedra in amorphous solid phase, in which silica rings are not uniform due to varying angle of Si-O-Si -bonds and non-bridging oxygens that are connected to other elements instead. (Rajabipour et al. 2015)*

Although the chemical and physical reaction mechanisms of alkali-silica reaction have been studied for decades, there is still significant knowledge gaps and lack of overall understanding of the phenomenon. As the name suggests, alkali-silica reaction occurs between the alkaline pore solution and metastable forms of silica present in aggregates (Leemann et al. 2016). In addition to reactive silica phase present, the total rate and magnitude of the reaction is dependent on wide combination of contributing factors that are not all thoroughly explained in this study. Other key parameters include temperature, relative humidity, calcium hydroxide, air entrainment, concrete paste porosity and water/cement ratio (Wigum et al. 2006). Interaction between all contributing factors is controlled by prevalent thermodynamics and kinetics that set the thresholds and limits for reactions (Rajabipour et al. 2015). Fundamentally ASR is a sequence of reactions occurring in high pH environment, in which certain unstable forms of silica are attacked by hydroxide ($OH^-$), sodium ($Na^+$) and potassium ($K^+$) ions present in concrete pore solution. Reaction results in formation of hydrous alkali silica gel that is prone to swelling due to imbibing of water (Figueira et al. 2019). Rajabipour et al. (2015) divides this sequence of reactions into I) dissolution of metastable silica, II) nano colloidal silica sol formation, III) formation of gel, and IV) gel swelling, which can be shortly presented as:

$$(SiO_2)_{solid} \rightarrow (SiO_2)_{aqueous} \rightarrow (SiO_2)_{sol} \rightarrow (SiO_2)_{gel} \rightarrow \text{swelling of gel.} \quad [1]$$

### 2.3.2 Silica dissolution

Hydrous dissolution of silica in the presence of $Na^+$, $K^+$ and $OH^-$ ions at high pH starts with breaking of silica bonds. Breaking is considered being mostly controlled by water molecules and OH-ions rather than alkali species Na and K, which are essential at later recombination stage (Broekmans 2004). The reaction initiates at the outer periphery near the surface of aggregate, and progressively migrates towards inner parts of the particle (Leemann et al. 2016). Simplified equation represents dissolution reaction:

$$(\equiv Si–OH)_s + 3(OH^-)_{aq} \leftrightarrow (Si(OH)_4)_{aq}, \quad [2]$$

in which hydroxyl ions react with silanol groups, forming an aqueous phase of $Si(OH)_4$ (Rajabipour et al. 2015). The overall solubility of silica is strongly connected to its crystallinity and temperature (Rajabipour et al. 2015; Leemann et al. 2016). Walther and Helgeson (1977) have investigated solubility of various polymorphs of $(SiO_2)_s$ in neutral water, and their results show solubility limit increasing as function of lowering and increment of temperature (table 2).

*Table 2. Thermodynamic solubility limits (mM) of certain silica polymorphs in neutral water in different temperatures. Calculations made by Rajabipour et al. (2015) derived from data provided by Walther and Helgeson (1977).*

| T (°C) | α-quartz | β-quartz | α-cristobalite | β-cristobalite | Amorphous silica |
|---|---|---|---|---|---|
| 0 | 0.03 | 0.06 | 0.13 | 0.42 | 1.01 |
| 25 | 0.10 | 0.19 | 0.36 | 0.99 | 1.93 |
| 50 | 0.24 | 0.42 | 0.74 | 1.81 | 3.12 |
| 75 | 0.46 | 0.79 | 1.32 | 2.88 | 4.57 |
| 100 | 0.80 | 1.32 | 2.11 | 4.22 | 6.30 |

Previous calculations indicate rather small solubility limit in neutral water, which brings up the significance of pH in the solution. Higher pH causes ionization of $Si(OH)_4$, converting it to highly soluble ions of $H_3SiO_4^-$ and $H_2SiO_4^{2-}$. Solubility limit of formed silica species is increased as function of pH as shown in Figure 2. Total alkalinity in the system is in addition affected by reactions occurring during other stages of ASR reaction sequence, thus alkalinity and its changes is concerned rather complex phenomenon to understand altogether. Previously mentioned dissolution and ionization reactions together with other contemporary ion exchange reactions tend to reduce the pH. On the other hand, later silica gelation can be associated with so called

alkali recycling, in which alkalis in the gel are replaced by calcium ions, returning alkalis to pore solution, hence increasing the pH. (Rajabipour et al. 2015)

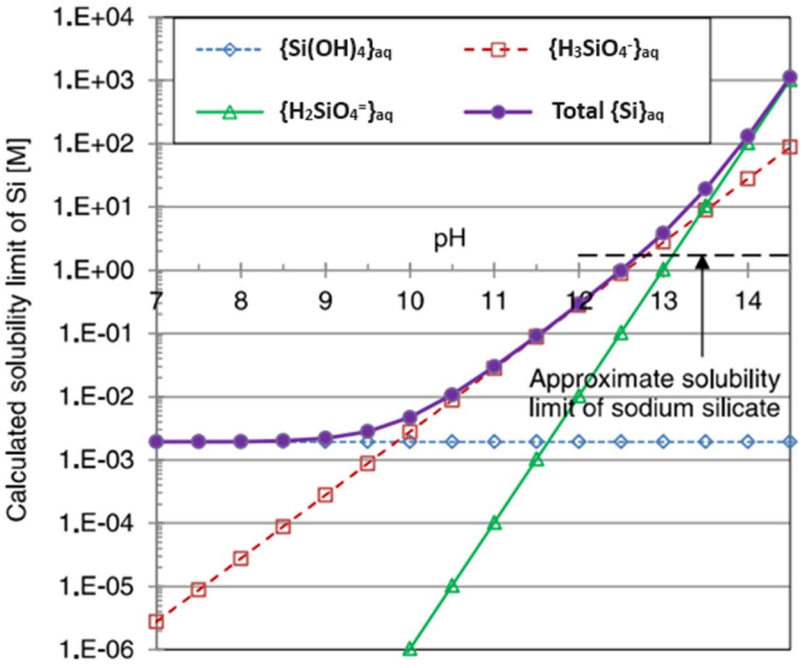


*Figure 2. Si activity of non-ionic and ionized silica species as function of pH at constant temperature of 25 degree Celsius. Note the constant solubility limit for non-ionized silica (Rajabipour et al. 2015).*

In addition to solubility limits determined by prevailing thermodynamics in the system, kinetics controlling the pace of silica dissolution plays equally important role when addressing the overall rate of ASR. Kinetics of the ASR is still not well introduced in literature and quantifying the dissolution rates with respect to these parameters demand further research work (Rajabipour et al. 2015). Maraghechi (2014) has demonstrated the contribution of pH and temperature on dissolution rates of soda-lime silica glass and concluded dissolution rate being function of hydroxide concentration up to pH of 14 and temperature of 60 degree Celsius. Above this, dissolution rate starts to decrease. In addition, the activation energy increases as function of pH, meaning that more energy is required for reaction to proceed (Rajabipour et al. 2015).

### 2.3.3 Colloidal silica and gelation

Formation of colloidal silica occurs after supersaturation of aqueous silica in solution, which is dominantly controlled by solution pH, temperature and present $Ca^{2+}$-ions. Ca-ions derived mainly from cement start to link silica ions, forming poly-metal-silicates. Continued condensation and clustering create nano-colloidal silica sol that is

essentially a continuous and space-filling silicate gel in pore solution that is generally called as ASR gel. (Rajabipour et al. 2015)

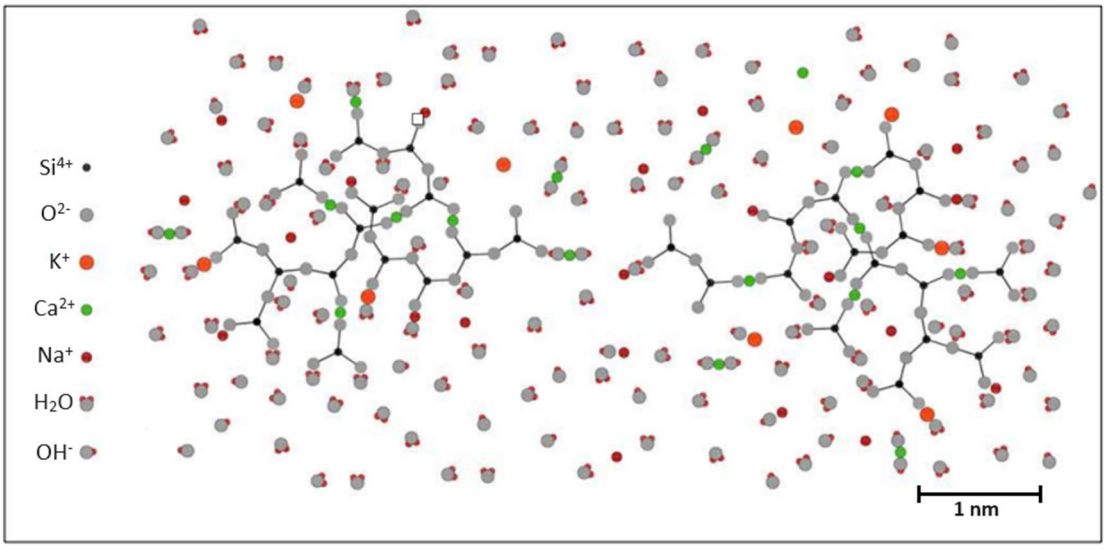


*Figure 3. Representation of ASR gel consisting of clustered colloidal silica particles (2 pcs) in gel's pore solution (modified from Rajabipour et al. 2015).*

### 2.3.4 Gel swelling

Porous ASR gel has a high surface area and has many hydrophilic groups within, such as -OH -O and Na. This enables water adsorption and osmosis that will result in swelling of the gel (Poole 1992). Swelling may ultimately lead to aggregate cracking, which leads to formation of even more reaction products, and reaction products are then extruded in the cement paste, filling cracks and voids (Leemann et al. 2016). The total expansion in concrete caused by gel swelling has been shown being dependent on the relative amounts of reactive constituents in aggregate material and available alkalis present for reactive material to react. The pessimum behaviour in concrete refers to ideal number of alkalis for all reactive material to react, resulting in the highest possible expansion to occur. By decreasing the amount of reactive material for the same number of alkalis, less expansion will occur. This is the case also when there is more reactive material than available alkalis needed for all of that to react. This is due to reactive grains sharing the alkalis, leading to only little expansion within the grains that is not sufficient to cause deleterious tensions within the concrete (Poole 1992).

## 2.4 Alkali-silica reaction in Finland

Finland has been previously considered as an alkali-silica reaction free country mainly due to geological and climatic factors (Ferreira & Holt 2013; Lahdensivu et al. 2018). As various granitoids and metamorphic rocks are largely present all over the country, they are favoured and widely used construction material in Finland. Granitoids are generally considered non- to low reactive in literature, which has formed a general presumption that these rocks are not eligible to react sufficiently that would cause deleterious reactions. Nonexistence of ASR has also been explained with low average annual temperatures due to northern geographical location, where the cold climate slows down the chemical reactions and this way prevents ASR from developing significant damage within the timeframe of the designed life of concrete structure (typically 50-100 years). This general view was outlined also in former versions of national concrete and aggregate durability guidelines, stating that common belief is that Finnish aggregates doesn't involve risk concerning ASR (Ferreira & Holt 2013).

First report regarding ASR in Finland was from damaged railway concrete sleepers in the 1990's (Lindgård et al. 2018). Cracking in the sleepers was in this case previously explained being caused by delayed ettringite formation due to heat-treatment during concrete precast (Tepponen & Eriksson 1987). More detailed investigations from the sleepers conducted by Shayan and Quick (1994) showed evidence of primary cause of cracking being due to ASR and ettringite was subsequently filling the formed cracks. During the last few years, dozens of cases of alkali-silica reaction have been observed from all around the country, especially in massive structures such as dams, highway passes, bridges, facades, balconies, swimming pools and foundations, which have lately drawn notable attention in Finnish concrete industry (Lahdensivu et al. 2018; Ferreira & Holt 2013). Finnish Transport Agency funded a survey regarding damaged structures in Finland in 2011. In this survey, a collection of petrographic reports from different Finnish concrete structures from the past 15 years was collected and collectively examined. Survey revealed that bridges and houses were the most common structures affected by ASR (Ferreira & Holt 2013). The age of affected bridges is typically high, in most cases between 40-50 years, and affected bridges of under 30 years are yet not detected with signs of ASR. On many occasions, the reaction has occurred in rock types that have been considered innocuous or low reacting (Lahdensivu et al. 2018).

Globally there are no published cases where ASR has led to terminal structural collapse. However, ASR has been noticed to create synergies with other deleterious mechanisms, including freeze/thaw damage, steel corrosion due to de-icing salt intrusion, or chloride intrusion in marine environments, so explanation for observed damage may not be straightforward cause of individual phenomenon, but instead a complex cause-and-effect sequence of several repetitive and continuous deleterious mechanisms strengthening one another (Scott IV 2020). In Finland, climatic conditions in which annual temperatures vary below and above freezing point, active chemical de-icing of roads during wintertime, and seashore at the western part of Finland expose concrete structures to many all beforementioned mechanisms with synergistic features with ASR, increasing the overall damaging potential. Macroscopically observable freeze-thaw damage is considered easy to confuse with damage caused by ASR as they both create cracking patterns in concrete surface. However, leached gel from the cracks on structure surface is a strong indicate for ASR that perceptive person can detect (Ferreira & Holt 2013). Because of this, Ferreira and Holt (2013) assume that in many former occasions, structures affected both by ASR and freeze-thaw damage has been falsely conducted as being solely caused by freeze-thaw damage. Due to general presumption of freeze-thaw induced cracking, field inspections have tended to focus on near surface area of structures. Freeze-thaw damage focuses near the surface area within concrete structures and the level of damage typically decreases towards deeper parts of structure. ASR instead affects within any part of the structure where conditions enable the reaction, thus damage may often remain unnoticed in inner parts, and at the time ASR is observable at the surface, structural damage is already significant. Due to confusing ASR and freeze-thaw damage, Holt and Ferreira (2013) think that the realistic amount of ASR affected concrete structures in Finland is likely much higher than current statistics indicate.

Holt and Ferreira (2013) emphasize that ASR was the main deleterious mechanisms only in small proportion of investigated structures, whereas freeze-thaw damage was more common and typically dominant damaging mechanism. Some industrial indoor structures were noticed being prone to reaction, in which temperatures between 30-40 degrees Celsius and high relative humidity create favourable conditions for ASR development. Other suitable structures with similar conditions are indoor swimming pools and spas, however according to Holt and Ferreira (2013) in Finland they are yet

not well studied, and number of confirmed cases caused by ASR damage is low. In all cases, structures were noticed being over 30 years old at the time of their investigation. This emphasized the assumption of ASR being relatively prolonged process in Finland that may eventually cause severe damage, and the risk of structure losing its required properties for its designed life due to ASR exists. Study included couple cases of bridges planned to be demolished and rebuilt due to damage that has been confirmed primary being caused by ASR. Holt and Ferreira (2013) consider ASR being mostly connected to certain rock types instead of geographical areas. Rock types that have been detected as reactive from ASR affected concrete structures in Finland are presented in Figure 4. Survey focused sampling on certain geographical areas, and some regions were not represented at all. Due to this, the statistical distribution is distorted, and this needs to be considered when evaluating regional occurrence of ASR in Finland. Increased awareness, better tools for ASR detection and the time period of intensive Finnish infrastructure building in 1970's is assumed to increase the amount of detected ASR-affected structures in Finland in the near future, since plenty of concrete structures are reaching the age that correspond to postulated time that ASR require advancing to observable damage (Ferreira & Holt 2013).

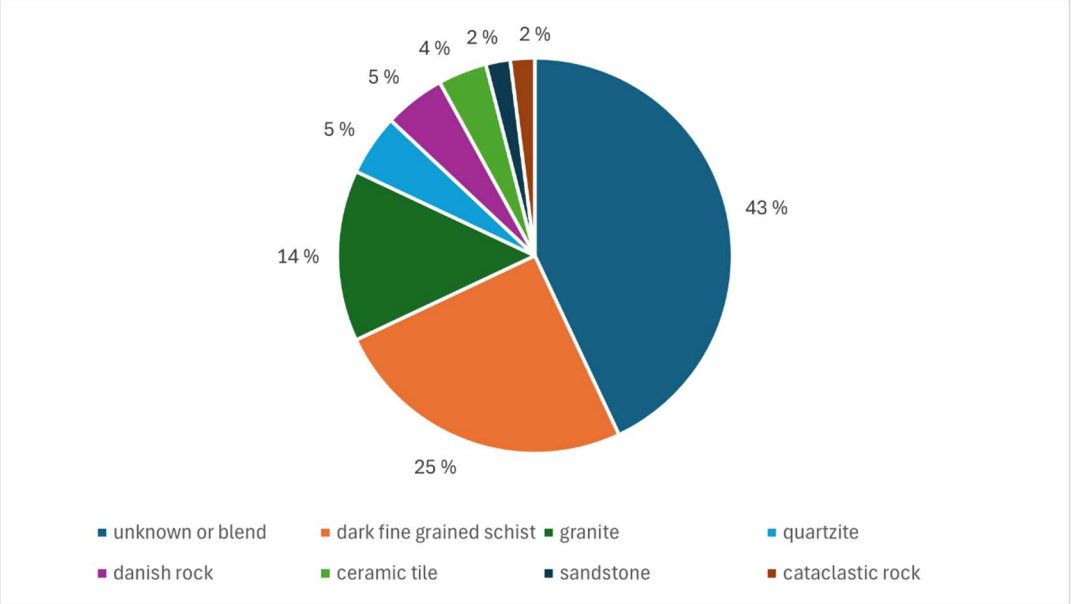


*Figure 4. Observed rock types of reacted aggregates in ASR affected concretes in Finland (Ferreira & Holt 2013).*

ASR is dependent of multiple factors that need to be simultaneously present for reaction to initiate or progress. Reaction needs suitable ingredients and conditions, and by influencing these factors ASR can be mitigated or optimally completely stopped.

Technically mitigation is achieved with proper concrete mixture design or controlling the conditions surrounding the concrete structure. From these two, mixture design is likely to be more conventional since non-reactive concrete structure is independent of environmental influence, thus reaction won't initiate or progress despite other conditional factors. Proper aggregate assessment based on optical or practical assessment is required to confirm ASR reactivity. Today, Finnish concrete norms demand concrete aggregate testing and classifying with respect to ASR, and reactive material is prohibited to use (Tikkanen et al. 2021). However, sometimes manufacturer may not have inert substitutive aggregates available, and Finnish Concrete Association has come up with updated guidance giving more detailed instructions regarding usage of reactive aggregate material (Klami et al. 2022). Reactive aggregate material will cause ASR only if concrete pore solution supplies suitable alkalinity and free alkalis contributing to reaction. Low alkali content cement has been shown to mitigate ASR. However, straightforward limiting of alkali content of cement may cause major inconveniences from productional perspective as large amounts of raw materials, mostly limestone, must be discarded from processing due to too high alkali content (Tapas et al. 2021). Other option for lowering cement alkali content is by utilizing bypass systems, but their disadvantage is increased energy requirement (Ferreira & Holt 2013). Quantitatively bulk of the used cements in Finland are manufactured by Finnsementti Oy, which produces clinker for its cements from domestic limestone quarries located in Parainen and Lappeenranta. Tapas et al. (2021) state commonly recommended total equivalent alkali content in cement to effectively mitigate alkali-aggregate reaction being 0.6%, but in bulk of used Finnish cements the content is averaged above that due to relatively high alkali content of exploited limestone, which makes high proportion of concrete produced in Finland having relatively high alkali content in used cement. Another solution for lowering alkali reactivity from binder perspective is by replacing cement partly with substitutive binding materials available in Finland such as fly ash, ground granulated blast furnace slag or silica fume. RILEM technical committee TC191-ARP has constructed a model regarding recommended amounts of substitute materials that should be used for efficiently mitigate reactivity for aggregates of different reactivity classes (Klami et al. 2022).

It is essential to acknowledge that total alkali content is later susceptible to change due to external alkali sources. Concrete can absorb alkalis after hardening for its whole

time in use, and the chemical potential for ASR may change significantly after additional alkali input overtime, especially when concrete has been cracked or highly permeable. Common external sources in Finland include seawater, groundwater, water from industrial processes, and de-icing salts used in road maintenance during wintertime. The rate of ASR induced by external alkalis are as such controlled by both permeability and the amount of free water (relative humidity) within the structure. External alkalis migrate as dissolved ions in water to reaction sites of reactive aggregate deeper in the structure along concrete porous channels. Reducing the permeability of concrete consequently restricts the movement of moisture and alkalis, lowering the susceptibility for ASR. Permeability can be reduced by lowering the water-cement ratio or using substitutive binding materials (Holt & Ferrera 2013). Increasing the total amount of binder and/or replacing a proportion of cement with certain substitutive materials will result in more compact and less permeable concrete, diminishing the mobility of ions (Tapas et al. 2021). Stark (1991) has investigated moisture conditions from field concrete structures exhibiting alkali-silica reactivity and concluded that measurements of over 80% of relative humidity in temperatures between 21 to 24 °C is required for expansive alkali-silica reactivity.

## 2.5 Features of silica affecting the alkali reactivity

### 2.5.1 Silica crystallinity, species and polymorphs

According to Broekmans (2004), a total volume of 12% of the earth's crust being consisted of pure $SiO_2$, making it a major crustal component. Silica may exist in several polymorphs, of which each have their distinct crystal structures differentiating them from each other. Temperature and pressure are the key factors controlling the organization of $SiO_4$-tetrahedra framework, and changes in prevailing temperature-pressure system may result in reorganization of these units, in other words polymorph conversion into another. Generally known polymorphs of silica are α-quartz, high temperature variants β-quartz, tridymite and cristobalite, and high pressure coesite and stishovite (Figure 5). Most abundant polymorph, α-quartz, is the second most abundant mineral in the crust and stabile in most prevailing temperature and pressure conditions in nature, whilst others are known being thermodynamically unstable (Ronov & Yaroshevsky 1969; Broekmans 2004). Even so, other silica polymorphs are still present in some rocks. Certain phase transformation processes are slow, and

sometimes the time needed for lattice reconstruction is insufficient within the timeframe of changes in prevalent conditions, and hence unstable polymorphs stay persist in low ambient temperatures. It is worth to note that high pressure silica polymorphs do not exist outside their stability zone since their phase transformation occurs immediately both directions, but temperature dependent phases may persist as high-end variants silica glass, cristobalite or tridymite when quenched. Phase transformations are possible also in authigenic conditions where devitrification of silica glass is a typical occurrence. For instance, devitrification forms cristobalite/tridymite intergrowths in obsidian, or up to α-quartz in case sufficient activation energy is available (Broekmans 2004). Poor crystallinity is another reactivity enhancing constituent in aggregates. Poor crystallinity may occur as result of deformation or very fast cooling of lava, in which sudden solidification will form volcanic glasses that don't have proper crystallographical structure and are thus thermodynamically unstable (Fournier and Bérubé 2000).

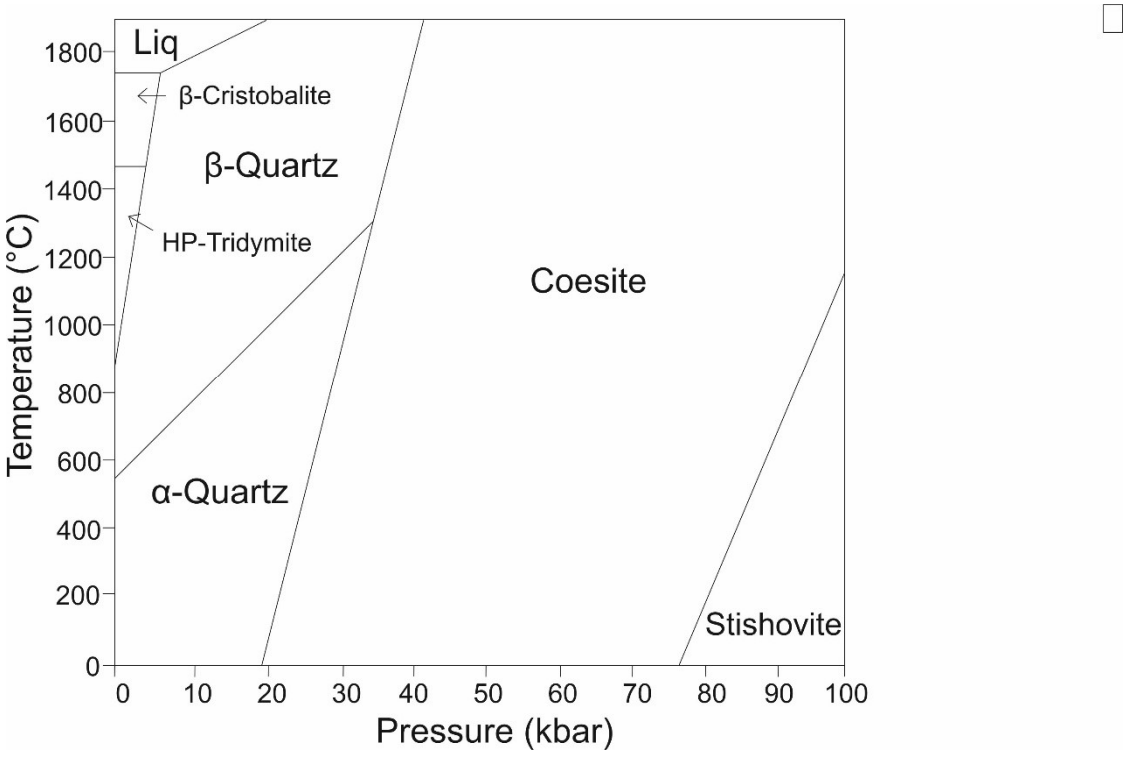


*Figure 5. P-T -diagram of silica system (Klein & Hurlbut 1993)*

Variations in thermodynamical stability of silica polymorphs affect their susceptibility for dissolution in alkaline environment. Effective concentration of dissolved silica in equilibrium is dependent on crystal structure and the crystallinity degree of solid silica phases, which makes phase recognition a relevant concern when evaluating aggregate

alkali reactivity (Broekmans 2004). Chemical tests have suggested that opal, a mixture of amorphous material and cristobalite and/or tridymite, has been noticed being generally the most reactive form of silica (Grattan-Bellew 1992).

### 2.5.2 Grain size

Reaction between reactive aggregate material and alkalis occurs mainly on the surface area of aggregate material in which reactants are in direct contact with each other. This is why total surface area of reactive aggregate material plays a significant role in determining the overall silica dissolution rate and extent. When more surface area is exposed for dissolution, reaction will speed up. Surface area is increased as function of diminishing grain size, in other words the total surface area increases whereas total reactive material volume stays constant, thus promoting reactivity potential. This makes the presence of microcrystalline quartz an essential factor affecting aggregate alkali-silica reactivity. Quartz microcrystals are small quartz grains of size <100 μm. Microcrystalline quartz forms either by crystallization and growth from precursor amorphous material such as opal, or by recrystallization of strained and deformed quartz under regional stress during metamorphism. Distinctive difference that can be observed in thin section is that microcrystalline quartz formed under metamorphic conditions tends to show undulatory extinction that exhibit crystal lattice mismatches and dislocations. Microcrystals are often localized within certain parts of the rock where differential stress is condensed such as shear joints and strongly dynamically recrystallized quartz clusters. Of these two origins, metamorphic microcrystalline quartz is suggested being more reactive as in addition to small grain size, crystal lattice contains imperfections that increase the intracrystalline energy. (Grattan-Bellew 1992)

### 2.5.3 Quartz lattice quality

Crystal lattice quality in nature is strongly connected to the deformation rock has experienced after initial solidification. Deformation of rock is a process in which external controls such as temperature, lithostatic pressure, differential stress, fluid pressure and externally imposed strain rate affect individual grains within the rock. Response of rock in contrast is dependent on its mineralogy, intragranular fluid composition, grain size, lattice-preferred orientation, porosity, and permeability (Passchier & Trouw 1998). A perfect crystal structure of quartz consists of $SiO_4$

tetrahedra units that are uniformly organized with respect to each other, in which the distance and angle between the units is identical. Perfect quartz structure is also purely consisted of $SiO_2$ without any other chemical constituents. As quartz is exposed to stress, its crystal structure starts to deform, forming displaces and deflects in the lattice (Tiecher et al. 2017). This affects the thermodynamical stability of present quartz (Ponce & Batic 2006). These displacements make lattice more distorted and favorable to accommodate foreign alkaline ions. In other words, quartz crystal holds high free intracrystalline energy that sets it vulnerable to aggressive agents attempting to break the stressed bonds. Quartz solubility is hence dependent on the lattice structural perfection. The reactivity of individual crystal is localized in the vicinity of displacements where the intracrystalline strain is condensed (Passchier and Trouw 1998).

Grain boundaries can be defined as misorientation angles between two volumes within the same crystal structure. This planar array of dislocations is considered either as one or two contiguous crystal structural entities by the angle of the dislocation arrays between separate volumes. Distinction between these two is arbitrary, but low angles tend to refer to a defect within single crystal, whereas high angles are regarded as two contiguous crystals with differently oriented lattices. Same fundamental applies for structures such as deformation lamellae and nonplanar or planar crystal twin interfaces (Broekmans 2004).

The level of deformation determines which deformational characteristics is being formed, and temperature and pressure conditions can be evaluated based on textural information observable from the rock. Typical observable quartz structures that are formed at low-grade PT-conditions include undulatory extinction, kind bands, pressure solution and redeposition (Passchier & Trouw 1998). Dolar-Mantuani (1981) introduces determination of the undulatory extinction angle as method for identifying potential alkali-reactive quartz grains. The angle is used as measure of the imperfections in the crystal lattice, which may assist in evaluating the level of intracrystalline strain. Extinction angle is determined by measuring the angle of microscope table rotation between the first appearance of extinction in any part of the quartz grain and the disappearance of the extinction in the grain area of the last extinction. Dolar-Mantuani (1981) suggested at least 10 measurements per thin section from rocks with medium to coarse grain size and set an undulatory extinction angles

of 15 degrees or more are as threshold to consider grain potentially alkali reactive. Grattan-Bellew (1992) however explains that results regarding correlation between quantified undulatory extinction and reactivity of quartz bearing aggregates are conflicting. This is due to problems limiting the accuracy of measuring the undulatory extinction angle; the size and orientation of the grain in thin section will affect the measured angle. Essentially, undulatory extinction and formation of microcrystalline quartz are part of the same process in which the quartz crystals are applied to stress, so observing either one of these features could be used as remark of enhanced reactivity.

## 2.6 Assessment of alkali reactivity potential of aggregates

### 2.6.1 Petrographic examination method from thin section

Petrographic examination of concrete aggregates is considered as a first step testing method assessing the alkali-reactivity of the rock. Method aims to determine the rock type and identify and quantify the amount of possibly reactive constituents. Comprehensive rock type classification is based on observing the mineral content, structure, texture and petrogenetic context from thin sections, of which calculating the modal contents of rock-forming minerals and describing texture is in key position.

Observation of thin sections is conducted by point counting method, which is a technique for calculating the modal composition of minerals and their microscopic grain size distribution. In point counting, thin section is divided into regular grids. Counting the number of individual minerals at grid intersections and calculating their relative proportions of total counted points constructs a modal proportion of each mineral in the rock. Counting is generally very slow process, in which the expertise of observer plays a major role. Nowadays digital image analysis offers assisting tools for point counting process that tend to reduce the amount of time required and simplify the workflow in general (Larrea et al. 2013). There are many international and national guides and recommendations for petrographic examination, one of which is the RILEMs (International Union of Laboratories and Experts in Construction Materials, Systems and Structures) recommended test method AAR-1. RILEM recommendation is widely adopted method, which is followed in Finland as well.

The principle of petrographic examination (AAR-1) is to distinguish rock types and minerals that are susceptible for alkali aggregate reaction. The objective of the examination is to classify aggregate reactivity potential in either unlikely, potentially, or likely reactive class. In case of Class I, no further testing is demanded, and aggregate is safe to use. Aggregates in classes II and III will need to be directed to further testing such as accelerated mortar-bar test or concrete prism test, which have their own recommended testing procedures also provided in RILEM recommendations (Sims & Nixon 2003b).

It is emphasized that rock naming is conducted in internationally acknowledged manner so that research work sustains global uniformity. RILEM AAR-1 suggests applying genetic, mineralogical, and preferred names. This division considers that in many cases petrographic examination is carried out for small amounts of aggregate fragments and particles, and thus no larger scale geological information is available. This reduces necessary information regarding rock origin and genesis that is often required for detailed specification. Of these, preferred name is the most accurate, in which the common geological rock and mineral name is being used. Mineralogical name is the next most satisfactory name that is derived from mineralogical composition. Genetic name is applied when naming is based on the least information, typically used for samples consisting of very small aggregate fragments and particles. Naming procedure also suggests giving additional supplementary information in brackets after aggregate name, such as special or local names, mineralogy, crystal size or any other relevant information. (Sims & Nixon 2003b)

RILEM doesn’t set any accurate limits for determining the reactive potential class, but instead emphasizes the importance of following national and regional experiences and recommendations. In Finland, Finnish Concrete Association (Betoniyhdistys) has published a national guide (by74, guide for controlling alkali aggregate reaction in concrete 2022) for controlling the alkali-aggregate reaction which follows the outlines RILEM offers for the general testing procedure, and in addition sets up limits for aggregate classification (Klami et al. 2022). These limits are set as follows:

Class I: The amount of quartz is <15 % or in case quartz grain size is >0,2 mm, the amount of quartz is not limited.

Class II: Quartz grain size is <0,2 mm, or >15% of quartz exhibits undeveloped or distorted crystalline structure.

Class III: Rock contains quartz that is very fine grained, mostly <0,060 mm, and >15% of quartz exhibits undeveloped or distorted crystalline structure.

(Sims & Nixon 2003b)

Suitability of petrographic method for assessing the potential of alkali-aggregate reaction has formerly been evaluated for instance in PARTNER-project (Lindgård et al. 2010). Petrographic assessment is seen as possibly the fastest and most efficient testing method of all, but the greatest disadvantages are linked to inconsistency regarding reactivity classification. It was observed that aggregates that react more rapid (5-20 years) as well as non-reactive aggregates were more successfully identified, whereas slowly reactive aggregates (greater than 20 years) were identified with less certainty.

### 2.6.2 Accelerated mortar-bar method

The accelerated mortar bar test (AMBT) is a common practical test for testing potentially alkali reactive aggregates. AMBT was developed in 1986 by Oberholster and Davies (1986) in South Africa which included immersion of mortar bars of size 20 x 25 x 285 mm in 1 M NaOH solution at 80 degrees Celsius for 14 days. Accelerated mortar bar test is nowadays widely adopted method worldwide, for example by American Society for Testing and Materials (ASTM), Canadian Standards Association (CSA) and International Union of Laboratories and Experts in Construction Materials, Systems and Strctures (RILEM). AMBT is typically used as secondary testing method in case the initial petrographic assessment has concluded the possibility for reactive constituents, but it can be implemented also without first-hand optical examination. Reactivity of aggregates is evaluated by the expansion mortar bars experience through testing period. There are differences in testing methods and suggested expansion limits for certain reactivity classes. For instance, ASTM and RILEM determine aggregates innocuous when expansion is less than 0.10 % at 14 days and reactive if more than 0.20%. Canadian Standard has set expansion limit of 0.15 % at 14 days, and Danish Standard has ruled two limits depending on environmental classes of 0.20 % for moderate environment and 0.10 % for aggressive environment (Alaejos et al. 2014).

Some studies also suggest modifications such as lowering the limit to 0.08 % at 14 days for better detection of slowly reactive aggregates (Shayan 2007). In Finland, the limits for reactivity classes are stated in Finnish national guide by74 (Klami et al. 2022). By74 grounds its thresholds to Swedish national guidance. This is because Swedish and Finnish bedrock share many similarities, and in Sweden, significantly more research work has been accomplished regarding local aggregate material behaviour in AMBT. There are three classes for reactivity with corresponding limits that are set as follows:

Class I - unlikely reactive: 14 days ≤ 0.08 % or 28 days ≤ 0.25 %.

Class II – possibly reactive: 0.08 % < 14 days ≤ 0.25 %.

Class III – likely reactive: 14 days > 0.25 %.

(Klami et al. 2022)

The advantage of AMBT over petrographic examination is generally better and more consistent ranking of the aggregates between laboratories which has been addressed for example in the EU Partner project. Partner project evaluated AMBT with 22 different types of aggregates from 10 different European countries that were tested in several laboratories. Results showed generally less than 1 standard deviation of the overall mean value of expansion, and the band of uncertainty in the limit of 0.10 % at 14 days less than 0.025 %. However, some studies have brought up some unconventionalities as well. AMBT has been considered overly severe as in some cases it has identified some aggregates reactive despite their good actual performance in the field and concrete prism tests conducted for the same aggregates. One essential reason for this is that because aggregate material is being crushed in fine-grained fractions of <4 mm, the surface area that exposes to reaction is drastically increased, promoting reactivity (Thomas et al. 1997; Thomas et al. 2006; Ideker et al. 2012). Thus, AMBT is generally recommended as test that only accepts but does not reject aggregates from being used. Field evidence has also shown that AMBT might not detect some slowly reactive aggregates such as granitic gneisses (Wigum & French 1996; Shayan 2007). Alaejos et al. (2014) commenced an experimental programme on AMBT in which rapid and slowly reactive aggregates were extracted from alkali silica reaction affected structures which were put into AMBT. Results showed that AMBT

correctly detected all reactive aggregates. However, for rapid reactive aggregates, a limit of 0.10 % at 14 days, and for slowly reactive aggregates, a limit of 0.20 % at 90 days was required for correct test result. Slowly reactive aggregates showed relatively low expansion results at 14 days (<0.10 %) even though they developed ASR in the structure they were extracted from. An extension to 90 days and expansion limit of 0.20 % was proved to show correct results for all slowly reactive aggregates tested.

# 3 Materials and methods

## 3.1 Sample gathering and field observations

For this study, a collection of rock samples gathered both from the bedrock outcrops and separate boulders from different locations around Finland. Object was to produce a collection of samples with varying optical characteristics of silica for the purpose of this study. Emphasis was on felsic igneous and metamorphic rocks that are known having potential for alkali-silica reaction and do commonly exist within Finnish bedrock. Sample collection included both outcrop and loose boulder samples. Samples consisted of one intact rock fragment instead of a mixture of fragments around the area. Outcrop samples were detached from bedrock using a rock hammer and their location coordinates were measured and stored using phone Global Positioning System (GPS) application. Observable macroscopic features were documented on site, including main mineral composition, assumed rock type and main textural characteristics.

| Sample | North | East |
|---|---|---|
| Leevi 1.1 | 6738308 | 213737 |
| Leevi 2.1 | 6735045 | 215960 |
| Leevi 3.1 | 6734559 | 215839 |
| Leevi 4.1 | 6703770 | 317034 |
| Leevi 5 | 6704024 | 317239 |
| Leevi 6 | 6823367 | 298299 |
| Leevi 7 | 6682930 | 310468 |
| Leevi 8 | 6681836 | 303516 |
| Leevi 9 | 6681869 | 303511 |
| Leevi 10.1 | 6681490 | 303746 |
| Leevi 11 | 6681493 | 303708 |
| Leevi 12 | 7059434 | 414566 |
| Leevi 13 | 6707785 | 258197 |
| Leevi 14 | 7108423 | 356656 |
| Leevi 15 | 7036298 | 418294 |
| Leevi 16 | 7036298 | 418294 |
| Leevi 17 | 7036298 | 418294 |
| Leevi 18 | 7036298 | 418294 |
| Leevi 19 | 6971800 | 394096 |

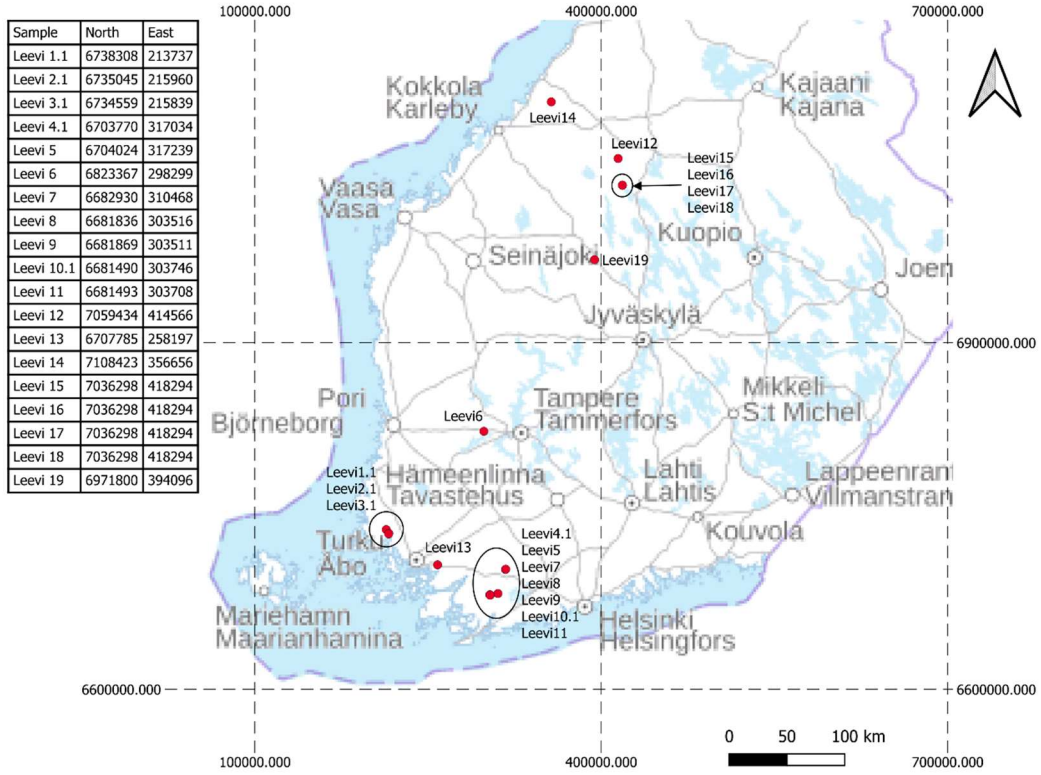


*Figure 6. Sample collection points projected on the map. Location coordinates are listed on the left. Coordinate system ETRS-TM35FIN.*

## 3.2 Petrographic examination

### 3.2.1 Thin section preparation

Thin section preparation work for petrographic examination was conducted in the laboratory of Geohouse, Turku University (Figure 7 & 8). One thin section was prepared from each of the 19 samples by technician Arto Peltola. Point of which thin section was prepared was chosen so that thin section represented the structure, texture, and bulk rock composition as well as possible.


*Figure 7. Rock samples after cutting. Size of the cutted samples is 3.5 x 2.5 mm.*

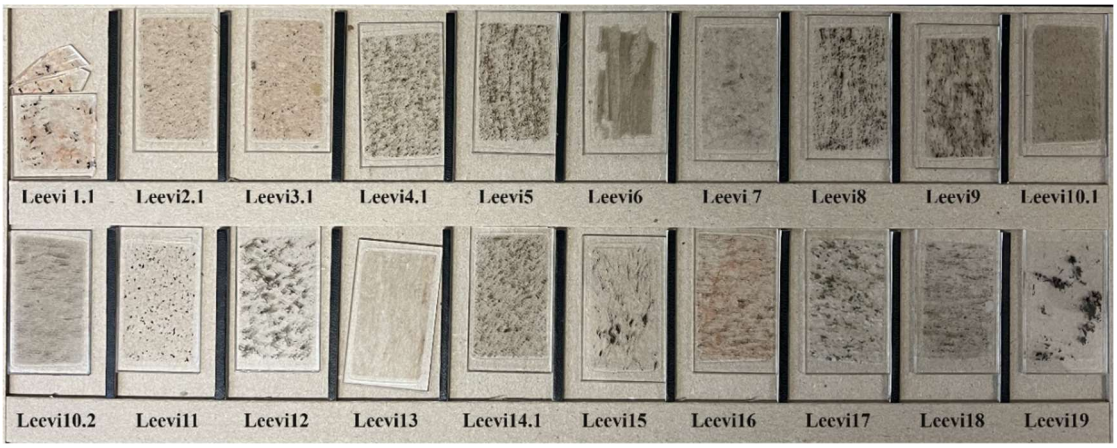


*Figure 8. Finished thin sections from rock samples. Thin section Leevi1.1 broke after examination.*

### 3.2.2 Naming of the rocks

Naming of the rocks followed the suggested nomenclature provided in RILEMs recommendation AAR-1 (Sims & Nixon 2003b). First, the modal mineralogy of samples was determined by calculating the percentage of each mineral in the rock. Calculation was based on counting the points of different minerals in thin section. Point counting was conducted with an electromechanical device attached to microscope, which moved thin section by regular steps in horizontal direction. Total amount of observed points was 1000 per thin section, which is considered representative by AAR-1 and by74 guidelines. (Sims & Nixon 2003b; Klami et al. 2022)

Three different classifications were used for rock naming according to RILEM's recommendation. Genetic name determines in which main rock group observed aggregate belongs to (igneous, metamorphic, sedimentary, artificial). Igneous rocks were divided into plutonic or volcanic type based on observed grain size. If the grain size was phaneritic (observable by naked eye), it was considered plutonic. Very fine-grained aphanitic rocks that needed microscope for determining the mineral composition were considered volcanic if known geological context didn't show otherwise. After this, mineralogical name was determined based on main mineralogy derived from modal composition determination. Lastly, preferred name was specified based on all available information gathered from both petrographic and field observations, giving the most accurate definition for the specific rock.

For intrusive igneous rocks the modal composition was plotted on the QAP triangle diagram according to Streckeisen (1974), of which each end represents one of three main minerals: quartz, alkali feldspar and plagioclase. After plotting, modal mineralogy was normalized by dividing quartz, alkali feldspar and plagioclase percentages by their combined percentage sum. Normalized modal composition is then read on QAP diagram, suggesting the preferred name based on composition. In case of volcanic rock, the compositionally equivalent extrusive name was applied. Determining preferred names for metamorphic rocks was based on the major features observable from the rock, such as present minerals, rock structure, nature of the rock prior to metamorphism (protolith), genetic conditions of metamorphism (pt-conditions, deformation), and rock chemical composition (Schmid et al. 2007).

### 3.2.3 Quartz classification

Simultaneously together with modal composition determination, point-counting included more detailed separation of quartz into three classes, aiming to categorize and quantify potentially reactive and innocuous forms of quartz by their optical characteristics. Quartz was qualified into one of the following: 1) undeformed and non-microcrystalline, 2) strained and, 3) microcrystalline quartz. Undeformed and non-microcrystalline quartz included crystals that showed none or faint undulatory extinction with angles of generally <10 degrees, grain shape was rather euhedral, grain bounders were clear, well crystallized, and straight. Quartz classified as strained included notable signs of deformation, lattice imperfections, intracrystalline strain or undeveloped crystallinity. Lattice imperfections included fluid inclusions, microcracks, deformation lamellae and undulatory extinction. Grain boundaries of strained quartz showed up as irregular, interlobating or sutured. Unclear grain boundaries were linked to undeveloped crystallinity. Strong grain elongation was also considered as notable indication of strain when present together with other beforementioned strain-indicating optical characteristics. Quartz included in microcrystalline class was based on measuring the grain size. Grains with longest diameter of <0.1 mm were considered as microcrystalline. Microcrystalline quartz that exhibited also strained features were qualified under microcrystalline class.

Reactivity classes for investigated samples were based on the modal content of possibly reactive components, consisting of combined amounts of quantified strained and microcrystalline quartz. Following reactivity class thresholds were applied:

Class I – unlikely reactive: modal composition of <15 % for reactive components and general grain size >0.1 mm,

Class II – potentially reactive: modal composition of >15 % for reactive components,

Class III – likely reactive: modal composition of >15 % for reactive components in which the general quartz grain size is <0.06 mm.

*Measuring extinction angle*

The amount of crystalline strain was quantified by utilizing extinction angle measurement according to Dolar-Mantuani (1981). Extinction angle measurement included determining the rotation angle of microscope table between the position of first appearance of undulatory extinction and the position at which the extinction band disappears. In total of 10 extinction angles measurements were taken from individual quartz grains from each of the sample thin sections. Measurements were taken from grains of size approximately 0.5-1.0 mm in diameter to acquire comparative results between the samples.

## 3.3 Accelerated mortar bar test

In total of 10 samples were chosen from sample collection and forwarded to accelerated mortar bar test. Mortar bar test was prepared and conducted in the laboratory of Mitta Oy in Oulu, Finland. Tested samples included both igneous and metamorphic rocks. Forwarded samples included different observed characteristics of possibly reactive quartz and variation in their relative proportions, so that their relationship and significance in alkali-silica reaction based on petrographic examination results could be assessed. In this study, RILEMs method AAR-2 for accelerated mortar bar test that is also adopted in by74, was applied. Aggregate material was crushed into five fractions and blended as follows:

1. 2.0-4.0 mm (10 wt-%)
2. 1.0-2.0 mm (25 wt-%)
3. 0.5-1.0 mm (25 wt-%)
4. 0.25-0.5 mm (25 wt-%)
5. 0.125-0.25 mm (15 wt-%)

Cement in use was CEM I 52,5 R Pikasementti (Finnsementti Oy). Cement Blaine fineness was 490-570 $m^2$/kg, and alkali content 1,3 % $Na_2O_{ekv}$. Three individual mortar bars of 40 x 40 x 160 mm in size were prepared for each of the rock samples (Figure 9). Water-cement ratio of mortar bars was 0.47. Mortar bars were left to cure for 3 days before immersing in alkaline water solution of 1 M NaOH with temperature of 80 degree Celsius. Before immersion, initial swelling during mortar curing was measured, and the length of mortar bar at this point was the reference length from which length changes were derived.


*Figure 9. Example picture of prepared mortar bars from rock sample Leevi19.*

Total of 10 measurements from each of the 3 individual mortar bars were taken during testing period of 28 days immersed in alkaline water solution. Four first measurements were taken within the period of days 1-13, one measurement at 14 days, four measurements between days 15-27, and final measurement at day 28. Measurements were taken simultaneously from each of the 3 mortar bars, and their average was considered as measurement result. Reactivity class was determined according to

suggestions stated in by74. Expansions of 0.08 % or under at 14 days, or 0.25 % or under at 28 days were included in class I, unlikely reactive. Expansions between 0.08 % and 0.25 % at 14 days were included in class II, potentially reactive. Likely potential reactivity class III was determined for samples with expansion of 0.25 % or above at 14 days.

# 4 Results

## 4.1 Field observations

### 4.1.1 Igneous rocks

There are in total of seven igneous samples with variations in grain size, deformation, and alteration. Four samples were gathered from SW Finland and two from central Finland (Figure 5), and their field observations are listed more detailed in Table 3. Samples Leevi1.1, Leevi 2.1 and Leevi3.1 are collected from Vehmaa batholith region at SW Finland (see Fig. 5). Vehmaa batholith belongs to a group of four large Finnish rapakivi intrusion regions that represent the anorogenic magmatic province. Rapakivi intrusions are comprised of series of granitic rocks associated with more mafic gabbroic bodies (Rämö & Haapala 2005). Leevi1.1. (Fig. 10a) represents a medium grained undeformed granite. Leevi2.1 (Fig. 10b) and Leevi3.1 (Fig. 10c) are fine-grained, mostly <1 mm, undeformed aplites. Aplites are very fine-grained compositionally granitic rocks that represent small intrusion phases within Vehmaa rapakivi batholith, mostly located at the eastern and western batholith margins (Lindberg & Bergman 1993). Sample Leevi19 is a coarse grained, undeformed porphyritic granite boulder collected from Karstula, Central Finland (Fig. 10d). Sample belongs to Central Finland Granitoid Complex. Sample Leevi11 (Fig. 10f) was detached from a boulder in Orijärvi area, Salo, SW Finland. This boulder has been derived from elsewhere to its current location as surrounding bedrock consists of metavolcanites and -sediments. Sample Leevi13 (Fig. 10e) was gathered from Paimio, SW Finland. Sample was detached from a shear joint of otherwise fine- to medium-grained, homogeneous, and undeformed granite intrusion. Sample Leevi16 (Fig. 10g) is a medium-grained, altered, recrystallized and deformed granite boulder gathered from sand pit, Pihtipudas, Central Finland.

Based on macroscopical field observations, igneous samples generally don't show evident signs of enhanced alkali reactivity. Sample Leevi13 is likely to contain the greatest number of reactive components such as strained and microcrystalline quartz that have been formed due to highly localized shear. Possible reactivity of aplite samples Leevi2.1 and Leevi3.1 is presumably linked to overall small grain size of the samples in which the quartz may be partly microcrystalline. Undeformed, medium- to coarse-grained samples Leevi19, Leevi1.1 and Leevi11 show no macroscopically observable signs of reactivity enhancing features.

*Table 3. A shortened summary of field observations of igneous samples with coordinates.*

| Sample | Sample type | Coordinates (ETRS-TM35FIN) | Main mineral assembly | Description |
|---|---|---|---|---|
| Leevi1.1 | Outcrop | N=6738308 E=213737 | Alkali feldspar, plagioclase, quartz, biotite, hornblende | Medium-grained (2-4 mm), undeformed, equigranular, homogenious granite |
| Leevi2.1 | Outcrop | N=6735045 E=215960 | Alkali feldspar, quartz, plagioclase, biotite | Fine-grained (1 mm), undeformed, equigranular, homogenious aplite with small mafic enclaves and sugary texture |
| Leevi3.1 | Outcrop | N=6734559 E=215839 | Alkali feldspar, quartz, plagioclase, biotite | Fine-grained (1 mm), undeformed, equigranular, homogenious aplite with small mafic enclaves and sugary texture |
| Leevi11 | Boulder | N=6681493 E=303708 | Alkali feldspar, plagioclase, quartz, biotite | Fine-to medium-grained (1-2 mm), undeformed, equigranular, homogenious granite |
| Leevi13 | Outcrop | N=6707785 E=258197 | Alkali feldspar, biotite, plagioclase, quartz | Fine-grained (up to 1 mm), stongly sheared and elongated granite from shear joint within granite intrusion. Crystals show up as sutured and their grain boundaries are unclear with unaided eye. |

| | | | | |
|---|---|---|---|---|
| Leevi16 | Boulder | N=7036298 E=418294 | Plagioclase, quartz, alkali feldspar, biotite | Medium-grained (1-3 mm), moderate preferred mineral orientation, altered granodiorite |
| Leevi19 | Boulder | N=6971800 E=394096 | Alkali feldspar, plagioclase, quartz, hornblende, biotite | Coarse-grained (2-5 mm), porphyritic, undeformed, homogeneous granite |

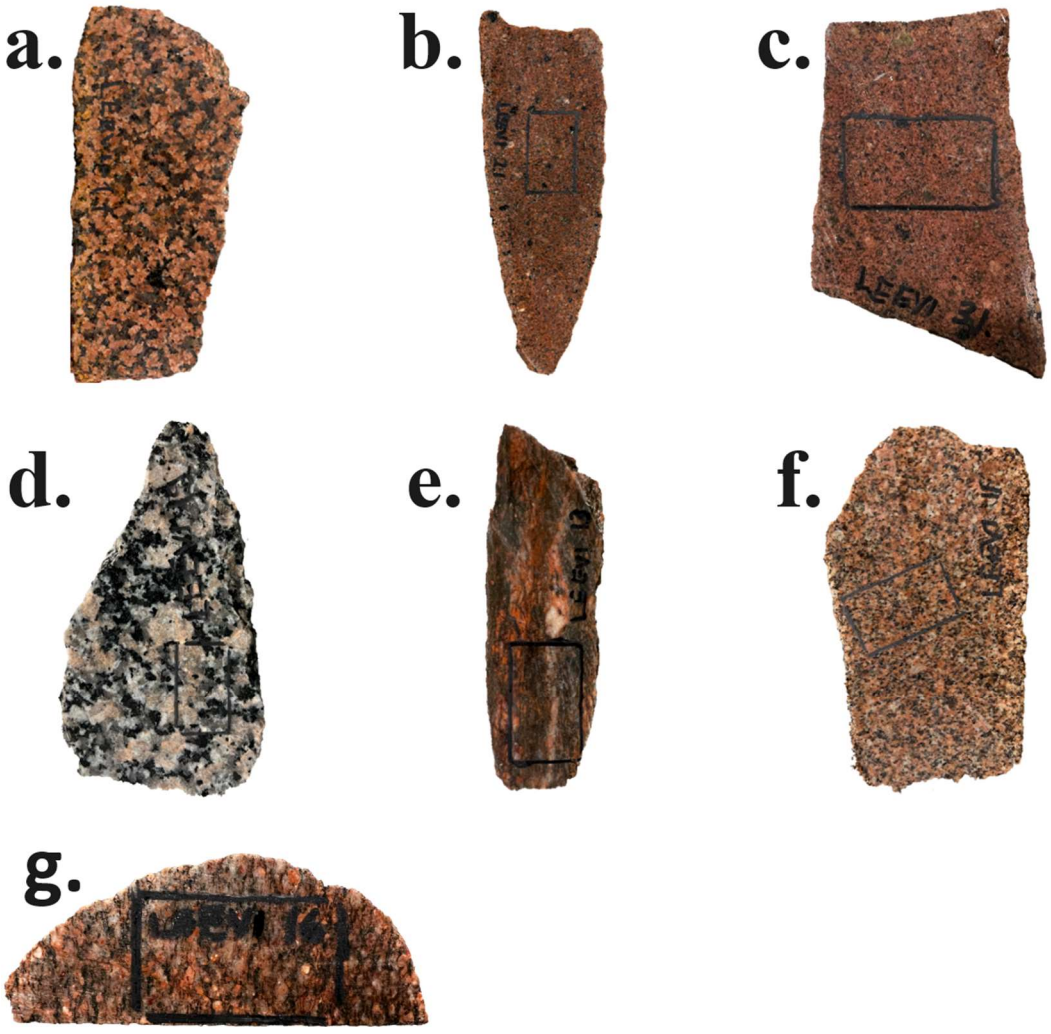


*Figure 10. Igneous samples. Rectangle marks the location within the sample where thin section has been obtained. a. Leevi1.1, medium-grained, undeformed granite, Vehmaa, SW Finland. b. Leevi2.1, fine-grained, undeformed aplite, Vehmaa, SW Finland. c. Leevi3.1, fine-grained, undeformed aplite, Vehmaa, SW Finland. d. Leevi19, coarse-grained and porphyritic granite, Karstula, Central Finland. e. Leevi13, fine-grained, sheared granite from shear joint of granite intrusion, Paimio, SW Finland. f. Leevi11, medium-grained granite from Salo, SW Finland. g. Leevi16, medoim-grained, altered and mildly oriented granodiorite from Pihtipudas, Central Finland. Black rectangles drawn on samples are 3.5 x 2.5 mm in size.*

### 4.1.2 Metamorphic rocks

In total of 12 metamorphic rocks are included in this study. Samples are gathered from several locations around south-western, western, and central Finland (see Fig. 5), and show variance in their mineralogical composition, metamorphic grade, deformation, structure, and texture. The detailed field observations are compiled in Table 4.

Distinctive set of samples was gathered from Orijärvi and Suomusjärvi areas, located in western part of the Uusimaa belt. Set consists of metamorphosed and deformed schistose and gneissic samples. Samples Leevi7, Leevi8, Leevi9 and Leevi10.1 (Fig. 11) are from Orijärvi area that is described consisting mainly of metamorphosed volcanic and volcaniclastic rocks that generally show low metamorphic grade, low strain, and well-preserved early structures (e.g. Väisänen & Skyttä 2007). Orijärvi region samples are either very fine or fine in grain size, felsic in composition and foliated from schistose to gneissic textures. Observed low grain size and texture indicate either volcanic or sedimentary origin of the samples that have undergone low temperature recrystallization, preserving the grain size. Based on felsic composition, small grain size and deformed texture it is assumed that Orijärvi area samples contain reactive siliceous components. Samples Leevi4.1 and Leevi5 (Fig. 11) were gathered from Suomusjärvi, approximately 25 km N-NE from Orijärvi. These two samples are taken from Suomusjärvi fault zone that has developed in ductile conditions (Lonka et al. 1998). Leevi4.1 and Leevi5 samples show typical gneissic mineralogical separation into layers with layer thickness varying from <1 mm to approximately 1 cm, and the thickest layers are consisted of recrystallized quartz.

Sample Leevi6 (Fig. 11g) is a metasediment taken from Tampere Schist Belt area. Tampere schist belt is a Proterozoic volcanic arc system that comprises metavolcanics and -sediments that are low metamorphic grade. Sample was taken from outcrop of very fine grained, homogeneous, and low metamorphic grade phyllite, where primary sedimentary layering is visible by naked eye. Due to very fine grain size, the amount or more detailed description of sample composition is hardly possible. Possible alkali reactivity is assumed relating mainly to small quartz grain size. Leevi12 (Fig. 11h) is a medium-grained gneiss from Haapajärvi, Central Finland. Mineralogical composition seems mafic where the total amount of silica is relatively low high. Leevi14.1 (Fig. 11i) is a metavolcanite boulder from Kainuu, Central Finland. Sample

is a separate boulder gathered from former quarry and represents the bulk rock material that has been excavated. Mineralogically sample consists mainly of mafic minerals and is thus considered mafic metavolcanite. Texture of the sample is homogeneous and equigranular with slight foliation observable from preferred breaking direction.

Samples Leevi15, Leevi17 and Leevi18 (Fig. 11) are all rounded boulder samples gathered from Pihtipudas, Central Finland. As samples are essentially boulders that have been delivered and deposited to their current placement, they do not represent the surrounding bedrock and are all evidently originated from different sources. This means that information regarding the origin and genesis of the samples is limited only to observable features from the boulders themselves. Sample Leevi15 is a granitic protomylonite that has undergone strong ductile shear. Rock consists of approximately 50% of larger, millimetre-to-centimetre scale feldspar porphyroclasts that have preserved after strong ductile shear that has caused mylonitic texture. Another 50% consists of strongly sheared groundmass. Since 50% of total rock volume consists of preserved feldspar porphyroclasts, rock is considered as protomylonite. Leevi17 is an unfoliated, medium-grained metamorphic rock that is compositionally heterogeneous; reddish parts of the rock are more rich in alkali feldspar, whereas within greyish parts it is lacking. Leevi18 is moderately deformed and recrystallized, fine-grained schist.

*Table 4. A shortened summary of field observations of metamorphic samples with coordinates.*

| Sample | Sample type | Coordinates (ETRS-TM35FIN) | Main mineral assembly | Description |
|---|---|---|---|---|
| Leevi4.1 | Outcrop | N=6703770 E=317034 | Biotite, quartz, feldspar | Medium-grained (1-2 mm) gneiss, foliated, recrystallized, equigranular, gneissic mineralogical layering with thickness of <1-5 mm |
| Leevi5 | Outcrop | N=6704024 E=317239 | Biotite, quartz, feldspar | Medium-grained (1-2 mm) gneiss, foliated, recrystallized, equigranular, gneissic mineralogical layering with thickness of <1-10 mm |
| Leevi6 | Outcrop | N=6823367 E=298299 | Quartz, muscovite, biotite, feldspar | Very fine-grained (<0.1 mm), low metamorphic grade, foliated phyllite. Minor deformation; |

| | | | | |
|---|---|---|---|---|
| | | | | preserved primary sedimentary bedding. Mineralogical composition hardly distinguishable with unaided eye due to low grain size. |
| Leevi7 | Outcrop | N=6682930 E=310468 | Quartz, feldspar | Very fine-grained (mainly <0.1 mm), recrystallzed, quartz-rich metavolcanite. |
| Leevi8 | Outcrop | N=6681836 E=303516 | Quartz, plagioclase, alkali feldspar, biotite | Strongly foliated fine-grained (0.1-1.0 mm) schist |
| Leevi9 | Boulder | N=6681869 E=303511 | Plagioclase, qiartz, biotite | Strongly foliated (<0.1-1.0 mm) schist. Unclear grain boundaries indicating imperfect crystallinity |
| Leevi10.1 | Boulder | N=6681490 E=303746 | Plagioclase, quartz, biotite | Very fine-grained (<0.5 mm), foliated, compositionally mafic metavolcanite |
| Leevi12 | Boulder | N=7059434 E=414566 | Plagioclase, quartz, biotite | Medium-grained (1-2 mm), foliated, compositionally mafic, recrystallized gneiss |
| Leevi14.1 | Boulder | N=7108423 E=356656 | Plagioclase, quartz, amphibole, biotite | Very fine-grained (0.1-0.5 mm), mildly foliated, compositionally mafic metavolcanite |
| Leevi15 | Boulder | N=7036298 E=418294 | Alkali feldspar phenocrysts, plagioclase, quartz, biotite | Granitic, strongly sheared protomylonite (50% alkali feldspar porphyroclasts (2-5 mm), 50% very fine-grained (<0.1 mm) groundmass) |
| Leevi17 | Boulder | N=7036298 E=418294 | Alkali feldspar, plagioclase, quartz, hornblende | Medium-grained (1-2 mm), recrystallized, compositionally heterogenous schist |
| Leevi18 | Boulder | N=7036298 E=418294 | Feldspar, quartz, biotite | Fine-grained (0.1-2.0 mm), foliated, recrystallized schist |

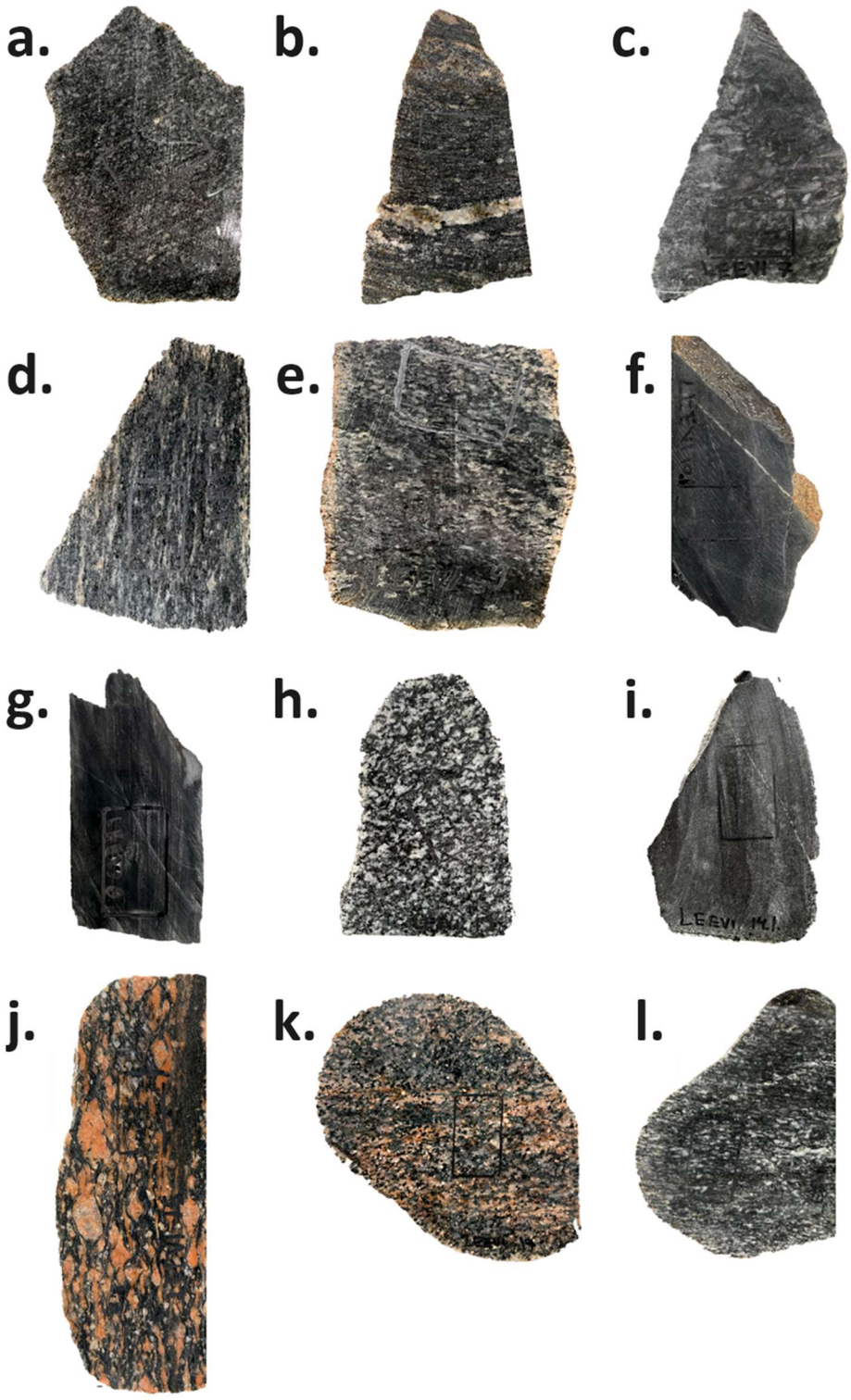


*Figure 11. Metamorphic rock samples. Rectangle marks the location within the sample where thin section has been obtained. a. Leevi4.1, medium-grained gneiss, Suomusjärvi, SW Finland. b. Leevi5, medium-grained gneiss from Suomusjärvi, SW Finland. c. Leevi7, very fine-grained metavolcanite from Orijärvi, SW Finland, d. Leevi8, fine-grained schist from Orijärvi, SW Finland. e. Leevi9, fine-grained schist from Orijärvi, SW Finland. f. Leevi10.1, very fine-grained metavolcanite from Orijärvi, SW Finland. g. Leevi6, low metamorphic grade phyllite from Tampere, W Finland. h. Leevi12, medium-grained, compositionally mafic gneiss from Haapajärvi, Central Finland. i. Leevi14.1, very fine-grained metavolcanite from Kannus, Central Finland. j. Leevi15, granitic protomylonite from Pihtipudas, Central Finland. k. Leevi17, medium-grained, compositionally geterogeneous schist from Pihtipudas, Central Finland. l. Leevi18, medium-grained, foliated, and recrystallized schist from Pihtipudas, Central Finlnd.Petrographical examination. Black drawn rectangles are 3.5 x 2.5 mm in size.*

## 4.2 Petrographical examination

### 4.2.1 Modal composition and rock naming

Of igneous rock samples, Leevi1.1, Leevi2.1, Leevi3.1, Leevi11, Leevi13 and Leevi19 represent a typical modal composition of granite. Leevi16 contained relatively high amount of plagioclase compared to alkali feldspar, classifying it as granodiorite. The alteration of feldspars is mild to moderate for coarser samples Leevi1.1 and Leevi19, and relatively stronger in fine grained aplites Leevi2.1 and Leevi3.1, deformed granite sample Leevi13 and granodiorite Leevi16. Coarse-grained Leevi19 also contained myrmekites that are intergrowths of quartz and plagioclase, which may contribute to alkali-silica reactivity.

Of metamorphic rocks, samples Leevi4, Leevi5, Leevi7, Leevi8, Leevi9, Leevi15, Leevi17 and Leevi18 represent a quartzo-feldspathic main modal mineralogical composition. Leevi4 and Leevi5 represent intensively deformed felsic gneisses. Leevi7 is compositionally felsic and recrystallized metavolcanite. Leevi8, Leevi9, Leevi17 Leevi18 are recrystallized and foliated felsic schists. Leevi15 is a quartzo-feldspathic mylonite which has experienced significant grain size reduction and recrystallization of groundmass after ductile shear deformation. Preserved phenocrysts consist of alkali feldspar and plagioclase that comprise in total of 47.4 % of modal composition, thus classifying rock sample as protomylonite. Leevi10.1, Leevi12 and Leevi14.1 are metamorphic rocks with mafic composition, indicated by high plagioclase and biotite, and low quartz contents. Small grain size of Leevi10.1 and Leevi14.1 indicate volcanic origin, classifying them as metavolcanites that have recrystallized in low temperature conditions. Leevi12 is fully recrystallized and banded gneiss. Leevi6 is a phyllite that consists of quartz, feldspars, and phyllosilicates. Textural characteristics indicate sedimentary origin that has undergone only minor deformation and low-grade metamorphosis, which has preserved the original sedimentary bedding structures.

Listed results of modal compositions are presented in table 5 and applied nomenclature in table 6.

*Table 5. Calculated modal compositions of studied thin sections.*

| Sample | Quartz | Alkali-feldspar | Plagioclase | Biotite | Muscovite | Others |
|---|---|---|---|---|---|---|
| Leevi1.1 | 27.0 % | 53.8 % | 11.4 % | 4.9 % | 2.9 % | |
| Leevi2.1 | 35.3 % | 44.2 % | 14.8 % | 2.6 % | 3.0 % | 0.1 % |
| Leevi3.1 | 33.4 % | 33.8 % | 23.8 % | 4.3 % | 4.7 % | |
| Leevi4.1 | 18.4 % | 42.3 % | 14.9 % | 24.0 % | 0.5 % | |
| Leevi5 | 19.2 % | 37.9 % | 8.1 % | 34.0 % | 0.0 % | 0.8 % |
| Leevi6 | 30.6 % | 15.8 % | 11.0 % | 16.6 % | 17.8 % | 8.2 % Chlorite |
| Leevi7 | 39.2 % | 38.6 % | 1.2 % | 8.4 % | 12.6 % | 0.0 % |
| Leevi8 | 30.9 % | 24.3 % | 22.0 % | 15.0 % | 0.5 % | 7.3 % Pyroxene |
| Leevi9 | 33.2 % | 17.6 % | 29.0 % | 20.2 % | 0.0 % | |
| Leevi10.1 | 26.4 % | 0.4 % | 41.6 % | 31.2 % | 0.4 % | |
| Leevi11 | 32.0 % | 41.6 % | 19.5 % | 6.5 % | 0.0 % | 0.4 % Opaque |
| Leevi12 | 24.4 % | 12.0 % | 41.4 % | 16.8 % | 1.2 % | 3.8 % Pyroxene<br>0.4 % Opaque |
| Leevi13 | 25.6 % | 23.2 % | 48.4 % | 2.8 % | 0.0 % | |
| Leevi14.1 | 17.8 % | 0.2 % | 52.6 % | 12.4 % | 0.0 % | 17.0 % Amphibole |
| Leevi15 | 43.2 % | 22.8 % | 24.6 % | 5.2 % | 0.0 % | 4.2 % Amphibole |
| Leevi16 | 23.6 % | 20.8 % | 48.6 % | 6.4 % | 0.0 % | 0.6 % Pyroxene |
| Leevi17 | 22.6 % | 29.4 % | 29.0 % | 0.2 % | 0.0 % | 18.8 % Hornblendite |
| Leevi18 | 22.8 % | 28.8 % | 28.8 % | 12.6 % | 0.0 % | 5.8 % Hornblendite |
| Leevi19 | 27.2 % | 44.8 % | 9.0 % | 10.8 % | 0.0 % | 7.8 % Hornblendite<br>0.4 % Pyroxene |

*Table 6. Applied names for studied rock samples.*

| Sample | Genetic name | Mineralogical name | Preferred name | Supplementary |
|---|---|---|---|---|
| Leevi1.1 | Plutonic rock | Quartzo-feldspathic rock | Granite | |
| Leevi2.1 | Plutonic rock | Quartzo-feldspathic rock | Aplite | |
| Leevi3.1 | Plutonic rock | Quartzo-feldspathic rock | Aplite | |
| Leevi4.1 | Metamorphic rock | Quartzo-feldspathic rock | Gneiss | Recrystallized, strained quartz |

| | | | | |
|---|---|---|---|---|
| Leevi5 | Metamorphic rock | Quartzo-feldspathic rock | Gneiss | Recrystallized, strained quartz |
| Leevi6 | Metamorphic rock | Argillaceous rock | Phyllite | Microcrystalline quartz |
| Leevi7 | Metamorphic rock | Quartzo-feldspathic rock | Metavolcanite | Low T recrystallization, strained and micro-/cryptocrystalline quartz |
| Leevi8 | Metamorphic rock | Quartzo-feldspathic rock | Schist | |
| Leevi9 | Metamorphic rock | Quartzo-feldspathic rock | Schist | Low T recrystallization, strained and micro-/cryptocrystalline quartz |
| Leevi10.1 | Metamorphic rock | Mafic rock | Metavolcanite | Microcrystalline quartz |
| Leevi11 | Plutonic rock | Quartzo-feldspathic rock | Granite | |
| Leevi12 | Metamorphic rock | Mafic rock | Gneiss | Recrystallized, myrmekite |
| Leevi13 | Plutonic rock | Quartzo-feldspathic rock | Granite | Sheared, strained and microcrystalline quartz condensed at the vicinity of zones of intense shear |
| Leevi14.1 | Metamorphic rock | Mafic rock | Metavolcanite | Microcrystalline quartz |
| Leevi15 | Cataclastic rock | Quartzo-feldspathic rock | Protomylonite | Strained quartz and microcrystalline quartz within the matrix |
| Leevi16 | Plutonic rock | Quartzo-feldspathic rock | Granodiorite | High T quartz recrystallization |
| Leevi17 | Metamorphic rock | Quartzo-feldspathic rock | Schist | Hornblende |
| Leevi18 | Metamorphic rock | Quartzo-feldspathic rock | Schist | |
| Leevi19 | Plutonic rock | Quartzo-feldspathic rock | Granite | Myrmekite |

### 4.2.2 Quartz classification and content of reactive phases

*Igneous samples*

The total amount of quartz in igneous samples varies from 23.6 % to 35.3 %. After quartz classification, the amount of unstrained quartz varies between 2.2 % and 27.7 %, strained quartz between 0.0 % and 19.2 %, and micro-/cryptocrystalline quartz between 0.5 % and11.8 %.

*Table 7. Modal compositions of classified quartz in studied igneous samples. Total amount of reactive quartz is the sum of strained and micro-/cryptocrystalline quartz. Reactivity class was determined based on total amount of reactive quartz.*

| Sample | Unstrained | Strained | Micro-/cryptocrystalline | Total amount of reactive quartz | Reactivity class |
|---|---|---|---|---|---|
| Leevi1.1 | 22.4 % | 3.7 % | 0.9 % | 4.6 % | I |
| Leevi2.1 | 26.7 % | 4.3 % | 4.3 % | 8.6 % | I |
| Leevi3.1 | 27.7 % | 1.3 % | 4.4 % | 5.7 % | I |
| Leevi11 | 12.3 % | 19.2 % | 0.5 % | 19.7 % | II |
| Leevi13 | 2.2 % | 11.6 % | 11.8 % | 23.4 % | II |
| Leevi16 | 4.0 % | 18.6 % | 1.0 % | 19.6 % | II |
| Leevi19 | 26.2 % | 0.0 % | 1.0 % | 1.0 % | I |

Medium- to fine-grained granite samples from Vehmaa rapakivi region, Leevi1.1, Leevi2.1 and Leevi3.1, and coarse-grained granite Leevi19 from Karstula, Central Finland, don't exhibit later recrystallization or deformation characteristics after their initial solidification (Figure 12). Quartz in samples Leevi1.1, Leevi2.1, Leevi3.1, and Leevi19 consists mainly of unstrained quartz, and only couple crystals exhibit undulatory extinction with angles sufficient to be classified as strained. Few percent of quartz grains have measured grain diameter of <0.1 mm which are classified as microcrystalline. Leevi19 contains moderate amounts of myrmekites, quartz intergrowths with feldspar which may enhance the reactivity potential. Other than that, quartz crystals in these samples exhibit intact euhedral crystals with straight and well-developed grain boundaries, referring to overall low reactivity. Total amount of

possibly reactive components for samples Leevi1.1, Leevi2.1, Leevi3.1 and Leevi19 was under 15 %, classifying them into unlikely reactive class.

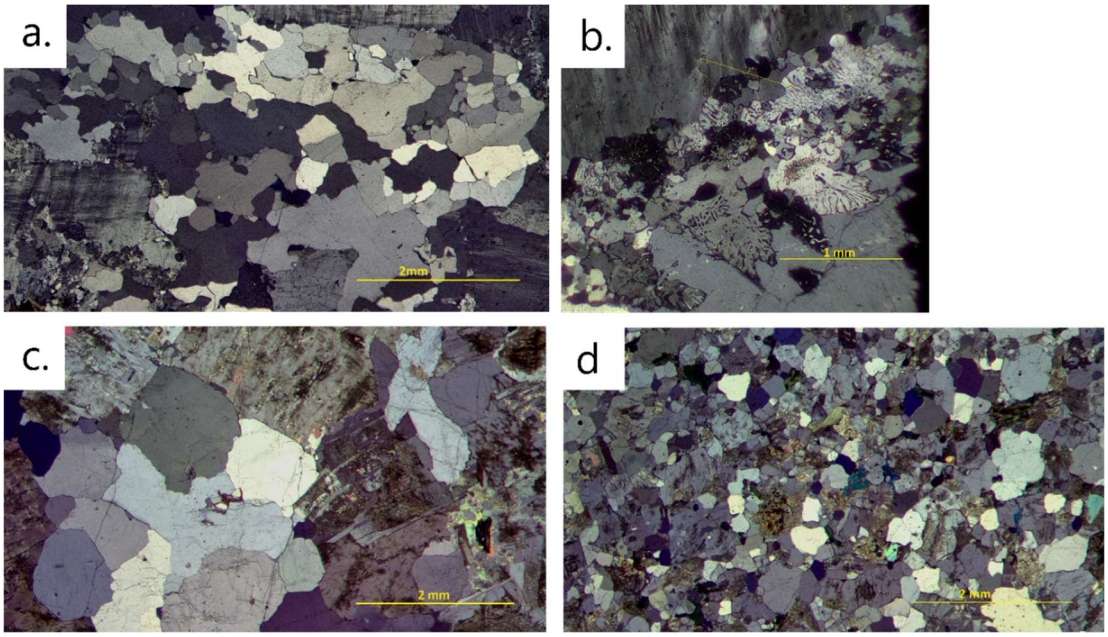


*Figure 12. Undeformed granite samples Leevi19 (a.), Leevi1.1 (c.) and Leevi2.1 (d.) contained very little forms of quartz linked to potential reactivity. Most significant reactivity enhancing feature was moderate amount of myrmekites present in Leevi19 (b.).*

Granite boulder from Orijärvi area, Leevi11, contains 19.2% of quartz that exhibit undulatory extinction, referring to strained quartz. Other metastable characteristics of quartz are not present, thus it is presumed that reactivity potential of the granite is generally low. Granite sample Leevi16 exhibits features of complete quartz recrystallization in moderate to high temperature conditions at around 500-550°C as recrystallization occurs as grain boundary migration type, in which the recrystallized crystals are relatively large, and no original grains have preserved (Stipp et al. 2002). Recrystallization has occurred contemporary or predated by deformation, which has led to elongated form of grains that exhibit mostly strain-free features (figure 12). Parts of the recrystallized quartz grains have developed subgrains that is evidence of dynamic recrystallization. Larger quartz grains and clusters exhibit moderate extinction angles in which the grain boundaries are also generally irregular and for some crystals also unclear, indicating lack of crystallinity. Granite sample Leevi13 detached from shear joint of granite intrusion includes considerable amounts of both strained and microcrystalline quartz. Intense shear has caused patterns of microfractures that cut through the rock parallel to shear direction, leading to formation of microcrystalline quartz that is concentrated in the vicinity of

microfractures where shear has been most intense. Modal contents of possibly reactive components of 19.7 % in Leevi11, 19.6 % in Leevi16, and 23.4 % in Leevi13 indicate possible reactivity for all the samples, classifying them into reactivity class II (Table 7).

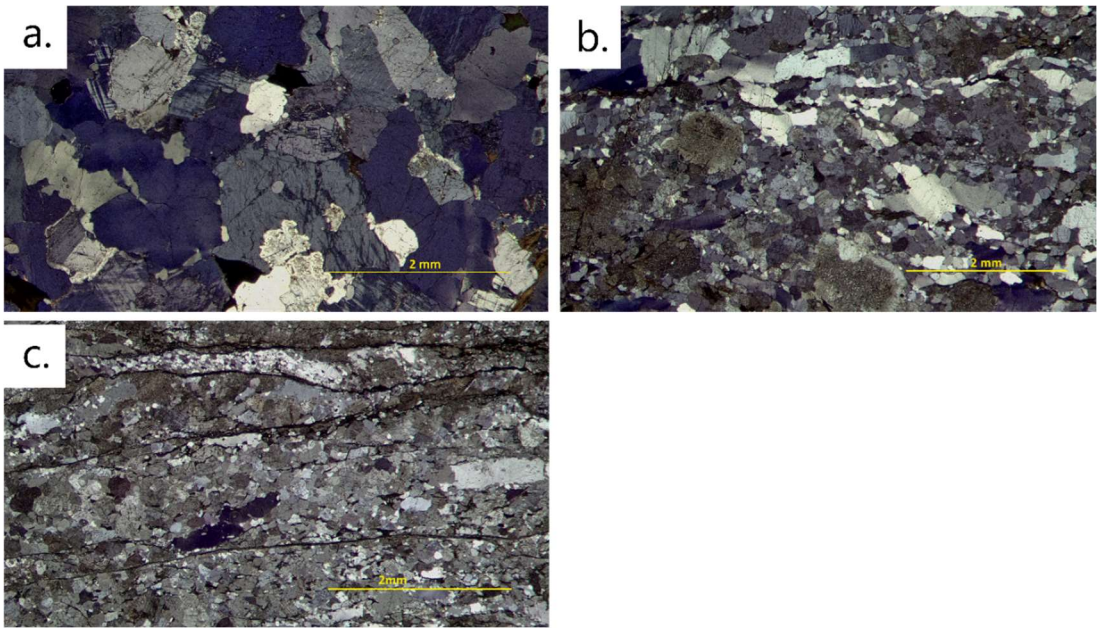


*Figure 13. Of igneous samples, granites Leevi11 (a.), Leevi16 (b.) and Leevi13 (c.) have experienced rock deformation which has formed strained and microcrystalline quartz. Microcrystalline quartz is especially present in Leevi13 which has experienced intense grain size reduction due intense localized shear.*

### *Metamorphic samples*

The modal proportion of quartz in metamorphic samples varies from 17.8 % to 43.2 %. After quartz classification, the amount of unstrained quartz varies between 0.0 % and 24.9 %, strained quartz between 0.0 % and 33.0 %, and micro-/cryptocrystalline quartz between 0.0 % and 30.6 %.

*Table 8. Modal compositions of classified quartz in metamorphic samples. Total amount of reactive quartz is the sum of strained and micro-/cryptocrystalline quartz. Reactivity class was determined based on total amount of reactive quartz.*

| Sample | Unstrained | Strained | Micro-/cryptocrystalline | Total amount of reactive quartz | Reactivity class |
|---|---|---|---|---|---|
| Leevi4.1 | 0.3 % | 14.4 % | 3.7 % | 18.0 % | II |
| Leevi5 | 0.0 % | 16.0 % | 3.2 % | 19.2 % | II |
| Leevi6 | 0.0 % | 0.0 % | 30.6 % | 30.6 % | II |

| | | | | | |
|---|---|---|---|---|---|
| Leevi7 | 0.2 % | 17.4 % | 21.6 % | 39.0 % | III |
| Leevi8 | 24.9 % | 0.8 % | 5.2 % | 6.0 % | I |
| Leevi9 | 0.8 % | 12.6 % | 19.8 % | 32.4 % | II |
| Leevi10.1 | 0.0 % | 0.0 % | 26.4 % | 26.4 % | II |
| Leevi12 | 24.4 % | 0.0 % | 0.0 % | 0.0 % | I |
| Leevi14.1 | 2.8 % | 0.4 % | 14.6 % | 15.0 % | II |
| Leevi15 | 3.0 % | 33.0 % | 7.2 % | 40.2 % | II |
| Leevi17 | 20.4 % | 1.8 % | 0.4 % | 2.2 % | I |
| Leevi18 | 12.8 % | 5.6 % | 4.4 % | 10.0 % | I |

Quartz in fine-grained phyllite sample Leevi6 and metavolcanites Leevi10.1 and Leevi14.1 are mainly consisted of microcrystalline size. Quartz within these samples is recrystallized, and the crystallinity of recrystallized quartz show up as mainly well-developed, which can be observed from distinct grain boundaries by which separate microcrystals are clearly distinguishable (Figure 13). In phyllite sample Leevi6, the quartz grain size tends to vary between the layers of original sedimentary bedding. Largest grains are present in phyllosilicate-poor layers consisting mainly of quartz and feldspar, whereas smallest grains are concentrated at phyllosilicate-rich layers. Grain lattices don't exhibit evident signs of intracrystalline strain, and the grain boundaries are well developed and angular. In metavolcanite samples Leevi10.1 and Leevi14.1, some individual larger quartz grains of 0.1-0.3 mm in diameter stand out from bulk of quartz grains by irregular grain boundaries and relatively strong undulatory extinction that are evident indication of strain. Modal content of possibly reactive components is 30.6 % for Leevi6, and due to possibly reactive components consisting solely of microcrystalline quartz, this sample is considered as likely potential class III as suggested in by74 (Klami et al. 2022). Reactive components with modal compositions of 26.4 % for Leevi10.1 and 15.0 % for Leevi14.1 determine these samples into possibly reactive class II (table 8).

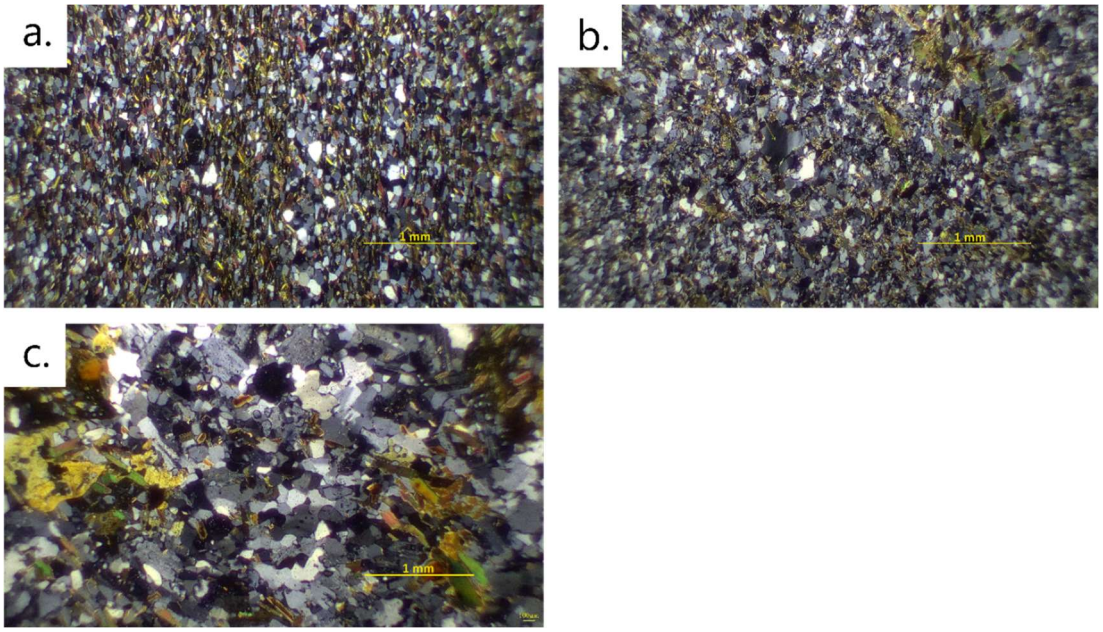


*Figure 14. Potential reactivity of phyllite sample Leevi6 (a.) and metavolcanite samples Leevi10.1 (b.) and Leevi14 (c) is linked to microcrystalline size quartz. Microcrystallinity dominates due to small initial grain size of protolith and low temperature metamorphosis that has preserved the general small grain size.*

Metavolcanite Leevi7 and felsic schist Leevi9 are characterised by the presence of both strained and microcrystalline forms of quartz (Figure 14). Quartz within these samples appear mainly as micro- and cryptocrystalline grains with unclear grain boundaries indicating low crystallinity. There are also larger clusters of recrystallized quartz that exhibit strong strained features of undulatory extinction, sutured grain boundaries, subgrain development and irregular grain shape. Microcrystalline quartz within the samples is scattered moderately even in the matrix and is relatively finer in metavolcanite Leevi7 (<0.06 mm) in comparison with schistose Leevi9 (<0.1 mm). Modal content of possibly reactive components for Leevi9 is 32.4 %, and for Leevi7 39.0 %, classifying these samples in class II (Table 8).

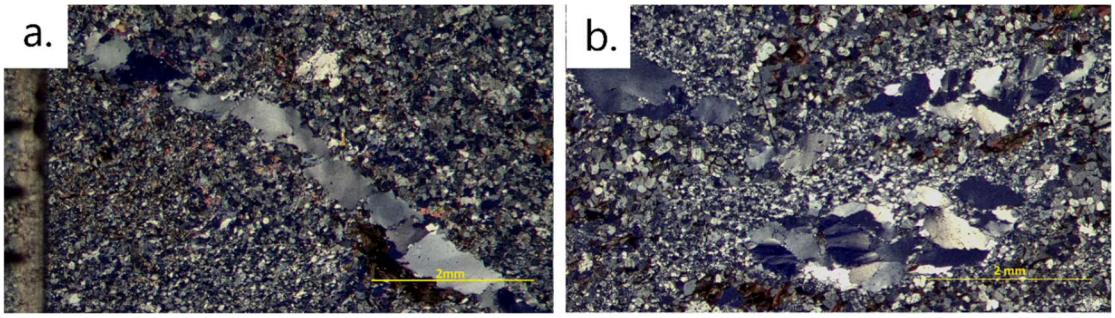


*Figure 15. Potential reactivity in metavolcanite sample Leevi7 (a.) and schist sample Leevi9 (b.) is linked to combination of microcrystalline quartz with undeveloped crystallinity that is scattered in the matrix, and individual clusters of larger quartz grains that exhibit strong strained characteristics.*

Strained quartz dominated in gneissic samples Leevi4.1 Leevi5 (Figure 14). The general grain size of quartz is 1.0-1.5 mm that is not linked to enhanced reactivity. Quartz is fully recrystallized during deformation but later overprinted by strong strained features. Ductile deformation has formed evident signs of intracrystalline stain that can be observed from sutured grains boundaries, intense microcracking, fluid inclusions, deformation lamellae and high extinction angles. Samples also contain small amount of recrystallized quartz microcrystals along grain boundaries of larger strained quartz grains and couple quartz intergrowths with feldspar that may have a small effect on reactivity. Quartz in protomylonite sample Leevi15 is dynamically recrystallized and deformed, containing mainly strained quartz with features of undulatory extinction and irregular grain shape along with subgrain development. The quartz grain size is homogeneous, the largest deformed quartz crystals and clusters are located between shear zones of highly localised strain, whereas the vicinity of shear zones has experienced intense grain size reduction, leading to formation of microcrystalline quartz (Figure 15). Modal content of possibly reactive components is 18.0 % for Leevi4.1, 19.2 % for Leevi5 and 40.2 % for Leevi15, classifying them in potentially reactive class II (table 8).

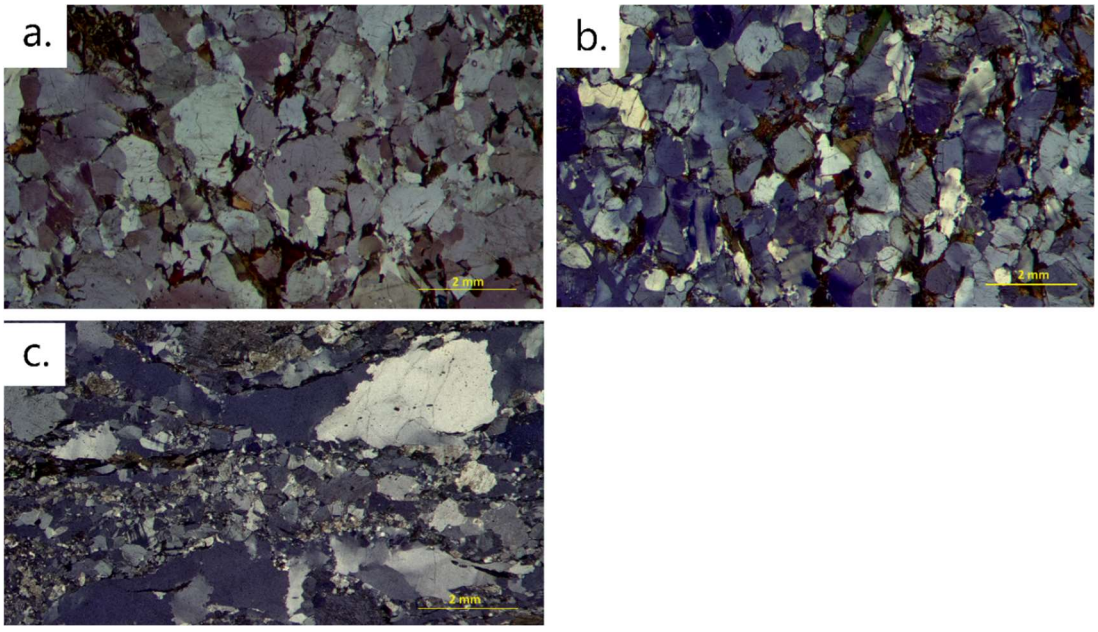


*Figure 16. Gneissic samples Leevi4.1 (a.), Leevi5.1 (b.), and protomylonite sample Leevi15 (c.) consist mainly of dynamically recrystallized quartz that has evident strained features referring to poor lattice quality. Protomylonite has more intense recrystallization of microcrystalline quartz along shear zones.*

Schist samples Leevi8, Leevi17 and Leevi18 and gneiss sample Leevi12 contained the lowest modal contents of quartz exhibiting reactive features. Samples are evidently

foliated and deformed but recrystallized in high temperatures leading to formation of quartz crystals of larger in size that have not experienced significant later deformation, thus grains tend to exhibit well-developed lattice quality. Quartz in Leevi8 is heterogeneous, containing a small proportion of quartz with lobate and interfingering grain boundaries and undulatory extinction that refer to higher intracrystalline strain. Major proportion of quartz is still fully recrystallized and healed in which these strained features are not present. Leevi18 stand out from this group with strong grain elongation parallel to general schistosity, of which some grains contain fluid inclusions. Despite evident grain elongation, quartz grains exhibit well-developed lattice quality and are not considered as strained. Gneissic sample Leevi12 contains some individual myrmekites, but the amount is very small which presumably won't significantly affect the reactivity potential. Modal content of possibly reactive components of 6.0 % for Leevi8, 0.0 % for Leevi12, 2.2 % for Leevi17 and 10.0 % for Leevi18 determines these samples in unlikely reactive class I (table 8).

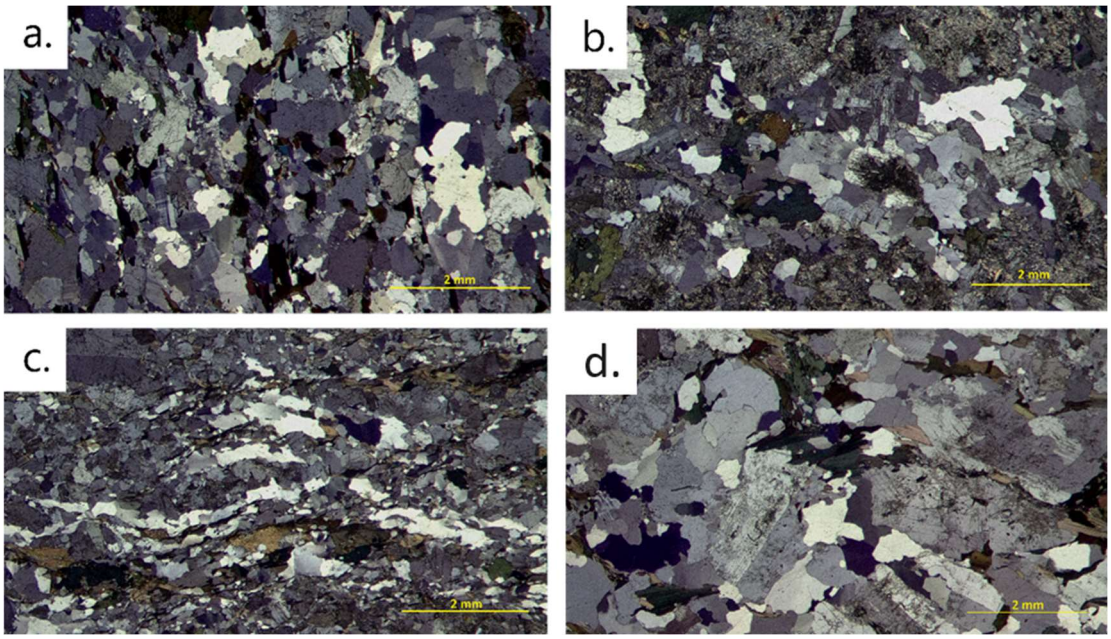


*Figure 17. Schist samples Leevi8 (a), Leevi 17 (b), Leevi18 (c), and gneiss sample Leevi12 (d) consist of dynamically recrystallized quartz that has sustained well-developed lattice quality after recrystallization.*

### *Undulatory extinction angle*

The average undulatory extinction angles within sample collection varies from 0.9 to 39.4 degrees. Highest average angles of >25° are present in metamorphic samples that have deformed in strong ductile deformation conditions, including gneissic samples Leevi4.1 (39.4°) and Leevi5 (34.3°) from bedrock outcrop in Suomusjärvi and

mylonizated boulder sample Leevi15 (26.0°) from Pihtipudas. Strong deformation of these samples was already clearly observable from the sample with unaided eye at the time of sample collection. Moderate extinction angles of 15 ≥ 25° are present in foliated metavolcanites Leevi7 (21.2°) and Leevi10.1 (17.5°), in schist samples Leevi9 (20.8°) and Leevi18 (21.3°), and in granite sample Leevi13 that was taken from shear joint (20.7°). Schistosity and foliation of these samples were evident indication of at least moderate undulatory extinction angles when making field observations. The lowest average angles of <15° are present in mafic metavolcanite Leevi14.1 (8.7°), schists Leevi8 (7.2°) and Leevi17 (7.7°), and mafic gneiss Leevi12 (7.7°). Other than sample Leevi13 from thin shear joint, igneous samples consisted of relatively small average angles. Average angle in granodiorite Leevi16 is 14.3°, and the measurements from the least deformed granite samples from Vehmaa rapakivi region and Karstula showed negligible angles of 5.0° in Leevi1.1, 1.0° in Leevi2.1, 0.9° in Leevi3.1, and 4.2° in Leevi19 which was presumable already when making field observations since macroscopical signs of deformation were either nonexistent or very mild. Low metamorphic grade phyllite Leevi6 consisted of such minute scale quartz grains that extinction angles could not be reliably measured from thin section. The same was in metavolcanite samples Leevi10.1 and Leevi14.1, which included only couple of larger crystals from which the angle was measurable.

*Table 9. Measured undulatory extinction angles of individual grains and their calculated average within the studied sample. Average grain size from measured grains also presented. Measures conducted following methodology of Dolar-Mantuani (1981).*

| *Sample* | *1* | *2* | *3* | *4* | *5* | *6* | *7* | *8* | *9* | *10* | *Avg angle* | *Avg size* |
|---|---|---|---|---|---|---|---|---|---|---|---|---|
| Leevi1.1 | 9 | 3 | 8 | 5 | 5 | 5 | 8 | 2 | 2 | 3 | 5.0 | 1.65 mm |
| Leevi2.1 | 1 | 0 | 2 | 0 | 1 | 2 | 3 | 0 | 0 | 1 | 1.0 | 0.70 mm |
| Leevi3.1 | 1 | 0 | 2 | 2 | 0 | 1 | 0 | 2 | 1 | 0 | 0.9 | 0.80 mm |
| Leevi4.1 | 27 | 24 | 48 | 34 | 44 | 31 | 41 | 56 | 54 | 35 | 39.4 | 1.00 mm |
| Leevi5 | 38 | 37 | 34 | 33 | 44 | 42 | 22 | 23 | 23 | 47 | 34.3 | 0.70 mm |
| Leevi6 | - | - | - | - | - | - | - | - | - | - | - | |
| Leevi7 | 18 | 15 | 25 | 14 | 21 | 32 | 20 | 30 | 24 | 13 | 21.2 | 1.15 mm |
| Leevi8 | 6 | 8 | 4 | 14 | 5 | 10 | 2 | 13 | 5 | 5 | 7.2 | 0.95 mm |
| Leevi9 | 24 | 25 | 26 | 18 | 24 | 20 | 14 | 12 | 30 | 15 | 20.8 | 1.20 mm |
| Leevi10.1 | 19 | 16 | - | - | - | - | - | - | - | - | 17.5 | 0.1 mm |
| Leevi11 | 7 | 7 | 9 | 6 | 11 | 12 | 9 | 15 | 11 | 18 | 10.5 | 1.20 mm |
| Leevi12 | 11 | 3 | 12 | 6 | 7 | 8 | 10 | 4 | 5 | 11 | 7.7 | 1.20 mm |
| Leevi13 | 11 | 32 | 24 | 13 | 20 | 26 | 16 | 30 | 23 | 12 | 20.7 | 1.35 mm |
| Leevi14.1 | 8 | 9 | 9 | - | - | - | - | - | - | - | 8.7 | 0.50 mm |
| Leevi15 | 16 | 23 | 25 | 15 | 36 | 44 | 21 | 22 | 21 | 37 | 26.0 | 1.35 mm |

| | | | | | | | | | | | | |
|---|---|---|---|---|---|---|---|---|---|---|---|---|
| Leevi16 | 8 | 15 | 22 | 13 | 6 | 13 | 24 | 18 | 9 | 15 | 14.3 | 1.10 mm |
| Leevi17 | 8 | 14 | 9 | 11 | 3 | 5 | 8 | 10 | 5 | 4 | 7.7 | 1.15 mm |
| Leevi18 | 22 | 21 | 24 | 25 | 36 | 12 | 28 | 11 | 18 | 16 | 21.3 | 0.75 mm |
| Leevi19 | 4 | 0 | 12 | 4 | 3 | 5 | 7 | 2 | 1 | 4 | 4.2 | 1.75 mm |

## 4.3 Accelerated mortar bar tests

The expansion measurements at different measurement times are listed in table 10 and presented in figure 18. Expansions varied at 14 days between 0.0280 % and 0.2262 %, and at 28 days between 0.0435 % and 0.3986 %.

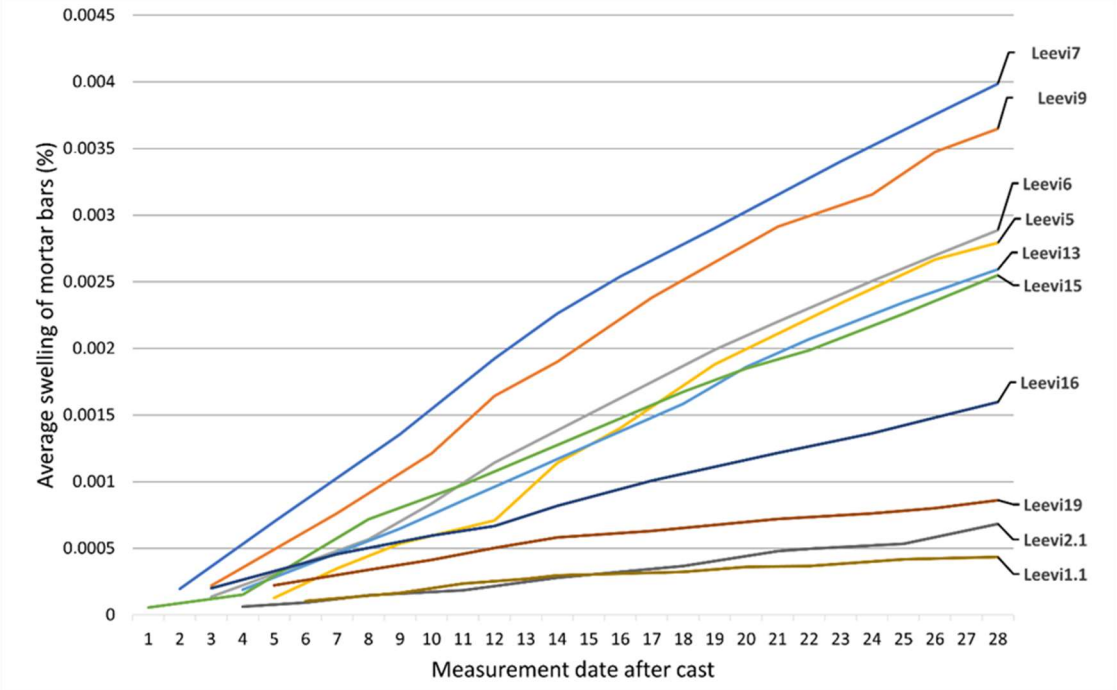


*Figure 18. Chart of mortar bar swell development of tested studied samples for 28 days period.*

Out of ten tested samples, five resulted in unlikely reactive class I and five in possibly reactive class II. Samples included in unlikely reactive aggregates are granite samples Leevi1.1, Leevi2.1, Leevi19 and Leevi16, and quartzo-feldspathic protomylonite sample Leevi15. Strongly deformed gneiss Leevi5, low grade phyllite Leevi6, felsic metavolcanite Leevi7, felsic schist Leevi9, and sheared granite Leevi13 are included in possibly reactive class. Expansion values of granite samples Leevi1.1, Leevi2.1 and Leevi19 are well below the limits to be considered possibly reactive, whereas foliated granite Leevi16 is just at the threshold to be reckoned as possibly reactive. Based on expansion, felsic metavolcanite Leevi7 is the most likely to be reactive, of which expansion at 14 days is close to be considered as likely reactive class III.

*Table 10. Measured expansions of accelerated mortar bar test at 14 days and 28 days. Expansion limits for reactivity classes adopted from by74.*

| Sample | Expansion at 14 days | Expansion at 28 days | Reactivity class |
|---|---|---|---|
| Leevi1.1 | 0.0296 % | 0.0435 % | Class I |
| Leevi2.1 | 0.0280 % | 0.0683 % | Class I |
| Leevi5 | 0.1141 % | 0.2792 % | Class II |
| Leevi6 | 0.1384 % | 0.2887 % | Class II |
| Leevi7 | 0.2262 % | 0.3986 % | Class II |
| Leevi9 | 0.1900 % | 0.3648 % | Class II |
| Leevi13 | 0.1169 % | 0.2592 % | Class II |
| Leevi15 | 0.1274 % | 0.2549 % | Class II |
| Leevi16 | 0.0818 % | 0.1597 % | Class II |
| Leevi19 | 0.0581 % | 0.0861 % | Class I |

*Class I:* $14 \text{ days} \leq 0.08\ \%$ *or* $28 \text{ days} \leq 0.25\ \%$

*Class II:* $0.08\ \% < 14 \text{ days} \leq 0.25\ \%$

*Class III:* $14 \text{ days} > 0.25\ \%$

# 5 Discussion

## 5.1 Alkali-silica reaction

Globally the most abundant type of AAR, ASR was detected in this study. AAR is divided into types of alkali-silica reaction, alkali-carbonate reaction and alkali-silicate reaction, of which the alkali-silica reaction is globally the most abundantly faced in damaged concrete structures, impacting over 50 countries (Jensen 20129; Bergmann et al. 2023). ASR occurs in concrete structures between metastable silica phases present in aggregates and alkalis that provided by cement in alkaline pore solution. ASR is a sequence of reactions that start with dissolution of metastable silica, followed by nano colloidal silica sol formation, gel formation and finally gel swelling after imbibing of water (Rajabipour et al. 2015). Gel swelling causes tensile stresses within the concrete structure which may ultimately lead to concrete cracking that directly affects to the demanded concrete properties such as compressive strength, but also in addition sets the concrete structure more vulnerable to other deterioration processes such as freeze-thaw damage, steel corrosion, and delayed ettringite formation (Thomas et al. 2011; Ferreira & Holt 2013).

AAR has formerly not been critically concerned as a problem in Finnish concrete structures as it has been presumed not being substantial deleterious mechanism around the country. This assumption has relied on local factors such as bedrock consisting mainly of rock types that have traditionally referred as not or weakly reacting in the literature, and low average annual temperatures which fundamentally could fully prevent or drastically decelerate the reaction progress (Lahdensivu et al. 2018). Because this topic has not been actively discussed, there has likely been situational shortage of awareness and knowledge regarding AAR in the industry. It is believed that this may have resulted in false conclusions in investigated damaged concrete structures in Finland, in which the ASR has been confused with other deleterious mechanisms of concrete such as freeze-thaw damage (Ferreira & Holt 2013). Today, ASR has been proven being involved in dozens of cases of damaged concrete structures in Finland, and more detailed national guidance has been provided in by74 published in 2022 (Klami et al. 2022). In this study, 70 % of the samples tested by AMBT and 42 % by petrographical examination were concluded as possibly reactive, which itself substantiate that ASR is viable in Finnish aggregate material and should be carefully considered when assessing aggregate suitability for concrete material.

### 5.1.1 Detected reactive components

In this study, possible alkali-silica reactivity enhancing features within collected rock samples were visually observed both during the field observations at the time of sample collection and microscopically from prepared thin section during petrographical examination. Observed reactive components of both igneous and metamorphic samples were primarily related to signs of intracrystalline strain, weak crystallinity, or exceptionally small grain size of quartz. Microcrystalline and/or strained quartz was identified in each of the investigated samples that were forwarded to accelerated mortar bar test. Myrmekites, quartz intergrowths with plagioclase, that may contain metastable silica that is prone to enhance alkali reactivity of the aggregate were also detected but is not considered here in more detail as it was only present in couple of samples which didn’t show high reactivity in mortar bar test. Thus, it is concluded that the ASR potential of aggregates is not highly affected by the presence of myrmekite. Other silica polymorphs that are generally linked to faster type of alkali-silica reaction such as amorphous silica or high temperature variants tridymite or cristobalite was not detected (Jensen 2012). Significance of observed possibly reactive

characteristics of silica was evaluated by comparing the qualification and quantification results from petrographical examination with measured expansions of accelerated mortar bar test by utilizing statistical analysis tool for detecting correlations and are explained in more detail in chapter 5.1.2. Spearman's correlation coefficient varies between values of 0 and 1 for positive, and values between 0 and -1 for negative correlation. Dependence between variables increase as correlation coefficient increase from 0 to 1 (or -1). Figure 15 shows the relation between the amounts of detected reactive components and expansion. The correlation between observed reactive component content and AMBT expansion is at 14 days is 0.867, and at 28 days 0.744, so both correlations are statistically significant, having strong correlation. In other words, the expansion increases as function of increment in modal content of reactive components in aggregate.

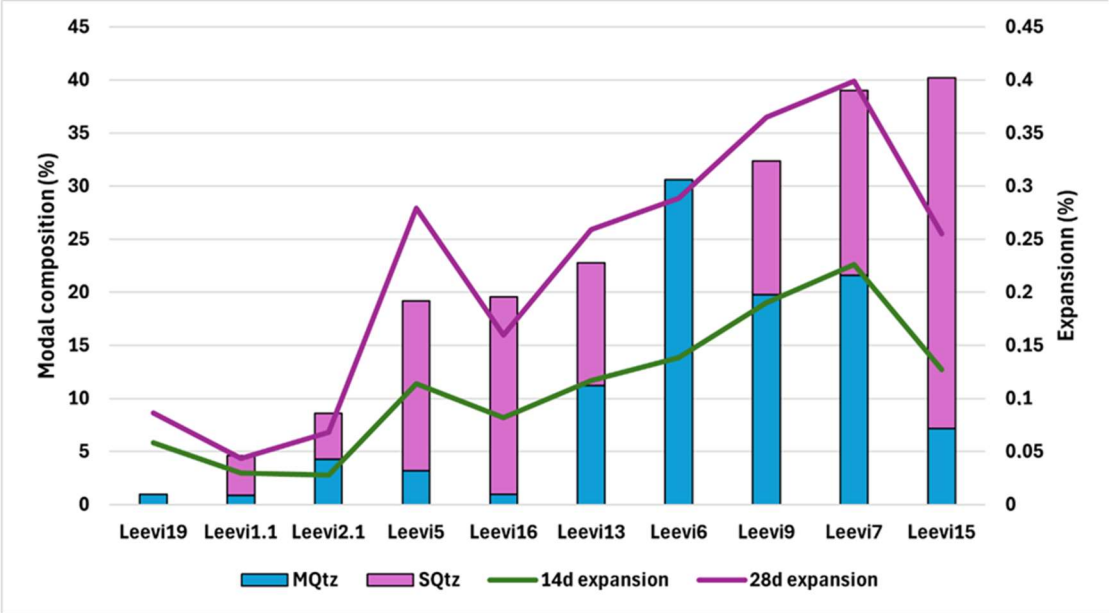


*Figure 19. Relation between modal compositions of potentially reactive forms of quartz and expansions at 14 and 28 days.. SQtz = Strained quartz. MQtz = Microcrystalline/cryptocrystalline quartz.*

### 5.1.2 Significance of field observations

Some of the observations made from the sample in field corresponded well to the known regional geological context, especially for samples that were clearly deformed and foliated in regional deformation. This compatibility between the presumptions of reactivity based on regional geological context and the results of applied assessment methods confirms that it is essential to be aware of broad-scale geological features at the first stages of aggregate assessment. Igneous samples collected from rapakivi

batholith area were presumed not reactive as rock types present in the area are not deformed and mainly plutonic, suggesting well developed crystallinity and absence of metastable silica variants (Fig. 10a, 10b, 10c). The absence of reactive components was confirmed in petrographical examination, and expansions in accelerated mortar bar test were well below the threshold indicating possibly deleterious reactivity. Tampere schist belt and Orijärvi and Kisko areas are known being affected by low grade regional metamorphosis and deformation, which led to initial presumption that reactive rocks are likely abundant in these areas. The most reactive samples based on petrographical examination and accelerated mortar bar test results were collected from these areas (Fig. 11b, 11c, 11e). Sample Leevi13 that was taken from a thin shear joint of otherwise undeformed granite on the other hand proved that relying on regional context can also lead to underestimating the reactivity of rock bodies with heterogeneous structural characteristics; highly localized deformation may sometimes be hardly distinguishable but still increase the overall reactivity of aggregate material extracted. This sample highlights the importance of comprehensive field observations and sample representativity.

Initial estimation regarding sample reactivity in this study was based on field observations from the field (Tables 3 and 4). Field observations gathered from collection sites provided essential first-hand information regarding evaluation of sample representativity and geological context for the alkali-aggregate reactivity assessment procedure. Geological context may refer to information regarding the lithological units and general rock types that are known to exist within the area, characteristics of regional metamorphism and deformation, structural information about faults, joints and thrust plates or glacial/fluvial processes that have transported local aggregate material. This piece of information is likely to help approaching the aggregate assessment when broad scale factors that may affect the aggregate reactivity are acknowledged (Sims & Nixon 2003b). Existing aggregate sources such as sand/gravel pits or excavated rock walls are especially beneficial as it allows fast and efficient mapping of aggregate source both vertically and laterally, from which the constituent rock types, structural characteristics and geological discontinuities can be more easily determined. This was the case with samples Leevi1.1 (Fig. 10a), Leevi12 (Fig. 10h) and Leevi14.1 (Fig. 11i). From these observations, special attention should be given to geological or petrographical features that are related to the presence and

distribution of potentially reactive rock material. Constructed model of the rock body or sand/gravel deposit may then be utilized as the basis for proper, representative aggregate sampling plan (Fournier & Bérubé 2000).

However, samples in this study were either detached fragments from small outcrops or individual separate boulders (Fig. 10 and 11), from which satisfactory larger scale bedrock features at collection sites could not be comprehensively described. This means that sample representativity was limited only to the collected sample itself, whereas the reactivity results cannot be used for evaluating the overall reactivity of local rock material at collection sites without a high level of uncertainty. The most evident sign of enhanced reactivity within studied samples was features of shear and foliation, which were especially abundant in samples gathered from Orijärvi and Kisko areas (Fig. 11a, 11b, 11c, 11d, 11e) and sheared granite Leevi13 from Paimio (Fig. 10e). It was concluded that proper assessment of the alkali-silica reactivity of investigated samples required distinguishing and quantifying the reactive components in more detail with microscopical instruments. This was because alkali-silica reactivity is associated with certain polymorphs and microstructural characteristics of silica of which presence and distribution was not reliably observable with unaided eye. Field observations themselves thus cannot be used for conclusive determination of material suitability for concrete in terms of ASR potential, but instead, consistent, and generally accepted assessment methods should be applied of which the petrographical examination is typically the preferred first-hand testing method.

### 5.1.3 Relation between petrographical examination and accelerated mortar bar test

Statistically significant correlation between modal content of reactive components and AMBT expansion together with conclusion of nine out of ten samples resulting in same reactivity class, petrographical examination and accelerated mortar bar are considered well comparable test methods for assessing aggregate alkali-silica reactivity. Determining the reactivity classes for investigated samples was based on thresholds provided in RILEM recommendations AAR-1 for petrographical examination and AAR-2 for accelerated mortar bar test (Sims & Nixon 2003a). Nine of the ten samples resulted in equivalent reactivity class for both testing methods (Table 11). Sample

Leevi7 resulted in likely reactive class III after petrographical examination, whereas AMBT resulted in possibly reactive class II.

*Table 11. Determined reactivity classes from petrographical examination and accelerated mortar bar tests for specific samples.*

| Sample | Petrographical examination reactivity class | AMBT Reactivity class |
|---|---|---|
| Leevi1.1 | Class I | Class I |
| Leevi2.1 | Class I | Class I |
| Leevi5 | Class II | Class II |
| Leevi6 | Class II | Class II |
| Leevi7 | Class III | Class II |
| Leevi9 | Class II | Class II |
| Leevi13 | Class II | Class II |
| Leevi15 | Class II | Class II |
| Leevi16 | Class II | Class II |
| Leevi19 | Class I | Class I |

Inconvenience regarding petrographical examination is the challenge of visually distinguishing the slowly reactive quartz phases, especially for strained quartz which may need additional equipment such as TEM in addition to polarization microscope for better detection (Tiecher et al. 2017). Expertise of petrographer plays a major role for correct assessment results. AMBT on the other hand has been noticed being oversevere in some cases, giving more pessimistic results than actual field performance of concrete structure (Thomas et al. 1997), and in some cases, has failed to detect the reactivity of tested aggregates (Wigum & French 1996). Despite these inconveniences, these two methods are largely favored as they are swift and relatively cheap testing methods, and thus they have their place in ASR assessment. Based on results of this study, petrographical examination and AMBT are good assessing methods for assessing Finnish aggregate material, but it is suggested that they are not considered as exclusive. In case aggregate fails to meet the demands in terms of alkali-silica reactivity, further and more reliable assessing methods such as concrete prism test should be carried.

When comparing the fundamental differences between petrographical examination and accelerated mortar bar testing methods, the most significant difference is that AMBT is a performance test in which the reactivity of assessed material is tested practically and evaluated based on expansion measurements caused by actual ASR, whereas petrographical examination results are based on subjective observations of petrographer. Petrographical examination is often conducted with polarization microscope, and thus the expertise of petrographer is essential for distinguishing possibly reactive forms and microstructures of silica from innocuous. It has also been demonstrated that in some cases traditional polarization microscope is insufficient to identify the presence and distribution of potentially reactive components. This is why sometimes complementary methods such as SEM, X-ray diffraction, image analysis, infrared spectroscopy, microprobe analysis or bulk chemical analysis are used for better identification of potentially reactive constituents in aggregates. Sometimes it might be taken for granted that in case of possible alkali-silica reactive aggregate after petrographical examination, next step in assessment is accelerated mortar bar test. This presumption is false as it has been shown that for some rock types, accelerated mortar bar test has failed to detect the potential alkali-reactivity, and for these certain rocks, other recommended testing methods such as concrete prism test should be applied. Thus, petrographical examination additionally serves as essential tool for choosing the right performance test when needed (Fournier & Bérubé 2000).

### 5.1.4 AMBT results versus field performance of concrete structures

There are many different performance test methods available for determining the aggregate alkali-reactivity potential, of which accelerated mortar bar test is globally widely used. The advantage in AMBT over many other performance testing methods is it low cost and swiftness, in which the results can be obtained within timeframe of weeks. According to Thomas et al. (1997), accelerated mortar bar test has been noticed overly severe, identifying many aggregates as reactive despite their good field performance. Due to this, accelerated mortar bar test is usually considered as only accepting and not rejecting testing method, meaning that in case of aggregate failing the test, more reliable testing method such as concrete prism test should be used to make the final conclusion about aggregate suitability as concrete ingredient.

Main challenges regarding developing accurate and reliable ASR performance testing methods are essentially linked to fact that concrete industry is favouring test methods that are inexpensive and rapid (Lindgård et al. 2012). None of the currently available and applied test methods can fulfil all the criteria for ideal test method, including the swiftness, reliability, and capability to determine the influence of aggregate reactivity, alkali availability and exposure conditions (Thomas et al. 2006). AMBT is a performance test that accelerates the alkali-silica reaction by elevating the storage temperature and humidity meaning that storage conditions differ substantially from the prevailing conditions the actual concrete structure is exposed to. This setup is contradictory in a sense that performance test should correspond the field performance of concrete structure typically for more than 50 years of exposure to the surrounding outdoor environment. Another important perspective is that concrete composition should represent the actual designed concrete mixture. Mortar bar testing includes crushing of aggregate material into more finer grain size, which may alter the reactivity behaviour of rock material. In addition to used aggregate material, binder type will also affect the alkalinity of pore solution (Tapas et al. 2021). Thomas et al. (2006) state that only way to reliably benchmark the performance tests is against real concrete structures, or alternatively against other kind of larger concrete blocks that are exposed to outdoor weathering conditions.

Comprehensive study that demonstrates the correlation between long-term field performance of concrete structure and laboratory testing methods has yet not been accomplished (Bergmann et al. 2023). Extensive data of outdoor exposure has been gathered as part of the European “PARTNER” project, in which several aggregate assessment methods were evaluated by comparing laboratory test results and field performance of specimens prepared from thirteen different aggregates that covered most types of known reactive aggregate types in Europe (Borchers et al. 2022). As a conclusion, AMBT was able to reliably differentiate the non- and highly reactive aggregates, whereas it showed variance in ability to moderately reactive aggregates. Concrete prism test was suggested as best testing methods for moderately reactive aggregates. Wigum and French (1996) also stated that AMBT appears to echo the alkali-aggregate reaction occurring in concrete structures in the field but noticed that test method has limitations regarding the field performance when aggregate material particle size is coarser and reaction rate slow. In these slow reacting aggregates, the

total expansion takes significantly more time but may eventually proceed to more deleterious level than AMBT would suggest. Thus, Wigum and French (1996) suggested that for slow type of aggregates, increasing the time period of expansion measurements would give more accurate results in terms of field performance.

## 5.2 Significance of detected potentially reactive components

The relative significance of possibly reactive components, microcrystalline and strained quartz, was evaluated based on comparing the petrographical examination results and accelerated mortar bar test expansions statistically and reflecting this information to literature and research work presented by other authors. Figure 20 illustrates the relationship between the modal compositions of different quartz classes and corresponding expansions measured at 14 and 28 days. Three separate groups can be distinguished; 1) the least expanded mortar bars dominated by unstrained quartz, 2) moderately expanded mortar bars dominated by strained quartz and 3) the most expanded mortar bars dominated by micro-/cryptocrystalline quartz. Aggregates consisting mainly of unstrained quartz (Leevi1.1, Leevi2.1, Leevi19) were all classified as unlikely reactive according to AMBT results, whereas aggregates consisting of predominantly microcrystalline or cryptocrystalline quartz (Leevi6, Leevi7, Leevi 9) were all included in possibly reactive class. Aggregates dominated by strained quartz (Leevi5, Leevi13, Leevi15, Leevi16) were also included in possibly reactive class after AMBT. Correlation coefficient between unstrained quartz and mortar bar expansion is -0.778 at 14 days, and -0.863 at 28 days, suggesting strong negative correlation where expansion decreases as function of increasing unstrained quartz content. This does not mean that less unstrained quartz will lead to more expansion, but quartz within these samples is mainly microcrystalline or strained which shows up as negative correlation for unstrained quartz. Correlation was statistically significant between the microcrystalline quartz content and both expansions at 14 and 28 days with positive correlation coefficient of 0.827, indicating strong correlation in which reactivity increases as function of increment in the content of microcrystalline quartz. Correlation coefficient between the amount of strained quartz and expansion at 14 days is 0.353, and at 28 days 0.292, suggesting statistically insignificant, low correlation (figure 23).

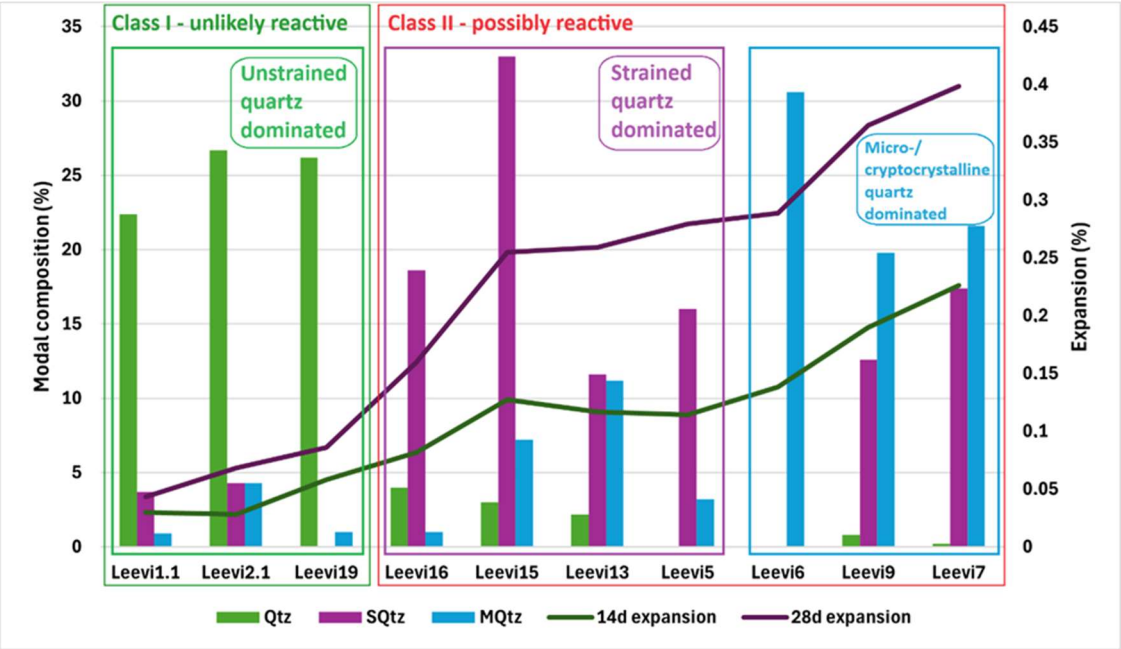


*Figure 20. Picture representing the relation between predominant quartz class and mortar bar expansion. Unstrained quartz dominates in least expanded mortar bars, whereas highest expansion occurs in mortar bars dominated by micro-/cryptocrystalline quartz. Strained quartz dominates in the middle of the least and most expanded mortar bars. 3 samples included in unlikely reactive class I and 8 samples in possibly reactive class II according to AMBT results. Qtz = Unstrained quartz. SQtz = Strained quartz. MQtz = Microcrystalline/cryptocrystalline quartz.*

### 5.2.1 Microcrystalline quartz

Strong correlation between the modal content of microcrystalline quartz and AMBT expansion suggests microcrystalline quartz being an essential factor for ASR development (Figure 21). Correlation also suggests that applied qualification method of setting the grain size of <0.1 mm as threshold to consider grain as reactive is well suitable for assessing alkali-silica reactivity in petrographical examination. Microcrystalline quartz has formerly been demonstrated being closely connected to alkali-reactivity of aggregates in literature, increasing the available surface area and allowing the interaction between alkali-silica reactants (eg. Jensen 2012; Grattan-Bellew 1992). Samples dominated by the presence of microcrystalline quartz did show relatively larger expansions compared to samples dominated by strained quartz, thus it seems that microcrystalline quartz develops alkali-silica reaction more rapidly than strained quartz. It is important to note that this considers only the rate of ASR within the timeframe of AMBT, but the final extent of reaction cannot be evaluated as expansions were measured over a short period of time; it is possible that strained quartz would ultimately result in equal expansion when given sufficient time due to its slow behaviour as stated by Velasco-Torres et al. (2010).

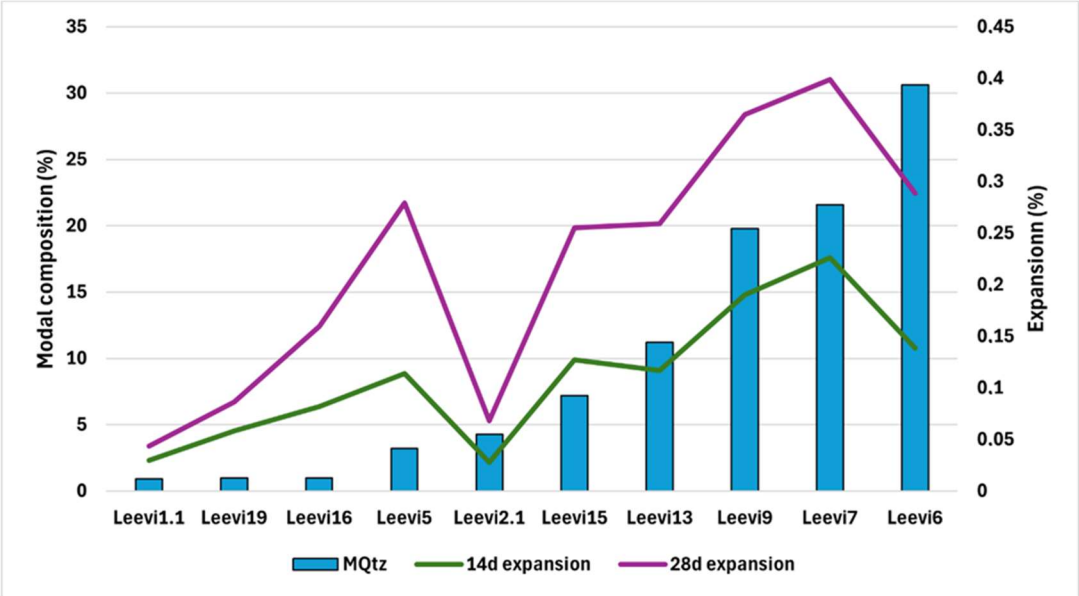


*Figure 21. Relation between the modal content of micro-/cryptocrystalline quartz and mortar bar expansion.*

When comparing the microcrystalline quartz dominated samples Leevi6, Leevi9, and Leevi7 in more detail, the level of crystallinity may also be a controlling factor in ASR development for microcrystalline quartz. Phyllite sample Leevi6 showed relatively good crystallinity, whereas in metavolcanite Leevi7, crystallinity was weaker, and in schist sample Leevi9, the least well-developed. Corresponding expansions were lower in sample Leevi6 with better crystallinity even though the microcrystalline content was highest, increasing towards the least crystallinity sample Leevi9 (Figure 22). This suggests that ASR potential in quartz seems to be highest in fine-grained, recrystallized quartz-rich felsic rocks which have deformed in low metamorphic facies. This conclusion is congruent with the results of Šachlová (2013), who described that low grain size together with low degree deformation and low temperature recrystallization that leads to formation of quartz with low crystallinity, is very prone to ASR. However, for these samples in this study, higher expansions can also be due to presence of strained quartz in samples Leevi7 and Leevi9, so this cannot be unambiguously concluded.

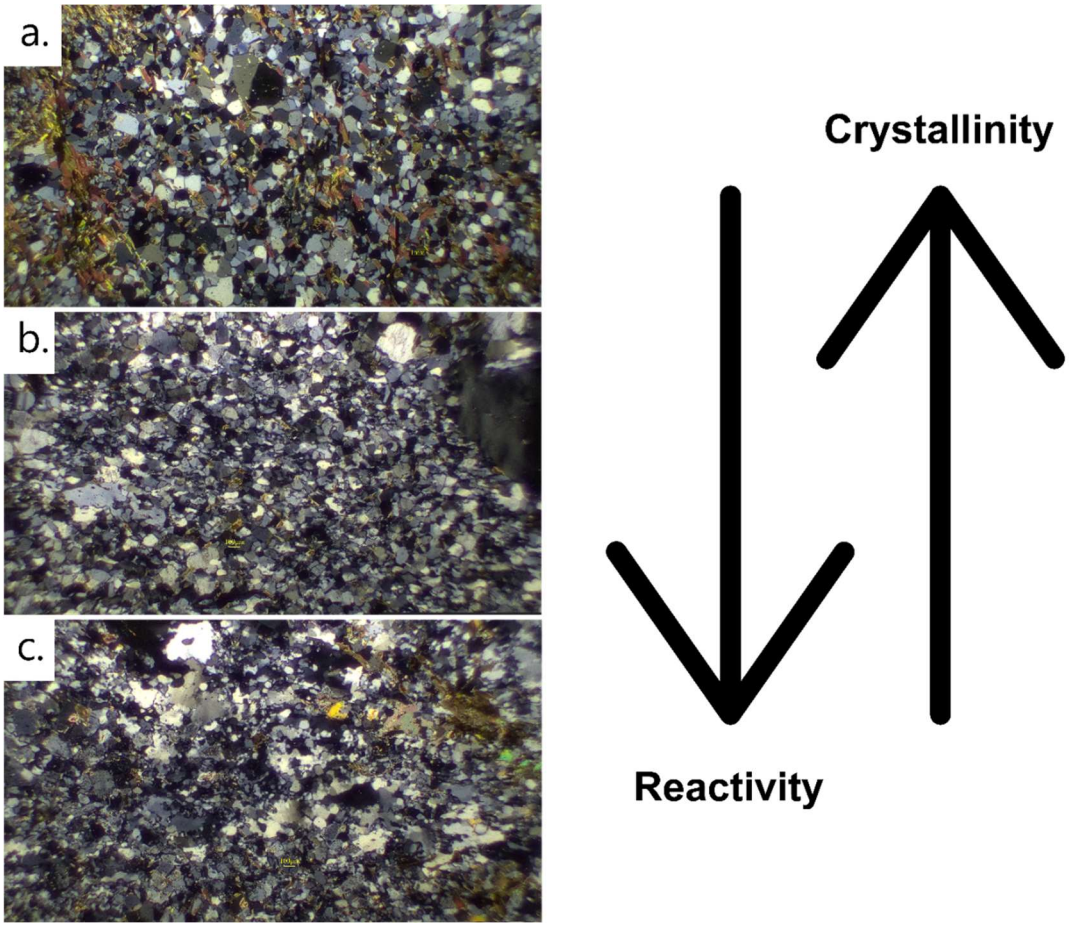


*Figure 22. The reactivity potential differences between samples dominated by microcrystalline quartz Leevi6 (a), Leevi9 (b) and Leevi7 (c) corresponded well to the observed general level of crystallinity of quartz. Size of the thin sections 2 x 3 mm.*

When quantifying microcrystalline quartz from thin section, it is important to know that the measuring of grain size may sometimes be ambiguous and lead to overestimation in the amount of microcrystalline quartz grains. This is due to thin section essentially being a random planar cross-section of the rock, in which the visible mineral crystals are arbitrary cut across. This means that the measured diameter in thin section represents always at least, but not necessarily the actual largest diameter of the grain. Because the crosscut is unlikely to travel along the actual largest diameter of the crystal, diameter measurements tend to be underestimated. It is likely that at least in undeformed granite samples Leevi1.1, Leevi2.1, Leevi3.1 and Leevi19, this phenomenon is mainly responsible for observed “microcrystalline” quartz grains as these samples showed very little reactivity according to expansions in accelerated mortar bar test results.

### 5.2.2 Strained quartz

Statistical analysis showed low and insignificant correlation between the modal content of strained quartz and AMBT expansions. Despite bad statistical correlation, strained quartz has been shown being linked to ASR development based on other research work (eg. Velasco-Torres et al. 2010; Jensen 2012; Trägårdh et al. 2013), and this result more likely points out the difficulty in qualificating and quantificating strained quartz from thin section with polarization microscope. Strained quartz has previously also noticed leading to slower and less extensive expansion in AMBT due to concrete pore solution entering relatively slower to reaction sites of reactive quartz when compared with microcrystalline quartz (Broekmans 2004; Velasco-Torres et al. 2010). This may lead to differences in reaction rates between the samples, and expansions at 14 and 28 days in AMBT may vary due to reactions being at different stages between the samples. Thus, it is suggested that the time period for measuring the expansion in AMBT should be prolonged for samples dominated by strained quartz.

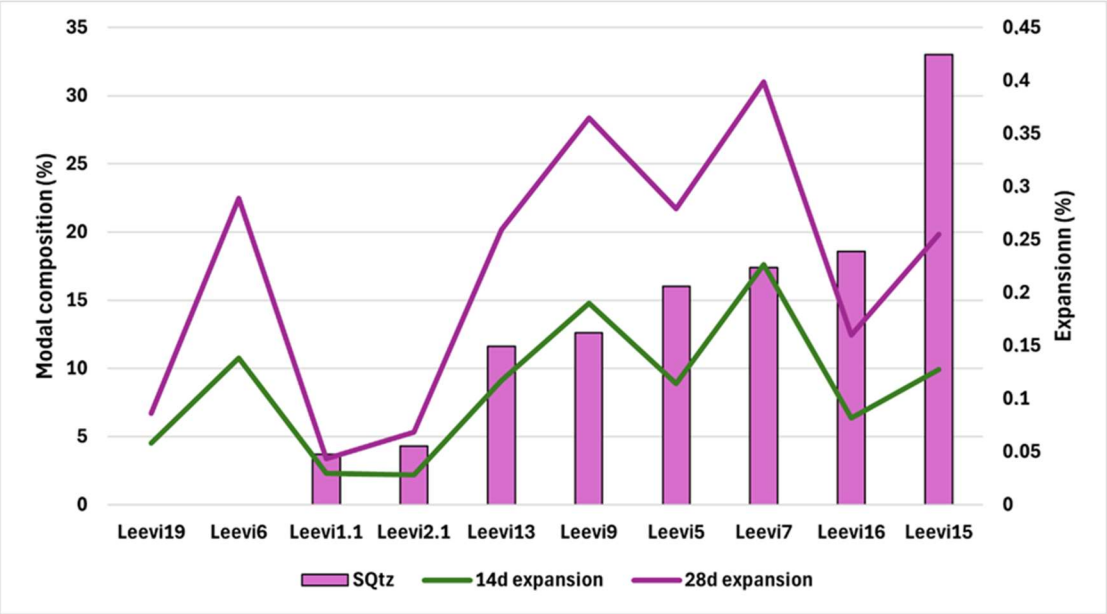


*Figure 23. Relation between the modal content of strained quartz and mortar bar expansion.*

A method for estimating the strain within the aggregate is to measure undulatory extinction angle, introduced by Dolar-Mantuani (1981). Undulatory extinction is one of the most evident features of crystalline strain. Correlation between measured undulatory extinction angle averages and expansion for both 14 and 28 days was statistically significant with coefficient of 0.767, indicating good correlation (Figure

24). Undulatory extinction angle averages varied between 1.0-26.0 degrees with average of 10.1 degrees for unlikely reactive aggregates according to AMBT results. Highest angles were measured from strongly deformed samples gathered from Orijärvi area (Leevi4.1, Leevi5) in which the mineralogical modal composition was mainly composed more of strained quartz (Table 8). Despite good correlation, due to factors such as grain size, shape and texture which will affect the measurement results of the undulatory extinction angle, it is not suggested to set thresholds for the angle which determines the reactivity class such as ones provided by Dolar-Mantuani (1981). It is stated in recommendation AAR-1 that undulatory extinction angles measurement should not be used as measurement of reactivity or even measured during petrographical examination. In this study, quartz grains with relatively equal size were picked for measurements with intention to eliminate these effects, which partly explains the good correlation of angle measurements between the samples. As opposed to AAR-1 recommendation, based on good correlation, undulatory extinction angle is considered as good tool for estimating the quartz strain and can be used to assist in petrographical assessment. However, it should not be used to deterministically evaluate the reactivity class.

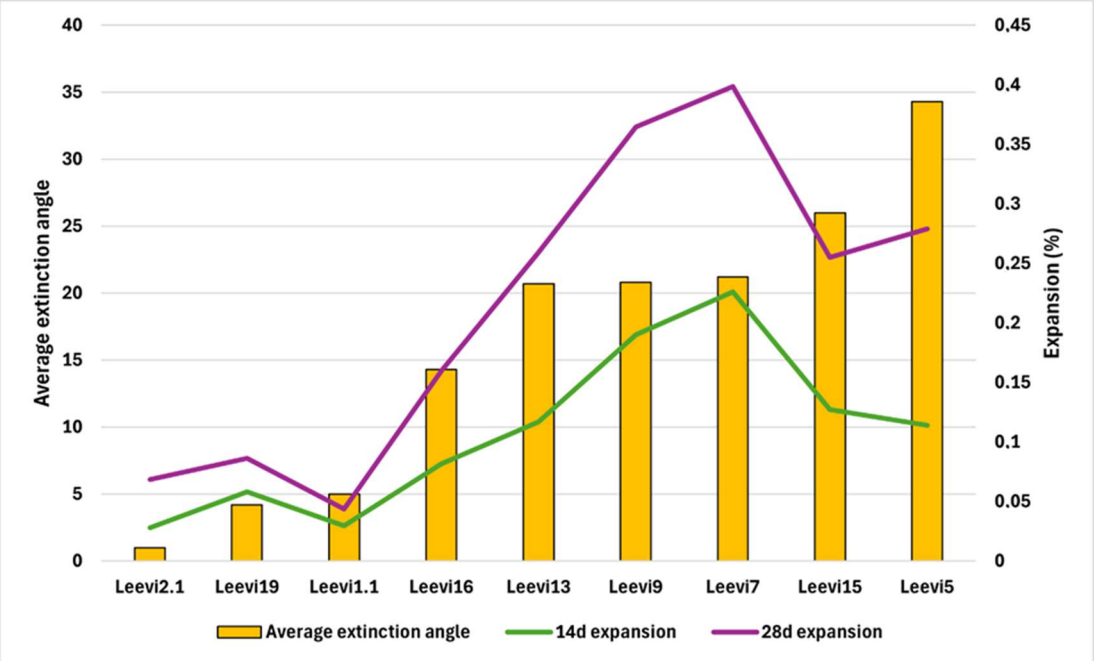


*Figure 24. Graph showing the relation between the expansion and measured average extinction angles.*

Determination of quartz as strained is based on occurrence of various visible signs of deformation such as undulatory extinction, irregular grain shape and grain boundaries,

fluid inclusions and deformation lamellae. Where the determination of microcrystalline quartz is fundamentally more straightforward based on measuring the grain diameter, determination of strained quartz seems to be ambiguous. It is often hard to determine the level and intensity of signs of deformation at which point the observed grain should be considered strained enough to potentially enhance alkali-silica reactivity, and this decision is based on subjective opinion of petrographer. Less correlation may also refer to that the reactivity of strained quartz is, in addition to imperfections in crystal lattice quality causing the intracrystalline strain, also dependent on its grain size. Because grain size is essential factor allowing the access of alkalis to reaction site within aggregate particles, large grain size may slow down or even prevent the reaction as reactants are not able to reach out and interact (Broekmans 2004). This would also explain why the rate and extent of ASR was relatively lower in samples dominated by strained quartz compared to samples dominated by microcrystalline quartz, as well as why trained quartz is generally described being involved in slow type of ASR (Jensen 2012). Currently there is no detailed research work completed that could comprehensively explain the qualification and quantification procedure for strained quartz optically based on polarization microscope analysis, and results regarding the significance of different strained features to quartz reactivity are somewhat incoherent. Because assessing strained features solely on polarization microscope is challenging, other instruments may offer substantial help in assessing the reactivity of strained quartz in petrographical examination. For example, Tiecher et al. (2017) managed to distinguish quartz structural factors that are associated with alkali-silica reaction development by utilizing transmission electron microscopy (TEM). With TEM it was possible to detect the presence of walls of metastable silica to better distinguish reactivity enhancing features in strained quartz grains.

## 5.3 Implications

To ensure successful aggregate assessment, testing laboratories should invest in offering comprehensive test services that include the testing procedure all the way from aggregate sampling at the site of aggregate source to final test results of either petrographical examination or selected performance test. An experienced petrographer should visit the aggregate material source to ensure representative sampling. This is especially important for quarries in which the bedrock is heterogeneous and thus reactivity may vary in different parts of the rock body.

This study suggests microcrystalline and strained quartz being most responsible factors increasing the alkali-silica reactivity in Finnish rock material. Correlation for microcrystalline quartz was strong, whereas correlation for strained quartz was not statistically significant. Correlation of total modal content of reactive components between petrographical examination and expansions in AMBT indicates that these metastable characteristics of quartz are possible to reliably identify utilizing petrographical method. Petrographers in Finland should have training in ASR assessment due to strong subjective influence on assessment results of petrographical examination, with focus on detecting the most significant components introduced in this study. Results are congruent with research work conducted in Sweden, which concluded microcrystalline and strained quartz as essential cause of ASR development in local rock material (Trägårdh et al. 2013). The necessity of other instruments alongside with polarization microscope for successful petrographical examination should be evaluated more in the future since based on results of this study, at least strained features of quartz might not be clearly distinguishable solely with polarization microscope.

Ambiguities regarding AMBT performance for Finnish rock material should be dealt with more research work mirroring the AMBT results and actual structure performance in nature. This development work would be best conducted together with other Fennoscandian countries due to similar bedrock and climatic features that should give comparative results, which could result in mutual, systematic assessment procedure of ASR between Fennoscandian countries. Special note should be focused on ASR development differences between microcrystalline and strained quartz based on results of this study and similar results from Sweden (Trägårdh et al 2013). Finally,

applicability of AMBT should be critically evaluated as it has been shown having ambiguities regarding detecting metastable phases of quartz. This need lots of collaborative research work between Nordic laboratories and testing with various rock types for comprehensive results. Based on this study, special attention should be paid to reactivity behaviour of strained quartz of which correlation was relatively poor between the results of petrographical examination and AMBT. Another consideration regarding AMBT is to test out the performance of aggregates together with other binder types. As concrete industry is currently moving forward in using substitutive binder types that replace traditional cement such as blast furnace slag and fly ash due to environmental ambitions, the concrete mix designs are constantly developing into less cementitious. This trend should also be reflected to performance tests as it is known that certain substitutive binders will affect the ASR development in concrete (Tapas et al. 2021).

# 6 Conclusions

- Understanding regional geological context provides essential first-hand information regarding the ASR potential of assessed aggregate material.

- Results from petrographical examination and accelerated mortar bar tests conducted according to RILEM's recommendations are consistent based on test results in this study, and thus these testing methods are considered well comparative.

- Main reactive components affecting alkali-silica reactivity of investigated samples were related to microcrystalline and strained features of quartz. Modal content of microcrystalline quartz had better correlation with AMBT expansions in contrast to modal content of strained quartz which is presumably due to difficulties regarding distinguishing reactive strained quartz from thin section and possibly relatively slower reaction rate of strained quartz in AMBT.

- Microcrystalline and strained quartz are generally connected to more slow type of alkali-silica reaction in which the reaction development and reaching the level that causes deleterious damage in concrete structures take typically more than ten years. Detected reactive components support the general

understanding of Finnish bedrock consisting mainly of rocks with relatively low or slow alkali-silica reactivity.

- Results indicating possible reactivity from petrographical examination or accelerated mortar bar test are not suggested to regard as conclusive whereby assessed aggregate should be rejected. Both test methods are ambiguous in terms of their reliability for detecting reactive components associated to slow type ASR. Petrographical examination disadvantages concern the inability to distinguish all reactive components and human error due to subjective qualification of reactive components, whereas accelerated mortar bar test has been noticed sometimes giving oversevere results and sometimes failing to identify reactive aggregates.

- Suitability of AMBT in assessing ASR of typical Fennoscandian rocks should be addressed by conducting more comparative studies between AMBT results and actual field performance of concrete in which the same aggregate material has been used. These studies would be best to conduct with other Fennoscandian countries for constructing mutual, systematic ASR assessment procedures for Fennoscandian countries that use similar aggregate material in concrete industry.

- Finnish petrographers should have more training in petrographical examination regarding ASR, focusing on distinguishing possibly reactive components introduced in this study.

# 7 Acknowledgements

Many thanks to my supervisor professor Esa Heilimo, firstly willing to accept to supervise this applied study, and secondly keeping me on the track throughout the writing process. Thanks to Kymppibetoni Oy for financial assistance, allowing to complete this study as it is, and Mitta Oy for preparing and conducting the accelerated mortar bar tests. Thanks to technician Arto Peltola for preparing the thin sections from rock samples. Lastly, thank you for family and friends, especially my wife for infinite support.

# 8 References

**Alaejos, P., Lanza, V., Bermudez, M.A., Velasco, A. 2014:** Effectiveness of the accelerated mortar bar test to detect rapid reactive aggregates (including their pessimum content) and slowly reactive aggregates. *Cement and Concrete Research*, 58, 13-19.

**Batic, O., Maiza P., Sota, J. 1994:** Alkali silica reaction in basaltic rocks – NBRI method. Cement and Concrete Research, 24(7), pp. 1317-1326.

**Bergmann, A., Medeiros, R., Sanchez, L. 2023:** The efficiency of laboratory test procedures for assessing field performance of concrete against alkali-aggregate reaction (AAR). *In:* Biondini, F., & Frangopol, D.M. (Eds.), Life-Cycle of Structures and Infrastructure Systems: Proceedings of the eighth international symposium on life-cycle civil engineering, CRC Press, Milan, Italy, 2211-2218.

**Borchers, I., Lindgård, J., Müller, C., 2022:** Evaluation of laboratory test methods for assessing the alkali-reactivity potential of aggregates by field site tests. *Materiales De Construcción*, 72(346), 10 pp.

**Broekmans M.A.T.M. 2004:** Structural properties of quartz and their potential role for ASR. *Materials Characterization*, 53, 129-140.

**Çopuroğlu, O., Andiç-Çakir, Ö., Broekmans, M.A.T.M., Kühnel, R. 2009:** Mineralogy, geochemistry and expansion testing of an alkali-reactive basalt from western Anatolia, Turkey. *Materials Characterization*, 60(7). 756-766.

**Dolar-Mantuani, L.M.M. 1981:** Undulatory extinction in quartz used for identifying potentially alkali-reactive rocks. *In:* Oberholster, R.E. (Ed.), *5th International Conference on Alkali-Aggregate Reaction in Concrete*, Cape Town, South Africa, pp. 1-6.

**Fernandes, I., Broekmans, M.A.T.M., Nixon, P., Sims, I., Ribeiro, M.A., Noronha, F., Wigum, B. 2012:** Alkali-silica reactivity of some common rock types – A Global petrographic atlas. *In:* Drimalas T., Ideker J.H., Fournier B. (Eds.), *14th International Conference on Alkali-Aggregate Reactions in Concrete*, Austin, Texas, USA, 10 pp.

**Ferreira, M. & Holt, E. 2013:** Addressing ASR in concrete construction in Finland. Nordic – Baltic mini seminar, alkali aggregate reactions (AAR) in concrete, Riga, Latvia, 15.

**Figueira, R.B., Sousa, R., Coelho, L., Azenha, M., de Almeida, J.M., Jorge, P.A.S., Silva, C.J.R. 2019:** Alkali-silica reaction in concrete: Mechanisms, mitigation and test methods. *Construction and Building Materials*, 222, 903-931.

**Fournier, B., Bérubé, M.A. 2000:** Alkali-aggregate reaction in concrete: A review of basic concepts and engineering implications. *Canadian Journal of Civil engineering*, 27, 167-191.

**Gillott, J.E. 1964:** Mechanism and kinetics of expansion in the alkali-carbonate rock reaction. *Canadian Journal of Earth Science*, 1(2), pp. 121-145.

**Gillott, J.E., Duncan M.A.G., Swenson, E.G. 1973:** Alkali-aggregate reaction in nova Scotia IV. Character of the reaction. *Cement and Concrete Research*, 3(5), 521-535.

**Grattan-Bellew, P.E. 1992:** Microcrystalline quartz, undulatory extinction & the alkali-silica reaction. *In: 9th International Conference on Alkali-Aggregate reaction*, London, England, 383-394.

**Ideker, J.H., Bentivegna, A.F., Folliard, K.J., Juenger, M.C.G. 2012:** Do current laboratory test methods accurately predict alkali silica reactivity?. *ACI Materials Journal*, 109(4), 395-402.

**Jensen, V., 2012:** Reclassification of alkali aggregate reaction. *In:* Drimalas T., Ideker J.H., Fournier B. (Eds.) *14th International Conference on Alkali-Aggregate Reactions in Concrete*, Austin, Texas, USA, pp. 10.

**Katayama, T., St John, D.A., Futagawa, T. 1989:** The petrographic comparison of some volcanic rocks from Japan and New Zealand – Potential reactivity related to interstitial glass and silica minerals. *In:* Okada, K., Nishibayashi, S., Kawamura, M. (Eds.) *Proceeding of the 8th International Conference on Alkali-Aggregate Reaction in Concrete*, Kyoto, Japan, pp. 537-542.

**Katayama, T. 1997:** Petrography of alkali-aggregate reactions in concrete – reactive minerals and reation products. *Proceedings of East Asia Alkali-Aggregate Reaction Seminar*, Tottori, Japan, pp. 45-59.

**Katayama, T. 2010:** The so-called alkali-carbonate reaction (ACR) – Its mineralogical and geochemical details, with special reference to ASR. *Cement and Concrete Research*, 40, 643-675.

**Klami, J., Lahdensivu, J., Pyy, H. 2022:** *Ohje Betonin Alkali-kiviainesreaktion Hallitsemiseksi 2022 by74*. Suomen Betoniyhdistys ry, 49 pp.

**Korsman, K., Koistinen, T. 1998:** Suomen kallioperän yleispiirteet. *In:* Lehtinen, M., Nurmi, P., Rämö, T. (Eds.), *Suomen kallioperä – 3 000 vuosimiljoonaa*, Suomen Geologinen Seura ry, Helsinki, pp. 93-104.

**Šachlová, S. 2013:** Microstructure parameters affecting alkali-silica reactivity of aggregates. *Construction and Building Materials*, 49, 604-610.

**Lahdensivu, J. Kekäläinen, P., Lahdensivu, A., 2018:** Alkali-silica reaction in Finnish concrete structures. *Nordic Concrete Research*, No. NCR 59(2), pp. 31-44

**Larrea, M.L, Castro, S.M., Bjerg, E.A. 2013:** A software solution for point counting. Petrographic thin section analysis as a case study. *Arabian Journal of Geosciences*, 7(8), 2981-2989.

**Leemann, A., Katayama, T., Fernandes, I., Broekmans, M.A.T.M. 2016:** Types of alkali-aggregate reactions and the products formed. *Construction Materials*, 169(3), 128-135.

**Lindberg, B., Bergman, L. 1993:** Vehmaan kartta-alueen kallioperä. Summary: Pre-Quarternary rocks of the Vehmaa map-sheet area. Geological map of Finland 1:100

000. Explanation to the maps of Pre-Quarternary rocks, Sheet 1042. Geological Survey of Finland, Espoo, 1-56.

**Lindgård, J., Nixon, P.J., Borchers, I., Schouenborg, B., Wigum, B.J., Haugen, M., Åkesson, U. 2010:** The EU "PARTNER" project – European standard tests to prevent alkali reaction in aggregates: Final results and recommendations. *Cement and Concrete Research*, 40, 611-635.

**Lindgård, J., Andiç-Çakır, Ö., Fernandes, I., Rønning, T.F., Thomas, M.D.A. 2012:** Alkali–silica reactions (ASR): Literature review on parameters influencing laboratory performance testing. *Cement and Concrete Research*, 42(2), 223-243.

**Lindgård, J., Grelk, B., Wigum, B., Trägårdh, J., Appelqvist, K., Holt, E., Ferreira, M., Leivo, M. 2018:** Nordic Europe. *In:* Sims, I. & Pole, A. (Eds.), *Alkali-aggregate reaction in concrete – A world review*. CRC Press, London, 804 p.

**Lonka, H., Schulmann, K., Venera, Z. 1998:** Ductile deformation of tonalite in the Suomusjärvi shear zone, south-western Finland. *Journal of Structural Geology*, 20(6), 783-798.

**Lopez-Buendia, A.M., Climent, V., Mar Uriquiola, M., Bastida, J. 2008**: Influence of dolomite stability on alkali-carbonate reaction. *In:* Broekmans M.A.T.M & Wigum, B.J. (Eds.), *Proceedings of the 13th International Conference on Alkali-Aggregate Reaction in Concrete*, Trondheim, Norway, pp. 10.

**Maraghechi, H. 2014:** Development and assessment of alkali-activated recycled glass-based concretes for civil infrastructure. College of Engineering, The Pennsylvania State University, 191 pp.

**Oberholster, R.E., Davies G. 1986:** An accelerated method for testing the potential alkali reactivity of siliceous aggregates, *Cement and Concrete Research*, 16, pp. 181-189.

**Passchier, C.W., Trouw, R.A.J. 1998:** *Microtectonics*. Springer, Berlin, Germany, 289 pp.

**Ponce, J.M., Batic, O.R. 2006:** Different manifestations of the alkali-silica reaction in concrete according to the reaction kinetics of the reactive aggregate. *Cement and Concrete Research*, 36(6), 1148-1156.

**Poole, A.B. 1992:** Introduction to alkali-aggregate reaction in concrete. *In:* R. N. Swamy (Ed.), *The Alkali Silica Reaction in Concrete*, Van Nostrand Reinhold, New York, 1-28.

**Rajabipour, F., Giannini, E., Dunant, C., Ideker, J.H., Thomas M.D.A. 2015:** Alkali-silica reaction: Current understanding of the reaction mechanism and the knowledge gaps. *Cement and Concrete Research*, 76, 130-146.

**Rämö, O.T., Haapala, I., 2005:** Rapakivi granites. *In:* Lehtinen, M., Nurmi, RA., Rämö, O.T. (Eds.), *Precambrian Geology of Finland – Key to the Evolution of the Fennoscandian Shield*, Elsevier B.V., Amsterdam, pp. 533-562.

**Šachlová, S. 2013:** Microstructure parameters affecting alkali-silica reactivity of aggregates. *Construction and Building Materials*, 49, 604-610.

**Scott IV, H.C. 2006:** Mitigating alkali silicate reaction in recycled concrete, Civil and environmental engineering, University of New Hampshire, 148 pp.

**Shayan, A. 2007:** Field evidence for inability of ASTM C-1260 limits to detect slowly reactive Australian aggregates. *Australian Journal of Civil Engineering*, 3(1), 13-26.

**Shayan, A. & Quick, G.W. 1994:** Alkali-aggregate reaction in concrete railway sleepers from Finland. *In:* 16th International Conference on Cement Microscopy, Richmond, USA, 69–79.

**Schmid, R., Fettes, D., Harte, B., Davis, E., Desmons, J., 2007:** A systematic nomenclature for metamorphic rocks: 1. How to name a metamorphic rock. Recommendations by the IUGS subcommission on the systematics of metamorphic rocks: Web version 01/02/07, 22.

**Sims, I., Nixon, P. 2003a:** RILEM recommended test method AAR-0: Detection of alkali-reactivity potential in concrete – Outline guide to the use of RILEM methods in assessments of aggregates for potential alkali-reactivity. RILEM Technical Committees, *Materials and Structures*, 36(7), pp. 472-479.

**Sims, I., Nixon, P. 2003b:** RILEM recommended test method AAR-1: Detection of potential alkali-reactivity of aggregates – Petrographic method. RILEM Technical Committees, *Materials and Structures*, 36(7), pp. 480-496.

**Stark, D. 1991:** The moisture condition of field concrete exhibiting alkali-silica reactivity. *In: Durability of Concrete. Second International Conference*, American Concrete Institute, Detroit, USA. p. 973-987.

**Stipp, M., Stunitz, H., Heilbronner, R. & Schmid, S. 2002:** The eastern Tonale fault zone: a ´natural laboratory´ for crystal plastic deformation of quartz over a temperature range from 250 to 700 ºC. *Journal of Structural Geology*, 24, 1861-1884.

**Streckeisen, A.L. 1974:** Classification and nomenclature of plutonic rocks: Recommendations of the IUGS subcommission on the systematics of igneous rocks. *Geologische Rundschau*, 63, 773-785.

**Tapas, M.J., Sofia, L., Vessalas, K., Thomas, P., Sirivivatnanon, V., Scrivener, K. 2021:** Efficacu of SCMs to mitigate ASR in systems with higher alkali contents assessed by pore solution method. *Cement and Concrete Research*, 142, 11 pp.

**Tepponen, P., Eriksson, B.E. 1987:** Damage in Concrete Railway Sleepers in Finland. *Nordic Concrete Research*, 6, pp. 199-209.

**Thomas, M.D.A., Hooton, R.D. Rogers, C.A. 1997:** Prevention of damage due to alkali-aggregate reaction (AAR) in concrete construction – Canadian approach. *Cement, Concrete and Aggregates*, 19(1), 26-30.

**Thomas, M., Fournier, B., Folliard, K., Ideker, J., Shehata, M. 2006:** Test methods for evaluating preventive measures for controlling expansion due to alkali-silica reaction in concrete. *Cement and Concrete Research*, 36(10), 1842-1856.

**Thomas, M.D.A., Fournier, B., Folliard, K.J., Resendez, Y.A. 2011:** Alkali-silica reactivity field identification book. United States, Highway Administration, Office of Pavement Technology, 69.

**Tiecher. F., Gomes, M.E.B., Dal Molin, D.C.C., Hasparyk, N.P., Monteiro, P.J.M. 2017:** Relationship between degree of deformation in quartz and silica dissolution for the development of alkali-silica reaction in concrete. Materials, 10(9), 1022.

**Tikkanen, J., Johansson, K., Kihula, J., Mantila, A., Punkki, J., Paukku, E., Ruuth, J. 2021:** *Betoninormit 2021 by65*. Suomen Betoniyhdistys ry, 157 pp.

**Trägårdh, J., Göransson, M., Döse, M., Appelquist, K. 2013:** Alkalisilica-reactivity of Swedish aggregates used for concrete, Alkali Aggregate Reactions (AAR) in Concrete: Workshop Proceeding No. 11, Nordic-Baltic Miniseminar, Riga, Latvia, 41-53 pp.

**Velasco-Torres, A., Alaejos, P., Soriano, J. 2010:** Comparative study of the alkali-silica reaction (ASR) in granitic aggregates. *Estudios Geológicos*, 66(1), 105-114.

**Väisänen, M. & Skyttä, P. 2007:** Late Svecofennian shear zones in southwestern Finland. GFF, 129, 55-64.

**Wakizaka, Y. 2000:** Alkali-silica reactivity of Japanese rocks. *Developments in Geotechnical Engineering*, 84, 293-303.

**Walther, J.V. & Helgeson, H.C. 1977:** Calculation of the thermodynamic properties of aqueous silica and the solubility of quartz and its polymorphs at high pressures and temperatures, *American Journal of Science*, 277(10), 1315-1351.

**Wigum, B.J. & French, W.J. 1996:** Sequential examination of slowly expanding alkali-reactive aggregates in accelerated mortar bar testing. *Concrete Research*, 48, pp. 281-292.

**Wigum, B.J., Pedersen, L.T., Grelk, B., Lindgård J. 2006:** PARTNER State-of-the art report: Key parameters influencing the alkali aggregate reaction. SINTEF Building and Infrastructure, Trondheim, Norway, 75 pp.

**Winkler, H.G.F. 1979:** *Petrogenesis of metamorphic rocks*. 7th edition, Springer, Berlin Heidelberg New York, pp. 348 pp.

## Attachments

| **Sample** | **Leevi 1.1** |
|---|---|
| Coordinates (ETRS-TM35FIN): | N=6738308<br>E=213737 |
| Sample type: | Outcrop |

| Petrographical analysis | | |
|---|---|---|
| Modal composition (Point count of 1000 observations) | Kfsp:<br>Plg:<br>**Qtz:**<br>**Qtz (s)**<br>**Qtz (m)**<br>Bt:<br>Msq: | 53.8 %<br>11.4 %<br>**22.4 %**<br>**3.7 %**<br>**0.9 %**<br>4.9 %<br>2.9 % |
| Rock type | Granite | |
| Undulatory extinction angles (angle and size of measured grain) | 1. 9° 1.5 mm<br>2. 3° 2.0 mm<br>3. 8° 2.0 mm<br>4. 5° 1.0 mm<br>5. 5° 1.5 mm<br>**Average: 5.0° 1.65 mm** | 6. 5° 1.5 mm<br>7. 8° 2.0 mm<br>8. 2° 1.5 mm<br>9. 2° 1.5 mm<br>10. 3° 2.0 mm |
| Grain size | Medium (1.0-4.0 mm) | |
| Texture | Undeformed, equigranular, homogeneous, not recrystallized, moderate feldspar (kfsp and plg) alteration | |
| Quartz description | Intact, faint undulatory extinction in some of the grains, euhedral crystal faces with clear grain boundaries | |

*Attachment figure 1. Picture of rock sample Leevi1.1. Width of the sample approximately 15 cm.*

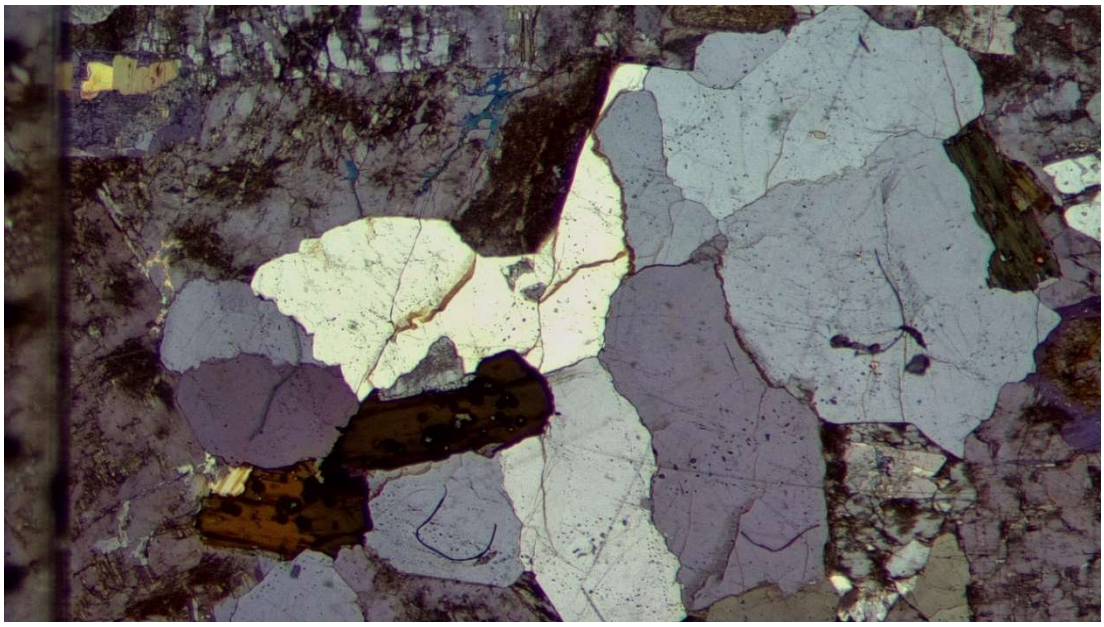

*Attachment figure 2. Xpl-image 1 of Leevi1.1. Image size 5x8 mm.*

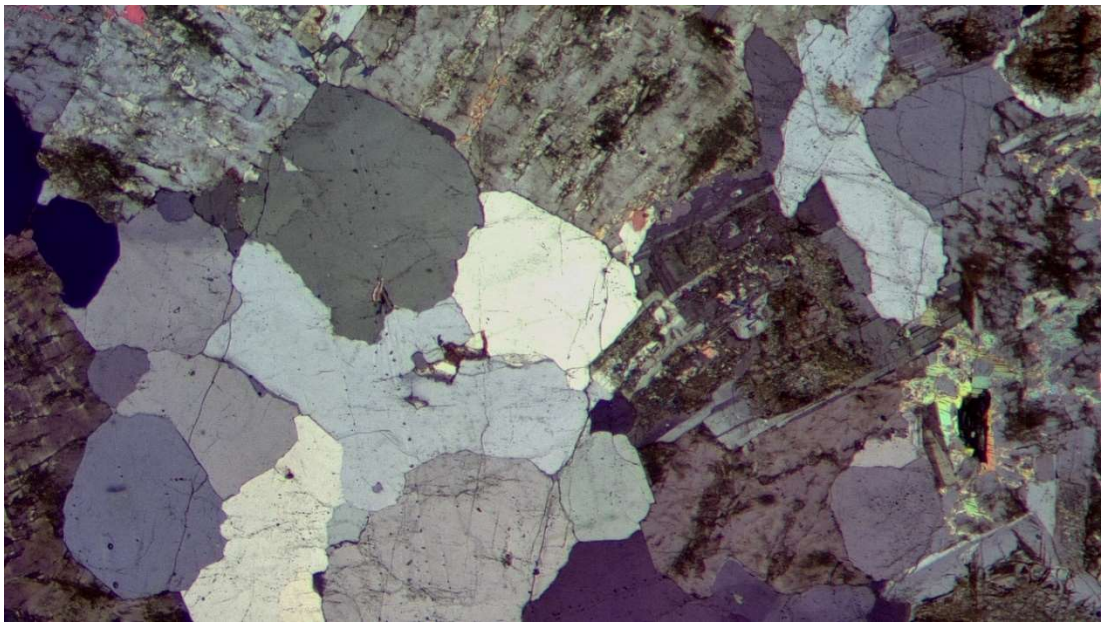

*Attachment figure 3. Xpl-image 2 of Leevi1.1. Image size 5x8 mm.*

| **Sample** | **Leevi 2.1** |
|---|---|
| Coordinates (ETRS-TM35FIN): | N=6735045<br>E=215960 |
| Sample type: | Boulder |

| **Petrographical analysis** | | |
|---|---|---|
| Modal composition (Point count of 1000 observations) | Kfsp | 44.2 % |
| | Plg | 14.8 % |
| | **Qtz** | **26.7 %** |
| | **Qtz (s)** | **4.3 %** |
| | **Qtz (m)** | **4.3 %** |
| | Msq | 3.0 % |
| | Bt | 2.6 % |
| Rock type | Granite | |
| Undulatory extinction angles (angle and size of measured grain) | 1. 1° 0.5 mm<br>2. 0° 1.0 mm<br>3. 2° 0.5 mm<br>4. 0° 1.0 mm<br>5. 1° 0.5 mm<br>**Average: 1.0° 0.7 mm** | 6. 2° 1.0 mm<br>7. 3° 1.0 mm<br>8. 0° 0.5 mm<br>9. 0° 0.5 mm<br>10. 1° 0.5 mm |
| Grain size | Fine (0.5-1.0 mm) | |
| Texture | Undeformed, equigranular, homogeneous, not recrystallized, strong feldspar (kfsp and plg) alteration | |
| Quartz description | Intact, undeformed, no undulatory extinction, euhedral crystal faces with clear grain boundaries | |

*Attachment figure 4. Picture of rock sample Leevi2.1. Width of the sample approximately 12 cm.*

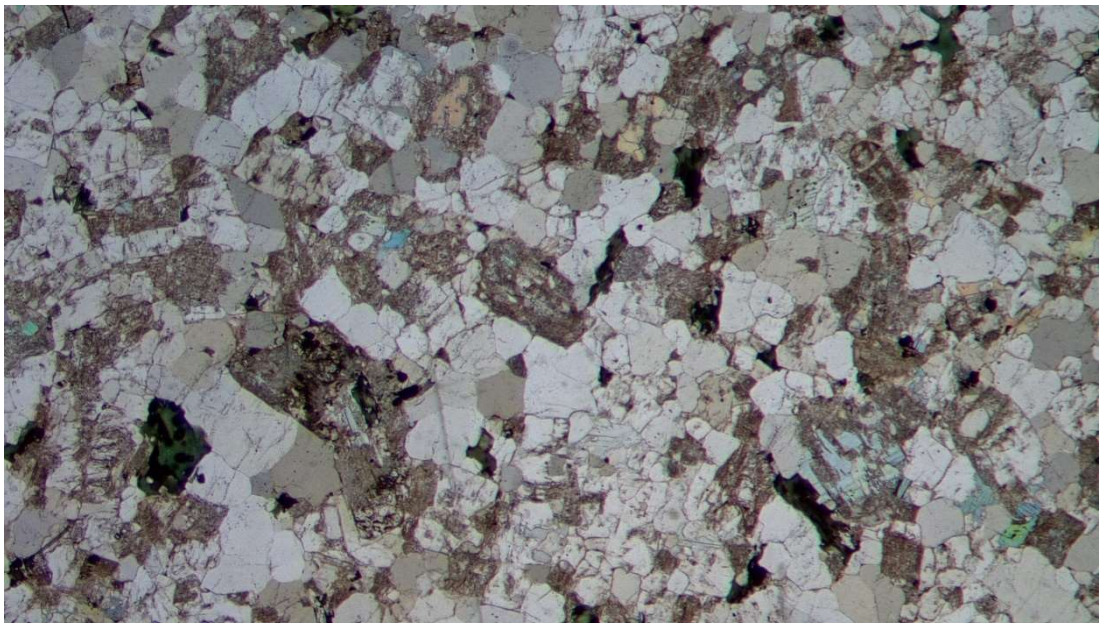

*Attachment figure 5. Ppl-image of Leevi2.1. Image size 5x8 mm.*

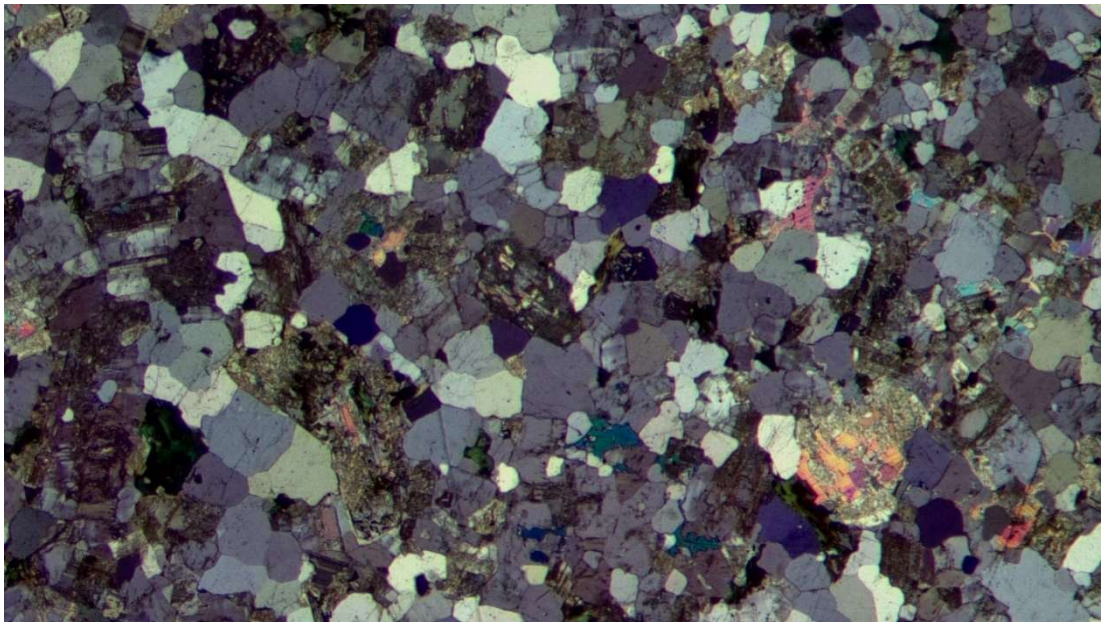

*Attachment figure 6. Xpl-image of Leevi2.1. Image size 5x8 mm.*

| **Sample** | **Leevi 3.1** |
|---|---|
| Coordinates (ETRS-TM35FIN): | N=6734559<br>E=215839 |
| Sample type: | Outcrop |

| **Petrographical analysis** | | |
|---|---|---|
| Modal composition (Point count of 1000 observations) | Kfsp | 33.8 % |
| | Plg | 23.8 % |
| | **Qtz** | **27.7 %** |
| | **Qtz (s)** | **1.3 %** |
| | **Qtz (m)** | **4.4 %** |
| | Msq | 4.7 % |
| | Bt | 4.3 % |
| Rock type | **Granite** | |
| Undulatory extinction angles (angle and size of measured grain) | 1. 1° 0.5 mm<br>2. 0° 1.0 mm<br>3. 2° 0.5 mm<br>4. 2° 1.0 mm<br>5. 0° 0.5 mm<br>**Average: 0.9° 0.8 mm** | 6. 1° 1.0 mm<br>7. 0° 1.0 mm<br>8. 2° 1.0 mm<br>9. 1° 1.0 mm<br>10. 0° 0.5 mm |
| Grain size | Fine (0.5-1.0 mm) | |
| Texture | Undeformed, equigranular, homogeneous, not recrystallized, strong feldspar (kfsp and plg) alteration | |
| Quartz description | Intact, undeformed, no undulatory extinction, euhedral crystal faces with clear grain boundaries | |


*Attachment figure 7. Picture of rock sample Leevi3.1. Width of the sample approximately 10 cm.*

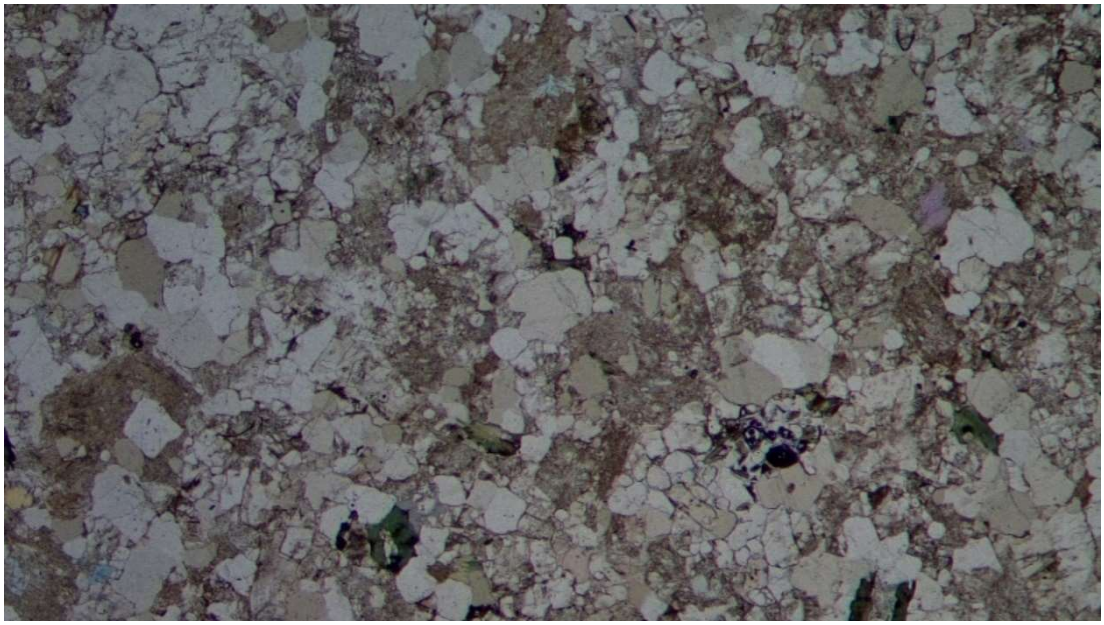

*Attachment figure 8. Ppl-image of Leevi3.1. Image size 5x8 mm.*

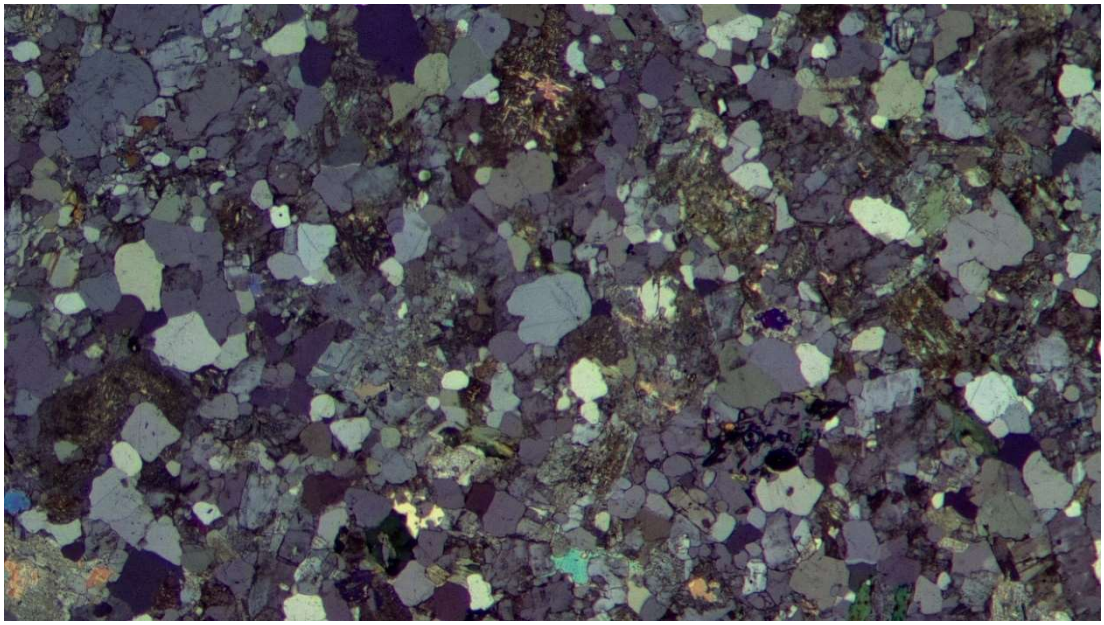

*Attachment figure 9. Xpl-image of Leevi3.1. Image size 5x8 mm.*

| **Sample** | **Leevi 4.1** |
|---|---|
| Coordinates (ETRS-TM35FIN): | N=6703770<br>E=317034 |
| Sample type: | Outcrop |

| **Petrographical analysis** | | | |
|---|---|---|---|
| Modal composition (Point count of 1000 observations) | Kfsp | 42.3 | % |
| | Plg | 14.9 | % |
| | **Qtz** | **0.3** | **%** |
| | **Qtz (s)** | **14.4** | **%** |
| | **Qtz (m)** | **3.7** | **%** |
| | Bt | 24.0 | % |
| | Msq | 0.5 | % |
| Rock type | **Quartz-biotite-feldspar gneiss** | | |
| Undulatory extinction angles (angle and size of measured grain) | 1. 27° 1.0 mm<br>2. 24° 1.5 mm<br>3. 48° 1.0 mm<br>4. 34° 1.0 mm<br>5. 44° 1.0 mm<br>**Average: 39.4° 1.0 mm** | | 6. 31° 1.0 mm<br>7. 41° 1.0 mm<br>8. 56° 1.0 mm<br>9. 54° 1.0 mm<br>10. 35° 0.5 mm |
| Grain size | Medium (0.5-2.0 mm) | | |
| Texture | Sheared, strained grains, plagioclase altered, augite altered to biotite, biotite orientation parallel to shear direction | | |
| Quartz description | Signs of strong shear and recrystallization, which occurs as<br>1) strongly strained and fractured larger 1,0-2,0 mm grains with fluid inclusions, and<br>2) small amount of recrystallized microcrystals along larger strained quartz grain boundaries and between other mineral grains. | | |

*Attachment figure 10. Picture of rock sample Leevi4.1. Width of the sample approximately 9 cm.*

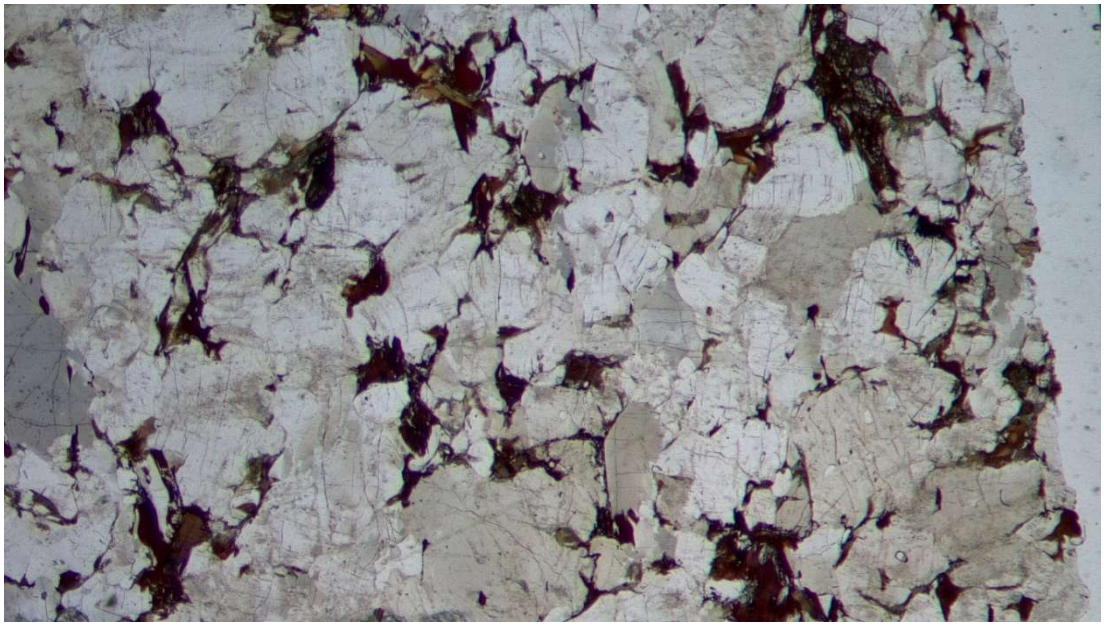

*Attachment figure 11. Ppl-image of Leevi4.1. Image size 5x8 mm.*

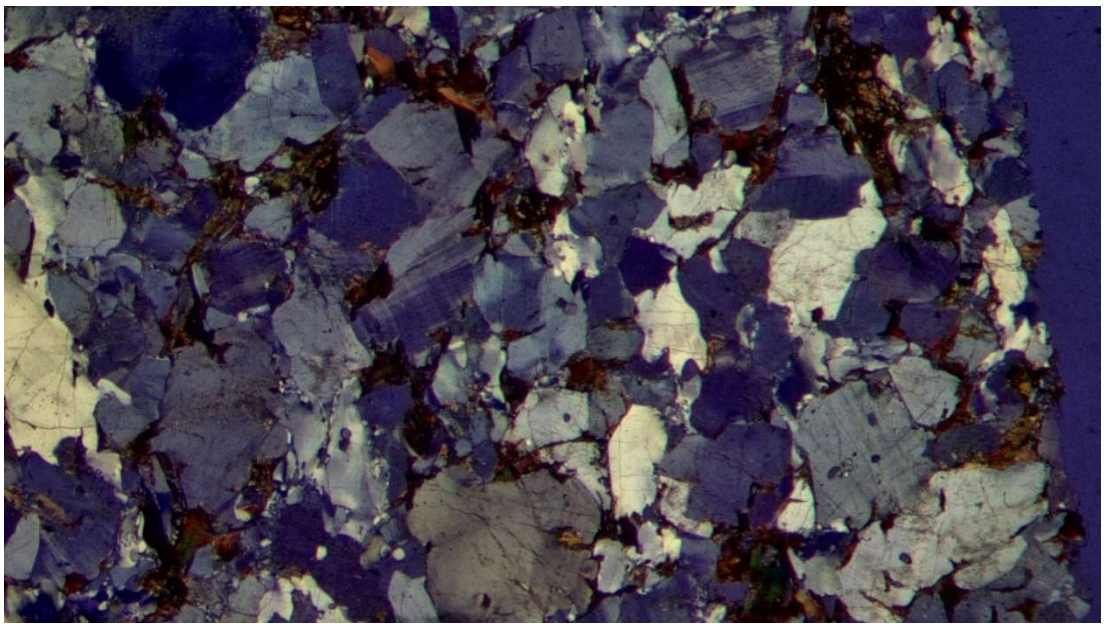

*Attachment figure 12. Xpl-image of Leevi4.1. Image size 5x8 mm.*

| **Sample** | **Leevi 5** |
|---|---|
| Coordinates (ETRS-TM35FIN): | N=6704024<br>E=317239 |
| Sample type: | Outcrop |

| **Petrographical analysis** | | |
|---|---|---|
| Modal composition (Point count of 1000 observations) | Kfsp | 37.9 % |
| | Plg | 8.1 % |
| | **Qtz (s)** | **16.0 %** |
| | **Qtz (m)** | **3.2 %** |
| | Bt | 34.0 % |
| | Op | 0.8 % |
| Rock type | **Quartz-biotite-feldspar gneiss** | |
| Undulatory extinction angles (angle and size of measured grain) | 1. 38° 0.5 mm<br>2. 37° 1.0 mm<br>3. 34° 1.0 mm<br>4. 33° 0.5 mm<br>5. 44° 0.5 mm<br>**Average: 34.3° 0.7 mm** | 6. 42° 0.5 mm<br>7. 22° 1.0 mm<br>8. 23° 0.5 mm<br>9. 23° 1.0 mm<br>10. 47° 0.5 mm |
| Grain size | Medium (0.5-2.0 mm) | |
| Texture | Sheared, strained grains, plagioclase altered, augite altered to biotite, biotite orientation parallel to shear direction, micrographic textures (qtz and kfsp intergrowths), microfractures filled with amorphous glass | |
| Quartz description | Signs of strong shear and recrystallization, which occurs as<br>1) strongly strained and fractured larger 1,0-2,0 mm grains with fluid inclusions,<br>2) small amount of recrystallized microcrystals along larger strained quartz grain boundaries and between other mineral grains, and<br>3) intergrowths with kfsp. | |

*Attachment figure 13. Picture of rock sample Leevi5. Width of the sample approximately 11 cm.*

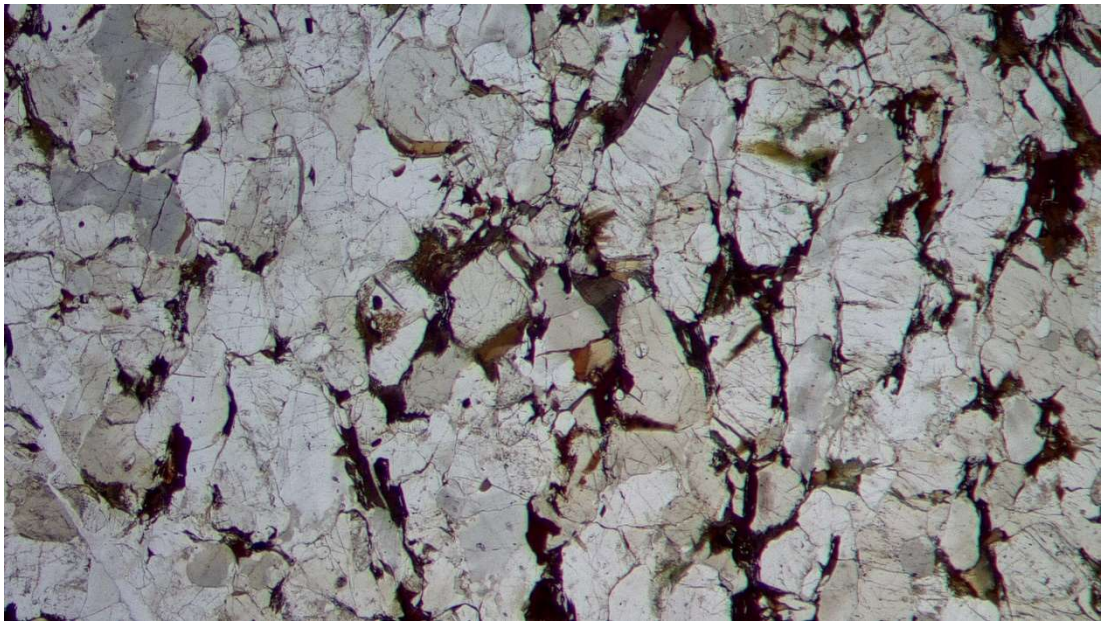

*Attachment figure 14. Ppl-image of Leevi5. Image size 5x8 mm.*

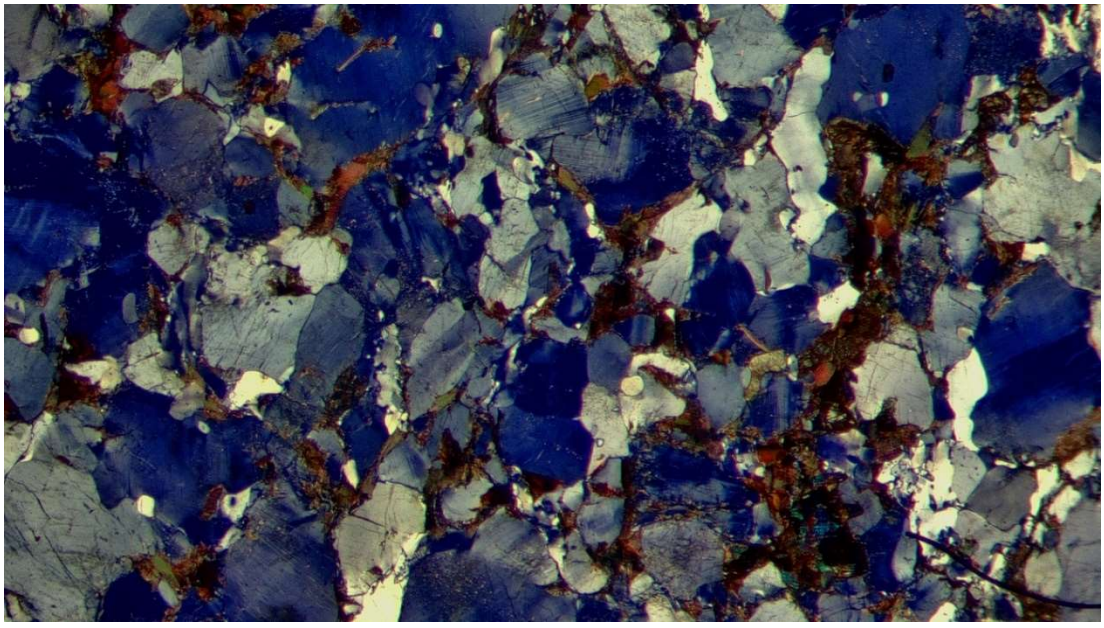

*Attachment figure 15. Xpl-image of Leevi5. Image size 5x8 mm.*

| **Sample** | **Leevi 6** |
|---|---|
| Coordinates (ETRS-TM35FIN): | N=6823367<br>E=298299 |
| Sample type: | Outcrop |

| **Petrographical analysis** | | |
|---|---|---|
| Modal composition (Point count of 1000 observations) | Kfsp | 15.8 % |
| | Plg | 11.0 % |
| | **Qtz (m)** | **30.6 %** |
| | Biotite | 16.6 % |
| | Msq | 17.8 % |
| | Chl | 8.2 % |
| Rock type | **Low metamorphic grade phylllite** | |
| Undulatory extinction angles (angle and size of measured grain) | Not measured. | |
| Grain size | Very fine (<0.1 mm) | |
| Texture | Low grade metamorphosis, heterogeneous, compositionally dispersed/oriented → primary sedimentary layering still observable as varying mica/chlorite-quartz/feldspar cleavage, intact matrix (only minor brittle or plastic deformation) | |
| Quartz description | Grain size microcrystalline (50-100 μm), intracrystalline strain not well observable due to very fine grain size, but straight and angular grain boundaries indicate very little deformation after initial deposition, suggesting grains being free of reactivity-enhancing intracrystalline energy. | |

*Attachment figure 16. Picture of rock sample Leevi6. Width of the sample approximately 8 cm.*

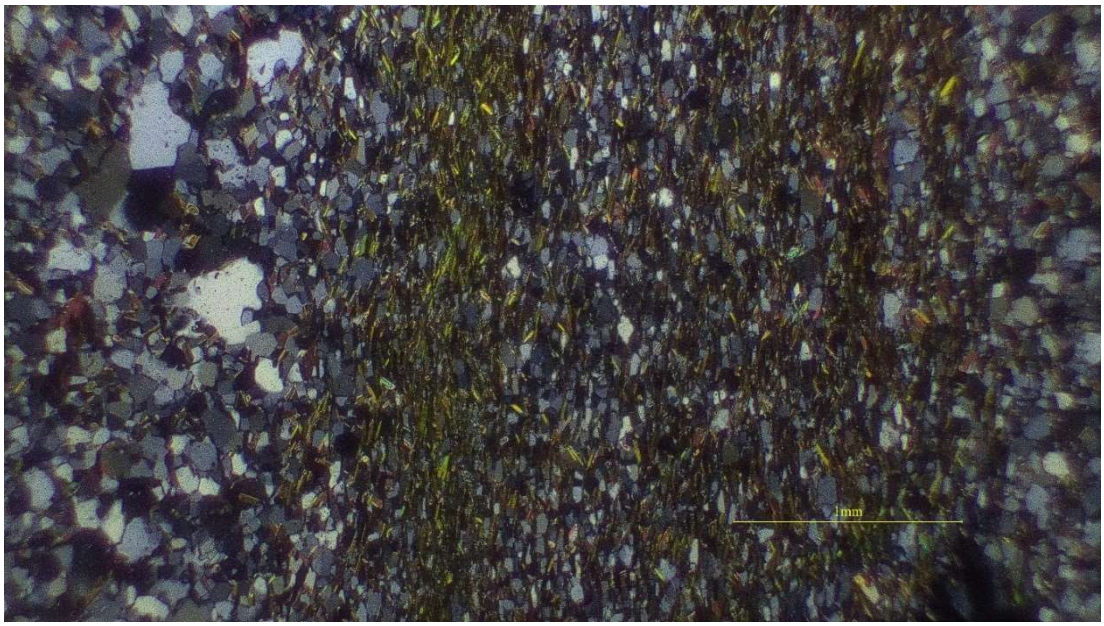


*Attachment figure 17. Xpl-image 1 of Leevi6. Image size 2x3 mm.*

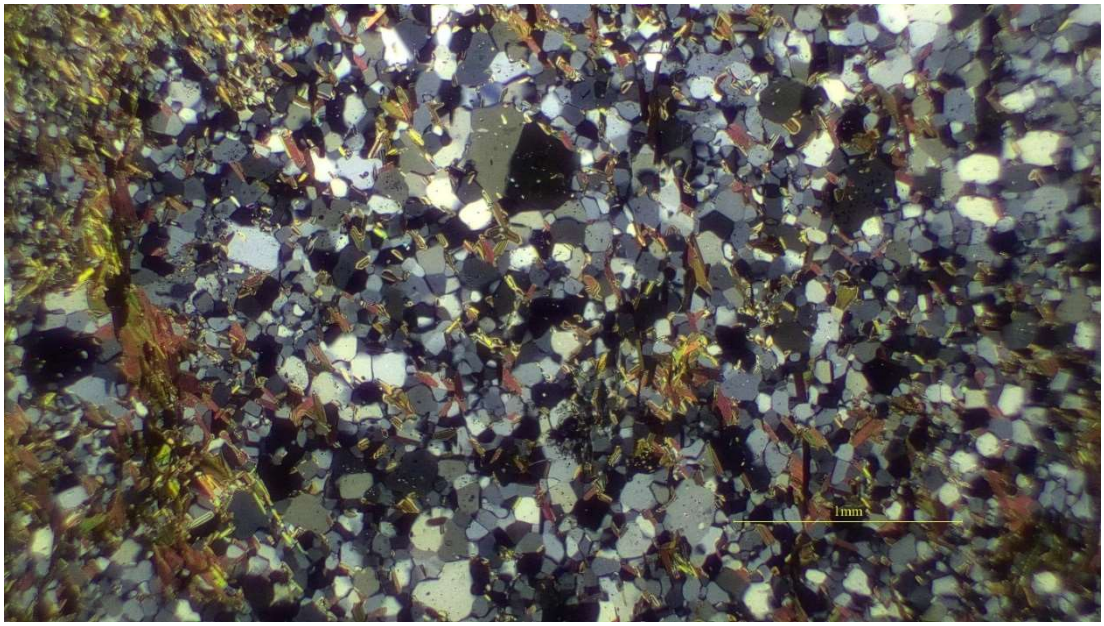


*Attachment figure 18. Xpl-image 2 of Leevi6. Image size 2x3 mm.*

| **Sample** | **Leevi 7** |
|---|---|
| Coordinates (ETRS-TM35FIN): | N=6682930<br>E=310468 |
| Sample type: | Outcrop |

| **Petrographical analysis** | | |
|---|---|---|
| Modal composition (Point count of 1000 observations) | Kfsp | 38.6 % |
| | Plg | 1.2 % |
| | **Qtz** | **0.2 %** |
| | **Qtz (s)** | **17.4 %** |
| | **Qtz (m)** | **21.6 %** |
| | Bt | 8.4 % |
| | Msq | 12.6 % |
| Rock type | **Biotite-quartz-feldspar metavolcanite** | |
| Undulatory extinction angles (angle and size of measured grain) | 1. 18° 1.0 mm<br>2. 15° 1.5 mm<br>3. 25° 1.0 mm<br>4. 14° 1.0 mm<br>5. 21° 0.5 mm<br>**Average: 21.2° 1.15 mm** | 6. 32° 1.0 mm<br>7. 20° 1.5 mm<br>8. 30° 2.0 mm<br>9. 24° 1.5 mm<br>10. 13° 0.5 mm |
| Grain size | Very fine (0.1-1.0 mm) | |
| Texture | Strong recrystallization, kfsp altered, mild mineral orientation, feldspars (kfsp and plg) altered, biotite occurs as scattered, fine crystals within matrix | |
| Quartz description | Represents grain boundary migration (GBM) quartz recrystallization → strongly sutured and interfingered, irregular grain boundaries<br>Occurs as<br>1) larger clusters of amoeboid quartz microstructures as product of GBM quartz recrystallization (17.4% of modal composition) and<br>2) recrystallized microcrystals of size <100μm (21.6% of modal composition) | |


*Attachment figure 19. Picture of rock sample Leevi7. Width of the sample approximately 10 cm.*

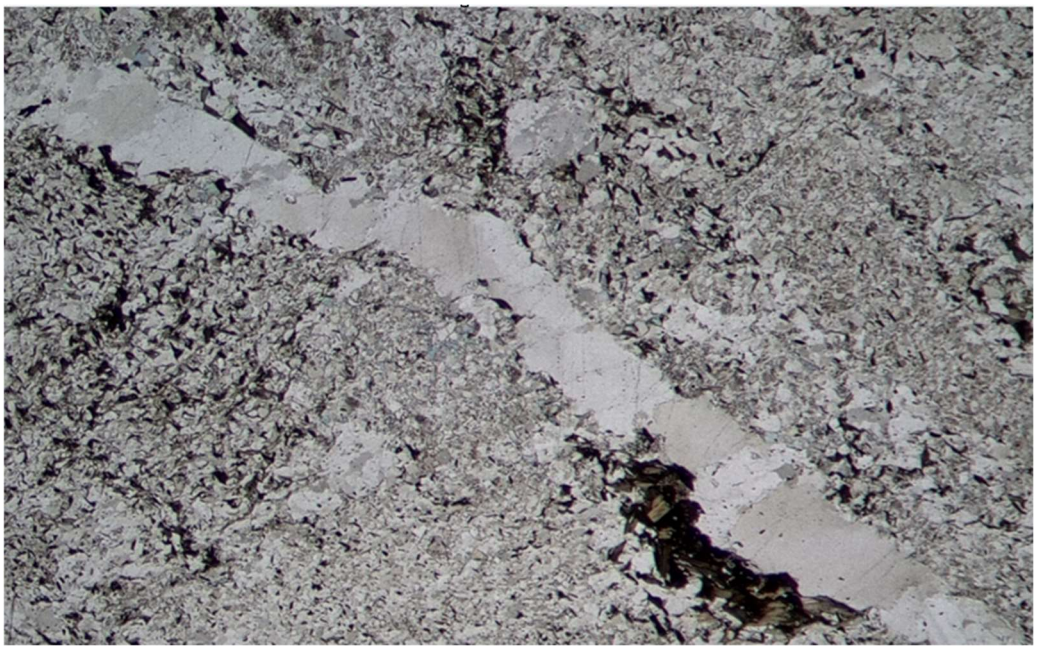

*Attachment figure 20. Ppl-image of Leevi7. Image size 5x8 mm.*

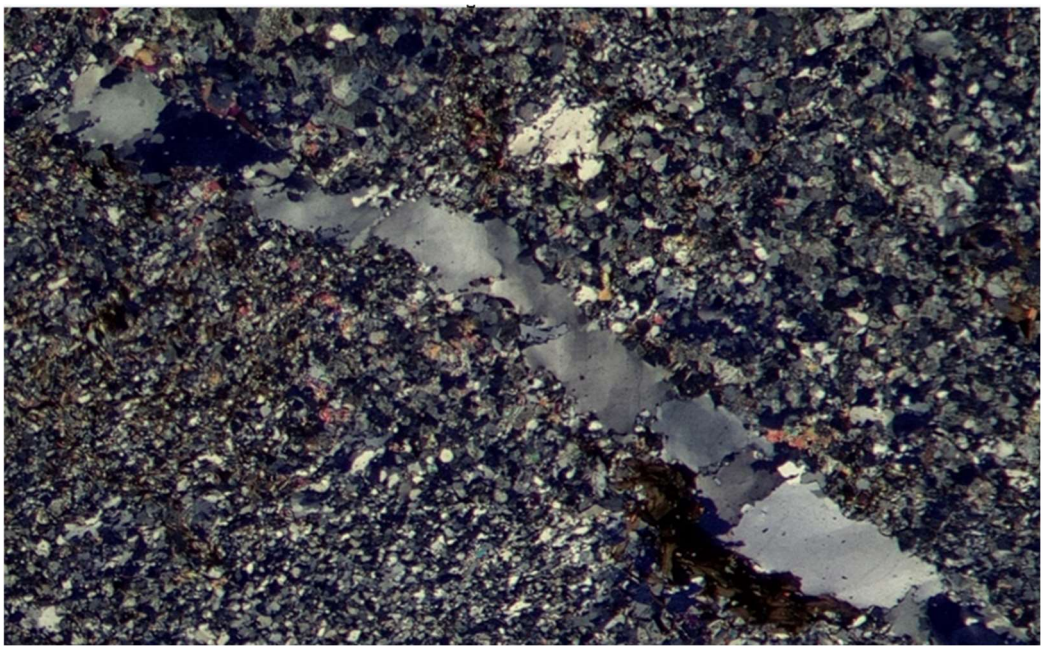

*Attachment figure 21. Xpl-image of Leevi7. Image size 5x8 mm.*

| **Sample** | **Leevi 8** |
|---|---|
| Coordinates (ETRS-TM35FIN): | N=6681836<br>E=303516 |
| Sample type: | Outcrop |

| **Petrographical analysis** | | |
|---|---|---|
| Modal composition (Point count of 1000 observations) | Kfsp | 24.3 % |
| | Plg | 22.0 % |
| | **Qtz** | **24.9 %** |
| | **Qtz (s)** | **0.8 %** |
| | **Qtz (m)** | **5.2 %** |
| | Bt | 15.0 % |
| | Px | 7.3 % |
| | Msq | 0.5 % |
| Rock type | **Biotite-quartz-feldspar schist** | |
| Undulatory extinction angles (angle and size of measured grain) | 1. 6° 1.0 mm<br>2. 8° 1.0 mm<br>3. 4° 1.0 mm<br>4. 14° 1.0 mm<br>5. 5° 0.5 mm<br>**Average: 7.2° 0.95 mm** | 6. 10° 0.5 mm<br>7. 2° 0.5 mm<br>8. 13° 1.5 mm<br>9. 5° 1.5 mm<br>10. 5° 1.0 mm |
| Grain size | Fine (0.1-1.0 mm) | |
| Texture | Homogeneous<br>Strong mineralogical alignment.<br>Minor feldspar (kfsp and plg) alteration. Individual myrmekites present. | |
| Quartz description | Signs of uneven recrystallization →<br>1) lobate and interfingering grain boundaries in larger grains with larger extinction angles<br>2) fully recrystallized and healed quartz clusters with no signs of intracrystalline strain (no undulatory extinction) and clear, straight grain boundaries | |

*Attachment figure 22. Picture of rock sample Leevi8. Width of the sample approximately 9 cm.*

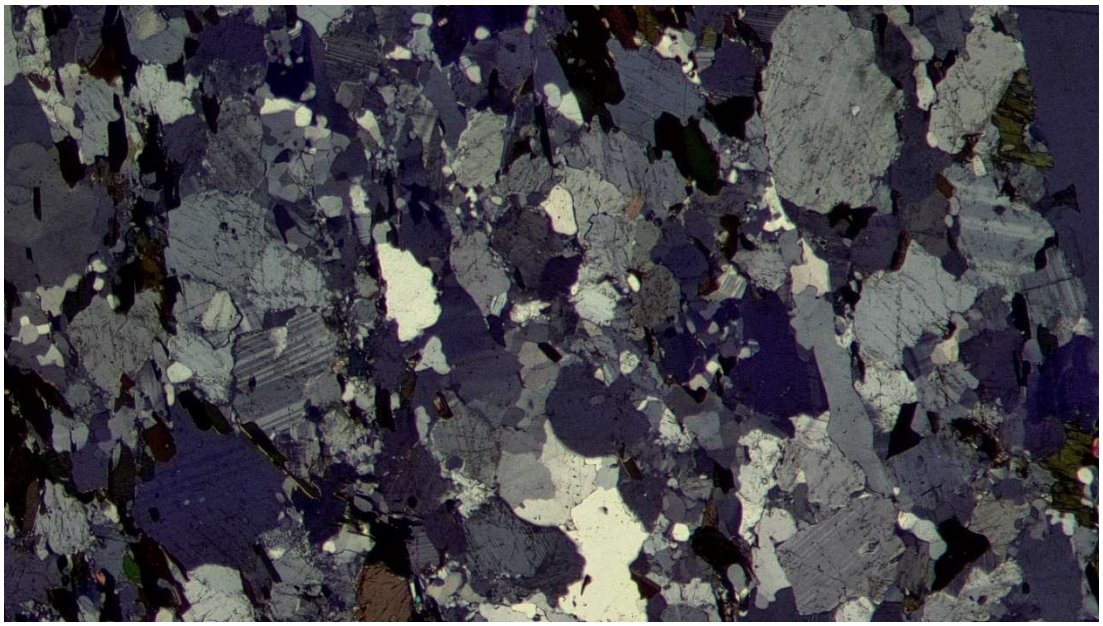

*Attachment figure 23. Xpl-image of Leevi8. Image size 5x8 mm.*

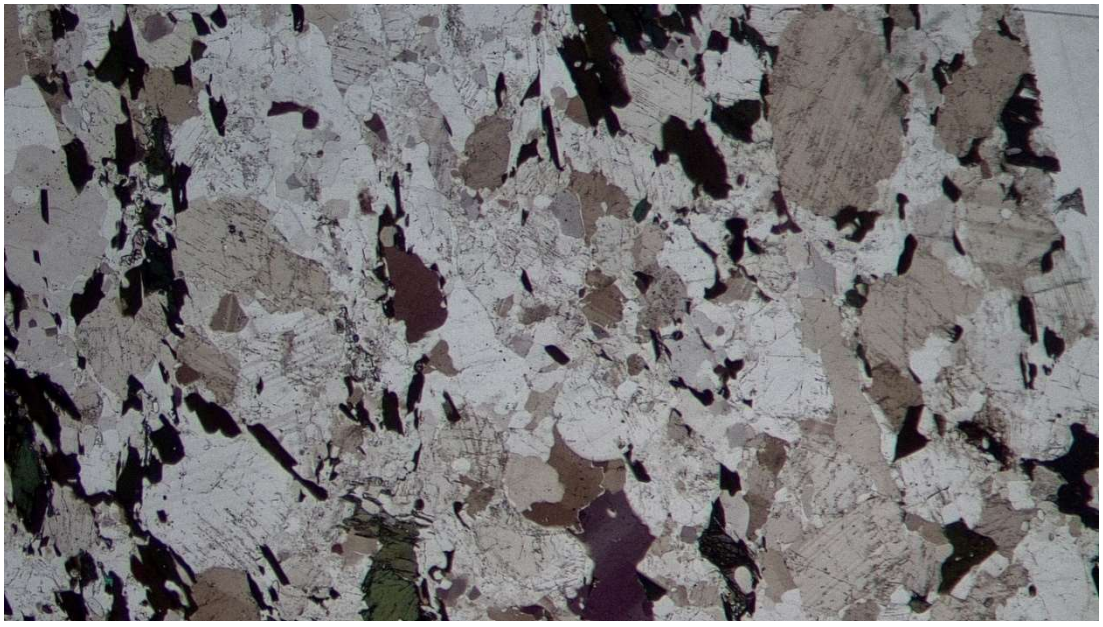

*Attachment figure 24. Ppl-image of Leevi8. Image size 5x8 mm.*

| **Sample** | **Leevi 9** |
|---|---|
| Coordinates (ETRS-TM35FIN): | N=6681869<br>E=303511 |
| Sample type: | Boulder |

| **Petrographical analysis** | | |
|---|---|---|
| Modal composition (Point count of 1000 observations) | Kfsp<br>Plg<br>**Qtz**<br>**Qtz (s)**<br>**Qtz**<br>**(m)**<br>Bt | 17.6 %<br>29.0 %<br>**0.8 %**<br>**12.6 %**<br>**19.8 %**<br>20.2 % |
| Rock type | **Biotite-quartz-feldspar schist** | |
| Undulatory extinction angles (angle and size of measured grain) | 1. 24° 1.0 mm<br>2. 25° 1.5 mm<br>3. 26° 1.5 mm<br>4. 18° 1.0 mm<br>5. 24° 1.0 mm<br>**Average: 20.8° 1.2 mm** | 6. 20° 1.5 mm<br>7. 14° 1.0 mm<br>8. 12° 1.0 mm<br>9. 30° 1.5 mm<br>10. 15° 1.0 mm |
| Grain size | Very fine to fine (0.1-1.0 mm). Larger. up to 4 mm quartz clusters. | |
| Texture | Grain size distributed in layers parallel to shear direction<br>Recrystallization that has been overprinted by brittle deformation which has developed microfractures parallel to shear direction | |
| Quartz description | Represents grain boundary migration (GBM) quartz recrystallization → strongly sutured and interfingered, irregular grain boundaries<br>Occurs as<br>1) larger clusters of amoeboid quartz microstructures as product of GBM quartz recrystallization (12.6% of modal composition), present especially along fracture zones and<br>2) recrystallized crypto- and microcrystals of size <100 µm (19.8% of modal composition) present around larger GBM clusters and along microfractures | |

*Attachment figure 25. Picture of rock sample Leevi9. Width of the sample approximately 8 cm.*

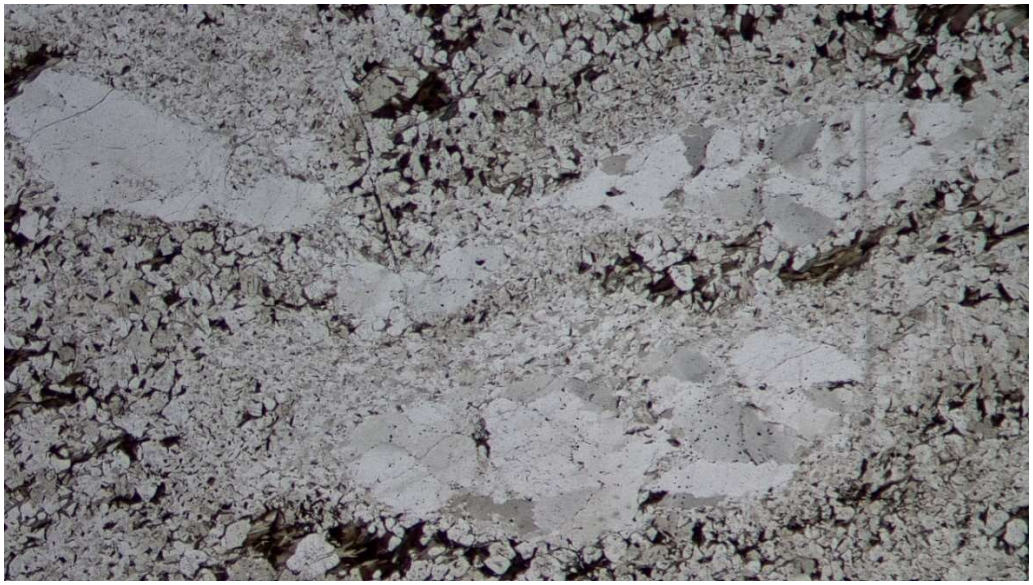

*Attachment figure 26. Ppl-image of Leevi9. Image size 5x8 mm.*

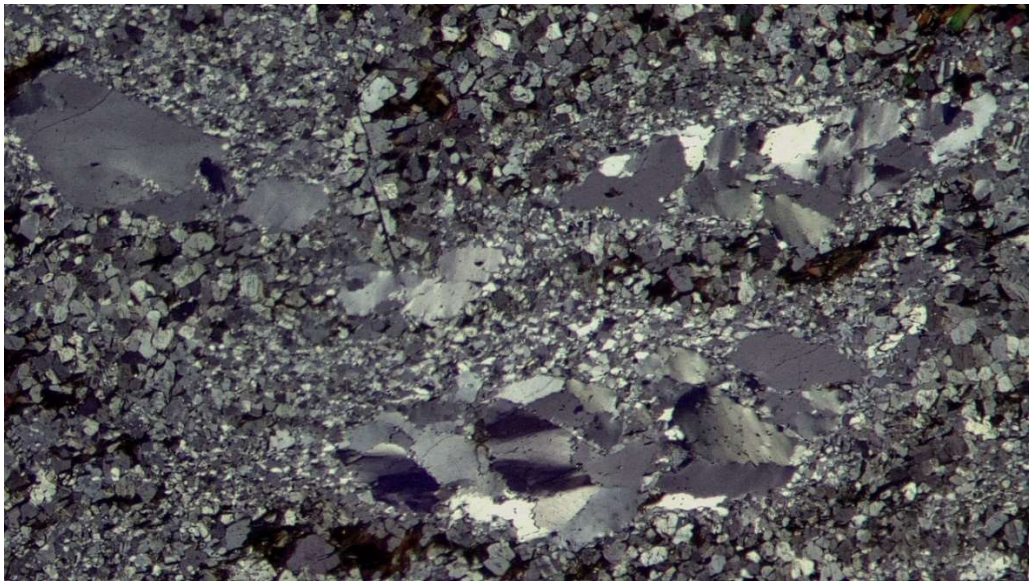

*Attachment figure 27. Xpl-image of Leevi9. Image size 5x8 mm.*

| **Sample** | **Leevi 10.1** |
|---|---|
| Coordinates (ETRS-TM35FIN): | N=6681490<br>E=303746 |
| Sample type: | Boulder |

| **Petrographical analysis** | | |
|---|---|---|
| Modal composition (Point count of 1000 observations) | Kfsp | 0.4 % |
| | Plg | 41.6 % |
| | **Qtz (m)** | **26.4 %** |
| | Bt | 31.2 % |
| | Msq | 0.4 % |
| Rock type | **Mafic metavolcanite** | |
| Undulatory extinction angles (angle and size of measured grain) | 1. 19° 0.1 mm<br>2. 16° 0.1 mm<br><br>**Average: 17.5° 0.1 mm** | |
| Grain size | Very fine (0.1-0.2mm) | |
| Texture | Mineral grains have a mild preferred orientation, recrystallized in low temperature conditions indicated by small grain size, plagioclase altered | |
| Quartz description | All quartz (26.4% of modal composition) is considered microcrystalline with size <100 μm. Due to very small size of crystals, comparative extinction angles are not measurable, however, 2 measured grains showed relatively high angles despite very small size. | |

*Attachment figure 28. Picture of rock sample Leevi10.1. Width of the sample approximately 8 cm.*

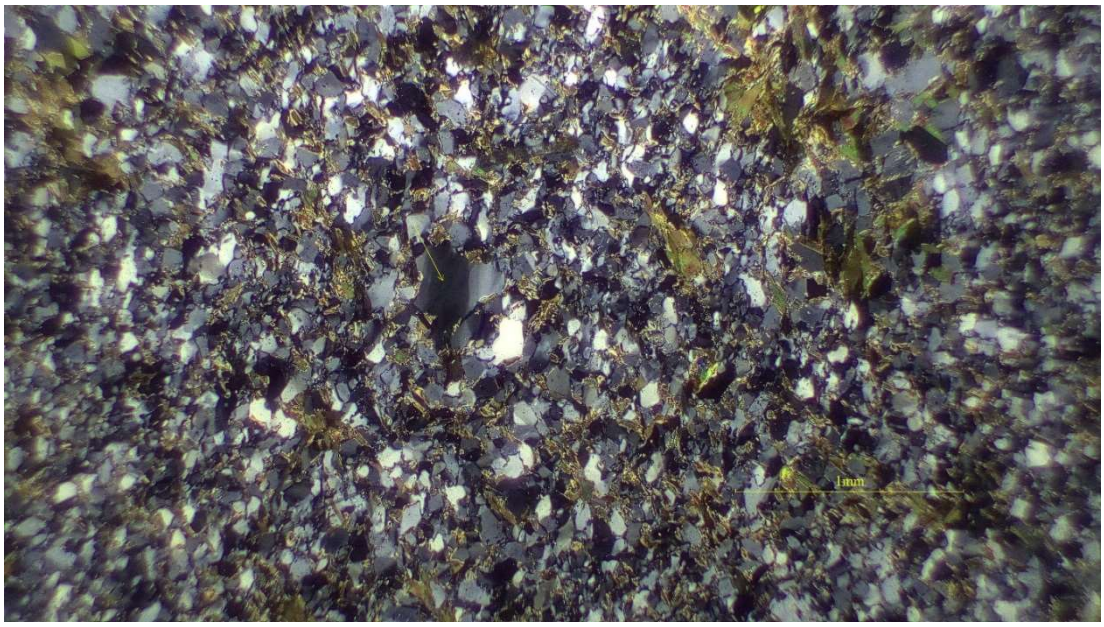


*Attachment figure 29. Xpl-image 1 of Leevi10.1. Image size 2x3 mm.*

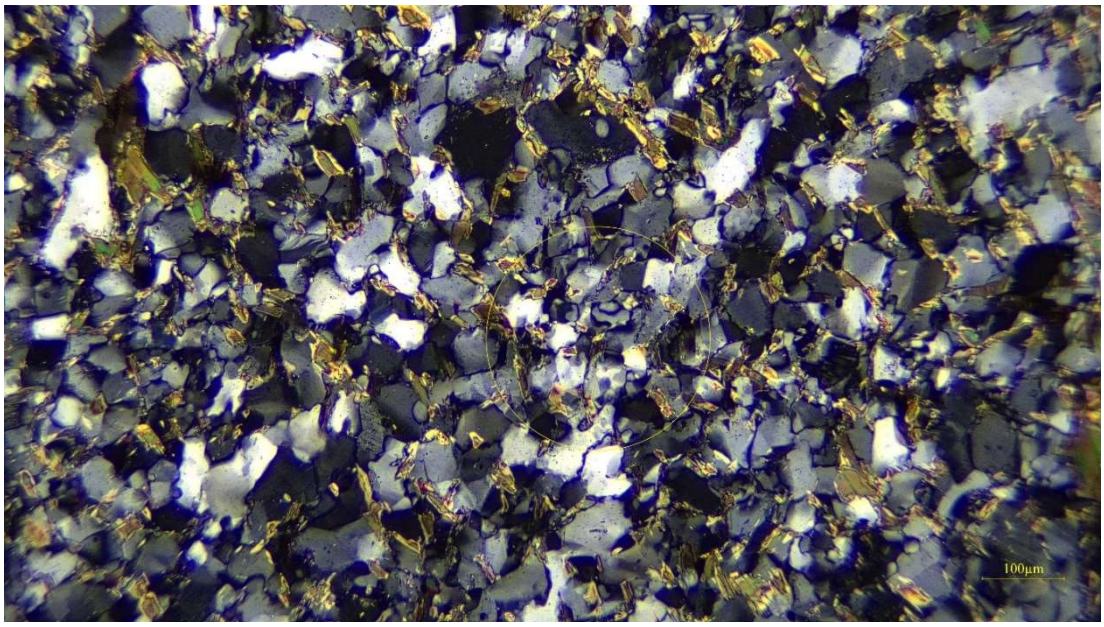


*Attachment figure 30. Xpl-image 2 of Leevi10.1. Image size 2x3 mm.*

| **Sample** | **Leevi 11** |
|---|---|
| Coordinates (ETRS-TM35FIN): | N=6681493<br>E=303708 |
| Sample type: | Boulder |

| **Petrographical analysis** | | | |
|---|---|---|---|
| Modal composition (Point count of 1000 observations) | Kfsp | 41.6 | % |
| | Plg | 19.5 | % |
| | **Qtz** | **12.3** | **%** |
| | **Qtz (s)** | **19.2** | **%** |
| | **Qtz (m)** | **0.5** | **%** |
| | Bt | 6.5 | % |
| | Op | 0.4 | % |
| Rock type | **Granite** | | |
| Undulatory extinction angles (angle and size of measured grain) | 1. 7° 1.0 mm<br>2. 7° 0.5 mm<br>3. 9° 1.5 mm<br>4. 6° 1.5 mm<br>5. 11° 1.5 mm<br>**Average: 10.5° 1.2 mm** | | 6. 12° 1.5 mm<br>7. 9° 1.0 mm<br>8. 15° 1.5 mm<br>9. 11° 1.0 mm<br>10. 18° 1.0 mm |
| Grain size | Medium (0.4-2.0mm) | | |
| Texture | Homogeneous, undeformed, moderate feldspar (kfsp and plg) alteration | | |
| Quartz description | Intact crystal faces without intracrystalline strain, shape of grain boundaries indicates recrystallization without significant deformation, low extinction angles | | |

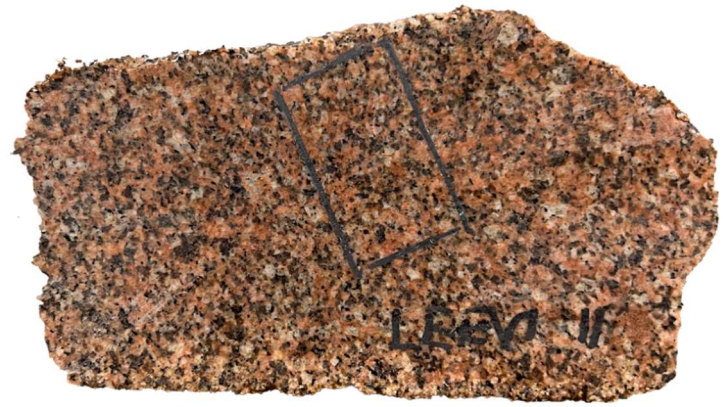

*Attachment figure 31. Picture of rock sample Leevi11. Width of the sample approximately 10 cm.*

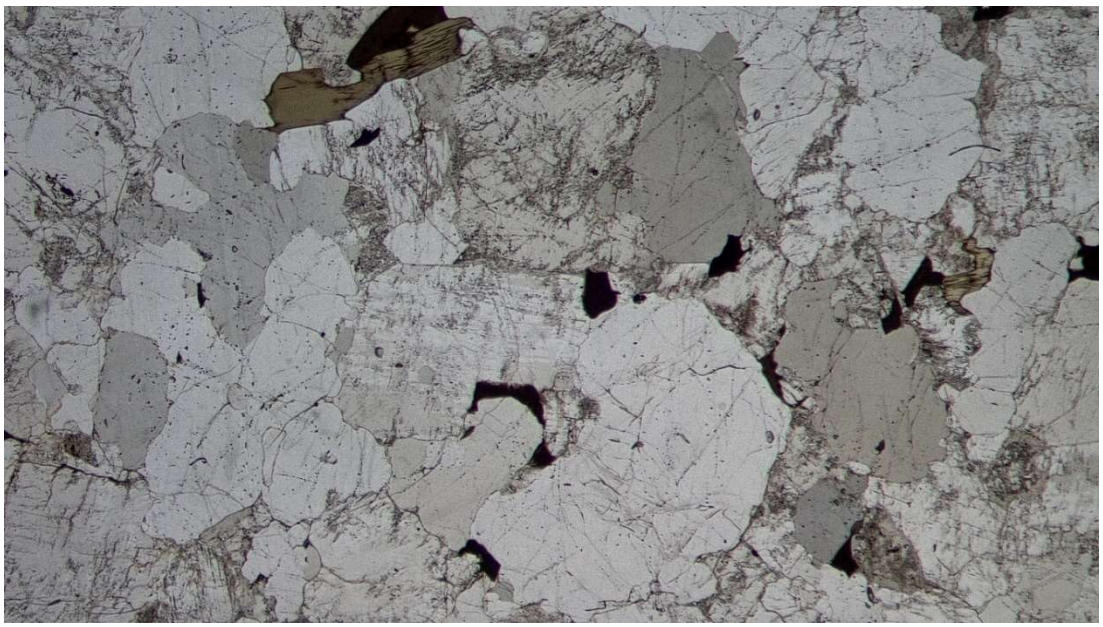

*Attachment figure 32. Ppl-image of Leevi11. Image size 5x8 mm.*

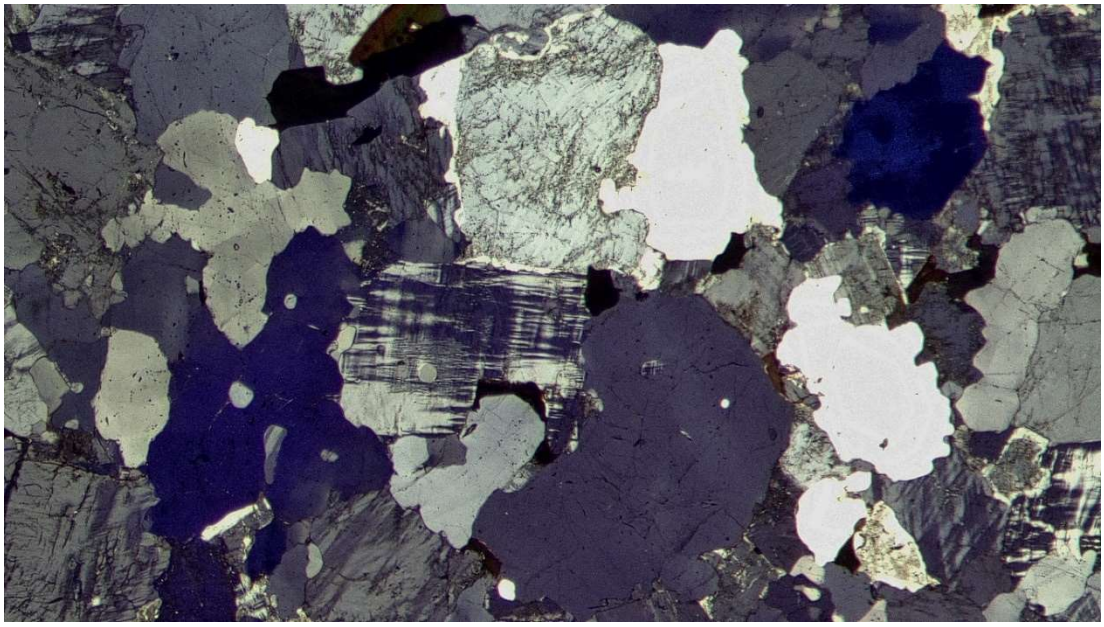

*Attachment figure 33. Xpl-image of Leevi11. Image size 5x8 mm.*

| **Sample** | **Leevi 12** |
|---|---|
| Coordinates (ETRS-TM35FIN): | N=7059434<br>E=414566 |
| Sample type: | Boulder |

| **Petrographical analysis** | | |
|---|---|---|
| Modal composition (Point count of 1000 observations) | Kfsp | 12.0 % |
| | Plg | 41.4 % |
| | **Qtz** | **24.4 %** |
| | Bt | 16.8 % |
| | Msq | 1.2 % |
| | Px | 3.8 % |
| | Op | 0.4 % |
| Rock type | **Mafic gneiss** | |
| Undulatory extinction angles (angle and size of measured grain) | 1. 11° 1.5 mm<br>2. 3° 0.5 mm<br>3. 12° 1.5 mm<br>4. 6° 1.5 mm<br>5. 7° 1.5 mm<br>**Average: 7.7° 1.2 mm** | 6. 8° 1.5 mm<br>7. 10° 1.0 mm<br>8. 4° 0.5 mm<br>9. 5° 1.0 mm<br>10. 11° 1.5 mm |
| Grain size | Medium (1,0-2,0 mm) | |
| Texture | Micrographic textures (myrmekites) around some feldspar crystals | |
| Quartz description | Fully recrystallized, quartz is sized >0.1 mm and fully recovered after deformation due to high temperature recrystallization, in which any signs of intracrystalline strain has not preserved. | |

*Attachment figure 34. Picture of rock sample Leevi12. Width of the sample approximately 9 cm.*

*Attachment figure 35. Ppl-image of Leevi12. Image size 5x8 mm.*

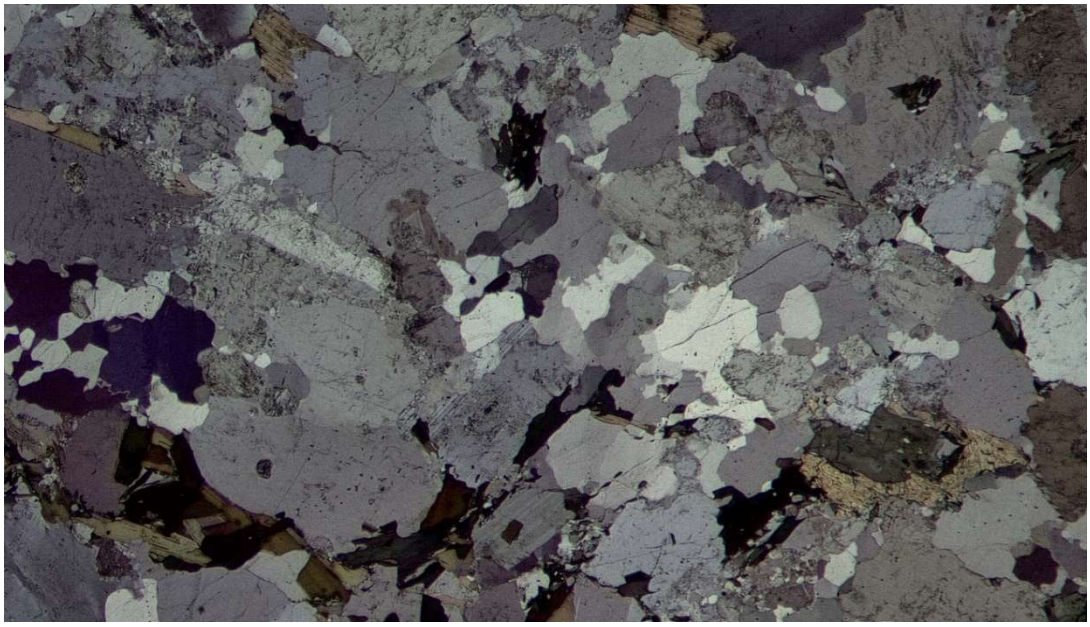

*Attachment figure 36. Xpl-image of Leevi12. Image size 5x8 mm.*

| **Sample** | **Leevi 13** |
|---|---|
| Coordinates (ETRS-TM35FIN): | N=6707785<br>E=258197 |
| Sample type: | Outcrop, sample taken from shear joint within otherwise undeformed and homogeneous fine-grained granite intrusion. |

| **Petrographical analysis** | | |
|---|---|---|
| Modal composition (Point count of 1000 observations) | Kfsp 23.2 %<br>Plg 48.4 %<br>**Qtz 2.2 %**<br>**Qtz (s) 11.6 %**<br>**Qtz (m) 11.8 %**<br>Bt 2.8 % | |
| Rock type | **Sheared granite** | |
| Undulatory extinction angles (angle and size of measured grain) | 1. 11° 1.0 mm<br>2. 32° 2.0 mm<br>3. 24° 2.0 mm<br>4. 13° 1.0 mm<br>5. 20° 1.0 mm<br>**Average: 20.7° 1.35 mm** | 6. 26° 1.0 mm<br>7. 16° 1.0 mm<br>8. 30° 1.5 mm<br>9. 23° 1.5 mm<br>10. 12° 1.5 mm |
| Grain size | Fine (0.1-1.0 mm) | |
| Texture | Unequigranular, strongly deformed and sheared, feldspars altered, elongated and strained grains up to 3 mm and several microcracks oriented parallel to shear direction. | |
| Quartz description | Around microfractures, quartz has largely recrystallized in microcrystals. Larger quartz crystals within more intact parts are generally irregularly elongated. Intracrystalline strain is easily observable from uneven extinction of larger grains and clusters. Extinction angle measurements taken from larger grains (listed above) are relatively high. | |


*Attachment figure 37. Picture of rock sample Leevi13. Width of the sample approximately 11 cm.*

*Attachment figure 38. Xpl-image 1 of Leevi13. Image size 5x8 mm.*

*Attachment figure 39. Xpl-image 2 of Leevi13. Image size 5x8 mm.*

| **Sample** | **Leevi 14.1** |
|---|---|
| Coordinates (ETRS-TM35FIN): | N=7108423<br>E=356656 |
| Sample type: | Boulder |

| **Petrographical analysis** | | | |
|---|---|---|---|
| Modal composition (Point count of 1000 observations) | Kfsp | 0.2 | % |
| | Plg | 52.6 | % |
| | **Qtz** | **2.8** | **%** |
| | **Qtz (s)** | **0.4** | **%** |
| | **Qtz (m)** | **14.6** | **%** |
| | Bt | 12.4 | % |
| | Amph | 17.0 | % |
| Rock type | **Mafic metavolcanite** | | |
| Undulatory extinction angles (angle and size of measured grain) | 1. 8° 0.5 mm<br>2. 9° 0.5 mm<br>3. 9° 0.5 mm<br>**Average: 8.7° 0.5 mm** | | |
| Grain size | Very fine (0.1-0.5 mm) | | |
| Texture | Mild mineral orientation, plagioclase altered, amphibole moderately altered to biotite. | | |
| Quartz description | Recrystallized, mild intracrystalline strain based on uneven extinction, which is not well measurable due to small grain size. 3 measurements were taken from individual larger crystals. | | |


*Attachment figure 40. Picture of rock sample Leevi14.1. Width of the sample approximately 8 cm.*

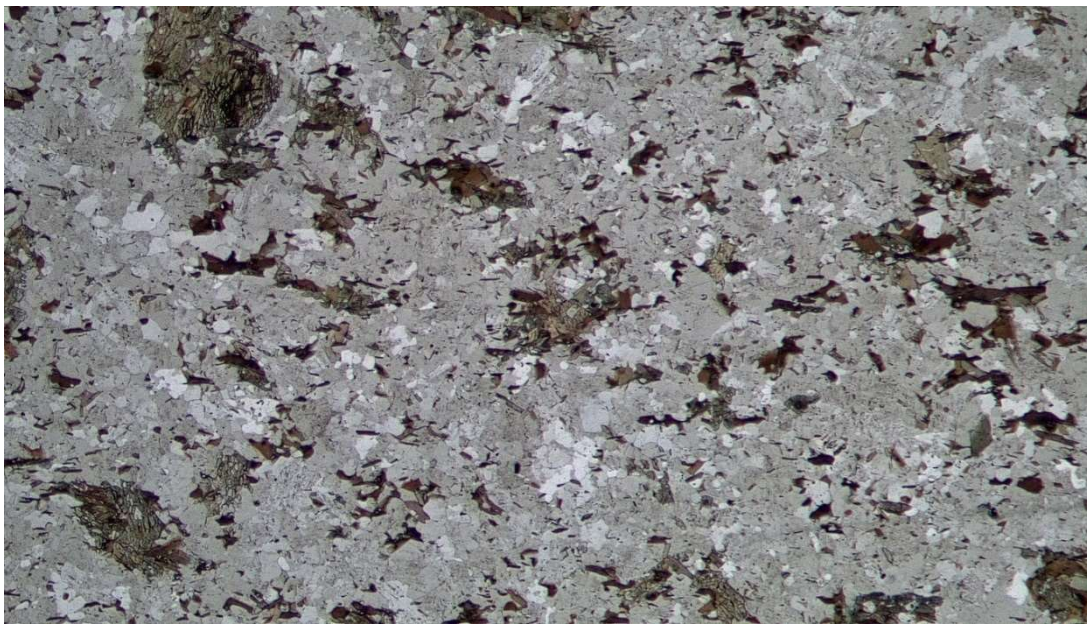

*Attachment figure 41. Ppl-image of Leevi14.1. Image size 5x8 mm.*

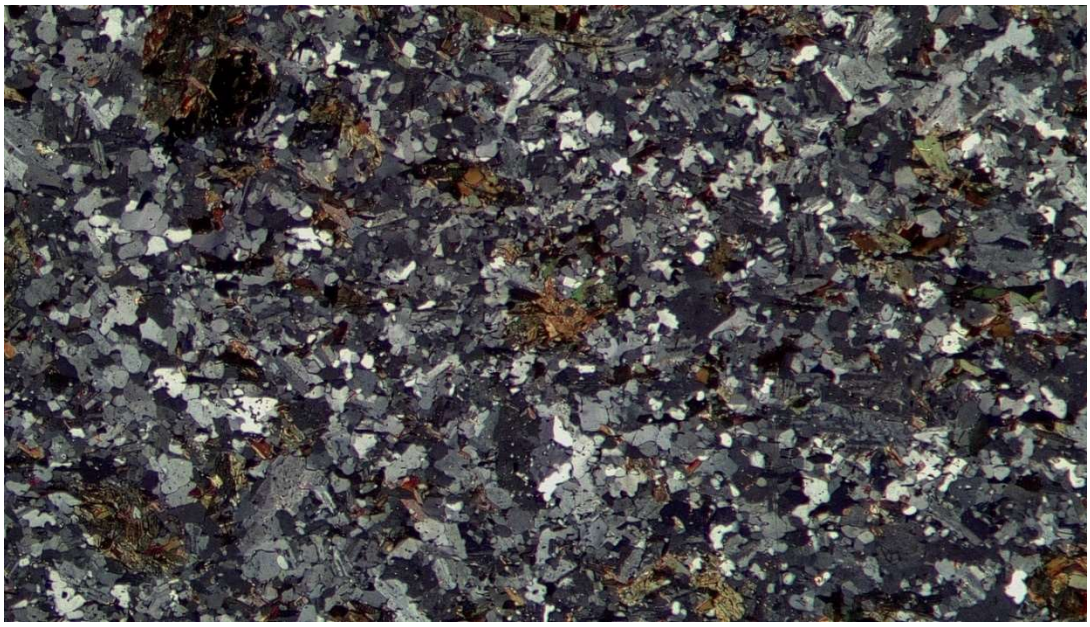

*Attachment figure 42. Xpl-image of Leevi14.1. Image size 5x8 mm.*

| **Sample** | **Leevi 15** |
|---|---|
| Coordinates (ETRS-TM35FIN): | N=7036298<br>E=418294 |
| Sample type: | Boulder |

| **Petrographical analysis** | | | |
|---|---|---|---|
| Modal composition (Point count of 1000 observations) | Kfsp | 22.8 | % |
| | Plg | 24.6 | % |
| | **Qtz** | **3.0** | **%** |
| | **Qtz (s)** | **33.0** | **%** |
| | **Qtz (m)** | **7.2** | **%** |
| | Bt | 5.2 | % |
| | Amph | 4.2 | % |
| Rock type | **Granitic protomylonite** | | |
| Undulatory extinction angles (angle and size of measured grain) | 1. 16° 2.0 mm<br>2. 23° 1.5 mm<br>3. 25° 1.0 mm<br>4. 15° 1.0 mm<br>5. 36° 1.5 mm<br>**Average: 26.0° 1.35 mm** | | 6. 44° 1.0 mm<br>7. 21° 1.0 mm<br>8. 22° 1.0 mm<br>9. 21° 2.0 mm<br>10. 37° 1.5 mm |
| Grain size | Fine matrix (0.5-1.0 mm), coarse feldspar phenocrysts (3.0-5.0 mm) | | |
| Texture | Unequigranular, heterogeneous, strong preferred orientation parallel to shear direction, schistosity bent around feldspar phenocrysts, matrix consists of fine-grained quartz, feldspars, amphibole and mica, of which quartz has formed larger, millimetre-scale individual grains and clusters up to 3 mm | | |
| Quartz description | Despite clear strong shear, bulk of quartz appears as larger quartz clusters that are strongly deformed (high extinction angles). Clusters include some subgrain rotation type quartz recrystallization.<br>Minor proportion show up as recrystallized microcrystal seams along microfractures and localized shear concentration areas within the matrix. | | |

*Attachment figure 43. Picture of rock sample Leevi15. Width of the sample approximately 15 cm.*

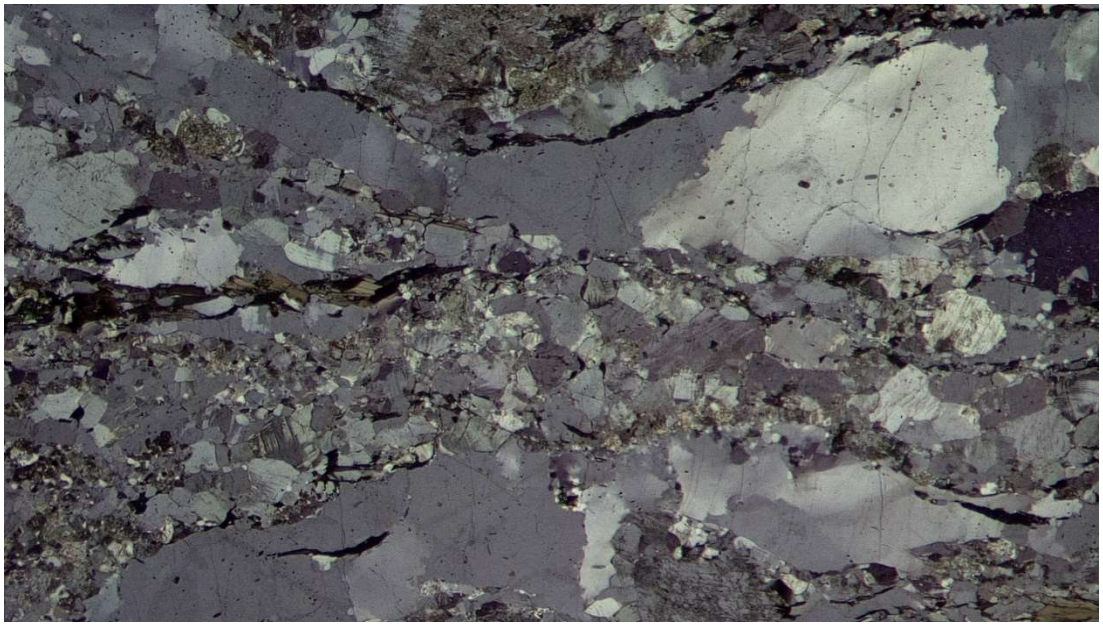

*Attachment figure 44. Xpl-image 1 of Leevi15. Image size 5x8 mm.*

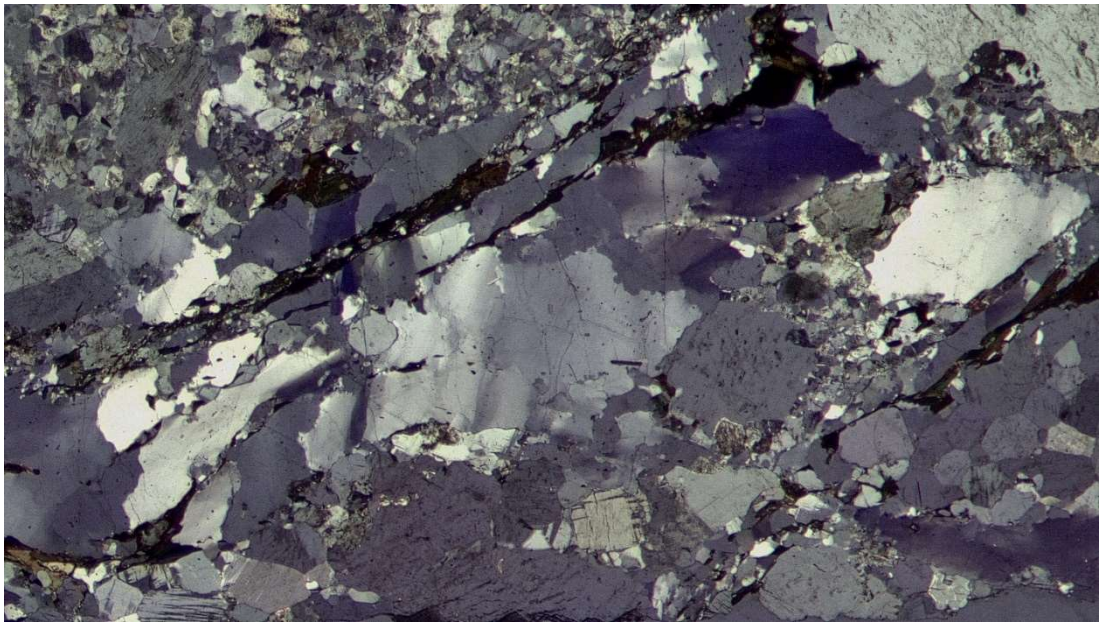

*Attachment figure 45. Xpl-image 2 of Leevi15. Image size 5x8 mm.*

| **Sample** | **Leevi 16** |
|---|---|
| Coordinates (ETRS-TM35FIN): | N=7036298<br>E=418294 |
| Sample type: | Boulder |

| **Petrographical analysis** | | |
|---|---|---|
| Modal composition (Point count of 1000 observations) | Kfsp | 20.8 % |
| | Plg | 48.6 % |
| | **Qtz** | **4.0 %** |
| | **Qtz (s)** | **18.6 %** |
| | **Qtz (m)** | **1.0 %** |
| | Bt | 6.4 % |
| | Px | 0.6 % |
| Rock type | **Granodiorite** | |
| Undulatory extinction angles | 1. 8° 1.5 mm<br>2. 15° 1.0 mm<br>3. 22° 1.0 mm<br>4. 13° 1.0 mm<br>5. 6° 1.0 mm<br>**Average: 14.3° 1.1 mm** | 6. 13° 1.0 mm<br>7. 24° 1.0 mm<br>8. 18° 1.0 mm<br>9. 9° 1.0 mm<br>10. 15° 1.5 mm |
| Grain size | Fine to medium (0.5-3.0 mm) | |
| Texture | One-way oriented fracturing goes through the whole rock. This brittle fracturing overprints deformation and is perpendicular to shear direction. Feldspars strongly altered (plg more altered that kfsp), myrmekites. | |
| Quartz description | Recrystallization which has been followed by brittle deformation, microfractures cut up through whole grains in direction perpendicular to shear direction, fluid inclusions present. | |


*Attachment figure 46. Picture of rock sample Leevi16. Width of the sample approximately 7 cm.*

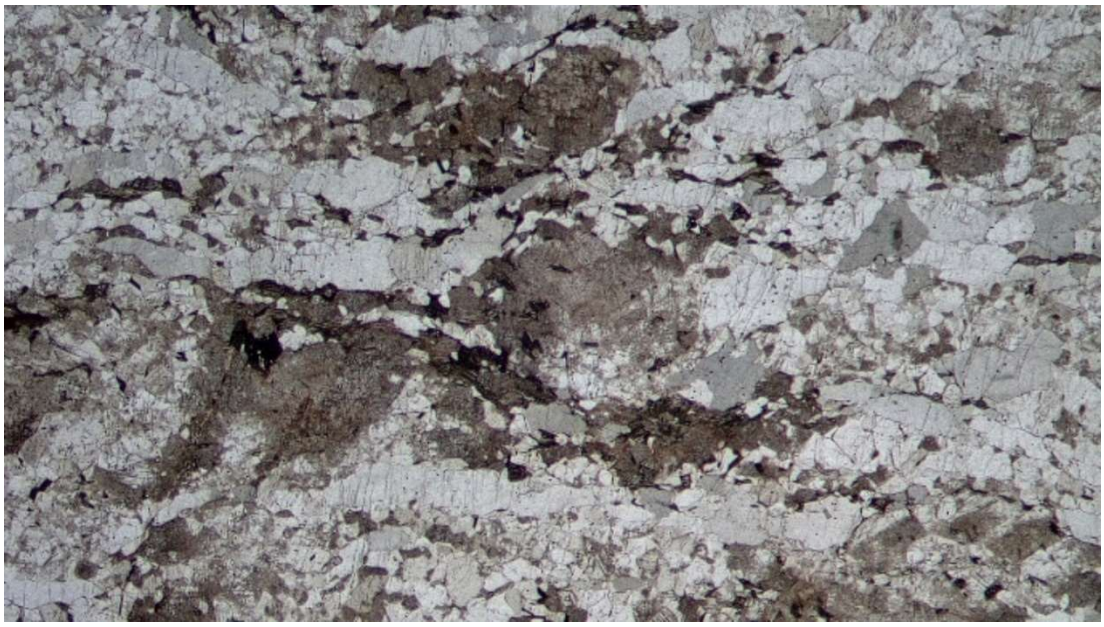

*Attachment figure 47. Ppl-image of Leevi16. Image size 5x8 mm.*

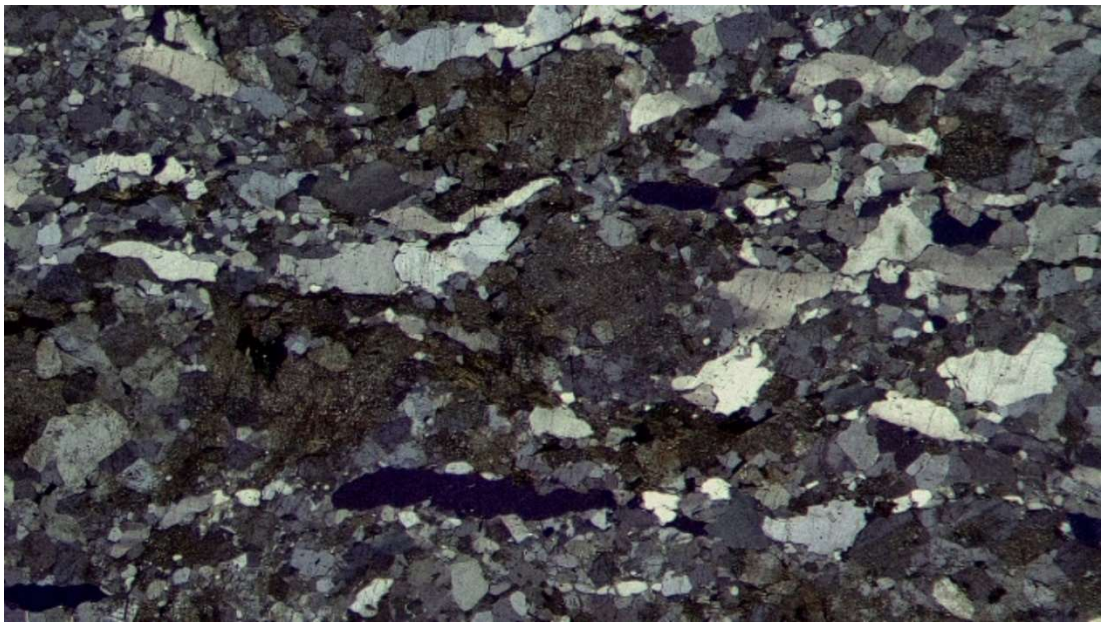

*Attachment figure 48. Xpl-image of Leevi16. Image size 5x8 mm.*

| **Sample** | **Leevi 17** |
|---|---|
| Coordinates (ETRS-TM35FIN): | N=7036298<br>E=418294 |
| Sample type: | Boulder |

| **Petrographical analysis** | | |
|---|---|---|
| Modal composition (Point count of 1000 observations) | Kfsp | 29.4 % |
| | Plg | 29.0 % |
| | **Qtz** | **20.4 %** |
| | **Qtz (s)** | **1.8 %** |
| | **Qtz (m)** | **0.4 %** |
| | Bt | 0.2 % |
| | Hbl | 18.8 % |
| Rock type | **Hornblende-quartz-feldspar-schist** | |
| Undulatory extinction angles (angle and size of measured grain) | 1. 8° 1.0 mm<br>2. 14° 1.0 mm<br>3. 9° 0.5 mm<br>4. 11° 1.5 mm<br>5. 3° 1.0 mm<br>**Average: 7.7° 1.15 mm** | 6. 5° 1.0 mm<br>7. 8° 1.5 mm<br>8. 10° 1.0 mm<br>9. 5° 1.5 mm<br>10. 4° 1.5 mm |
| Grain size | Medium (1.0-2.0 mm) | |
| Texture | Equigranular, strong sericitic alteration. Mineralogical variation, variating between more reddish colored and kfsp rich and greyish zones that lack kfsp. | |
| Quartz description | Recrystallized, where round grain shapes indicate more static recrystallization. Static recrystallization may have healed former more unstable quartz phases, leading to quartz structures with less free energy. Most of quartz show up as stabile, unstrained crystals, only minor proportion exhibits mild undulatory extinction with relatively low extinction angles. | |

*Attachment figure 49. Picture of rock sample Leevi17. Width of the sample approximately 10 cm.*

*Attachment figure 50. Ppl-image of Leevi17. Image size 5x8 mm.*

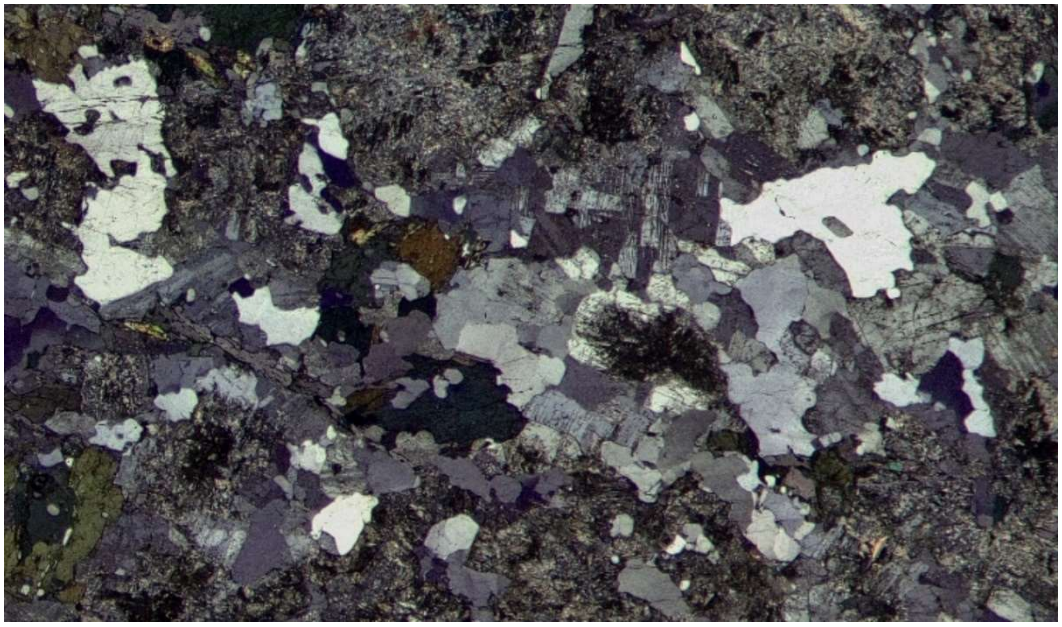

*Attachment figure 51. Xpl-image of Leevi17. Image size 5x8 mm.*

| **Sample** | **Leevi 18** |
|---|---|
| Coordinates (ETRS-TM35FIN): | N=7036298<br>E=418294 |
| Sample type: | Boulder |

| **Petrographical analysis** | | |
|---|---|---|
| Modal composition (Point count of 1000 observations) | Kfsp | 28.8 % |
| | Plg | 28.8 % |
| | **Qtz** | **12.8 %** |
| | **Qtz (s)** | **5.6 %** |
| | **Qtz (m)** | **4.4 %** |
| | Bt | 12.6 % |
| | Hbl | 5.8 % |
| Rock type | **Biotite-quartz-feldspar schist** | |
| Undulatory extinction angles (angle and size of measured grain) | 1. 22° 0.5 mm<br>2. 21° 0.5 mm<br>3. 24° 1.0 mm<br>4. 25° 0.5 mm<br>5. 36° 1.0 mm<br>**Average: 21.3° 0.75 mm** | 6. 12° 0.5 mm<br>7. 28° 1.0 mm<br>8. 11° 1.0 mm<br>9. 18° 0.5 mm<br>10. 16° 1.0 mm |
| Grain size | Fine (0.2-1.0 mm) | |
| Texture | Grains strongly elongated and oriented parallel to schistosity, most feldspar grains altered, amorphous glass in microscopic shear zones and joints | |
| Quartz description | Elongated parallel to schistosity and recrystallized. Grain shape suggests high temperature recrystallization where grain boundaries are migrated but show either no or only minor undulatory extinction. Some grains hold fluid inclusions. | |

*Attachment figure 52. Picture of rock sample Leevi18. Width of the sample approximately 9 cm.*

*Attachment figure 53. Ppl-image of Leevi18. Image size 5x8 mm.*

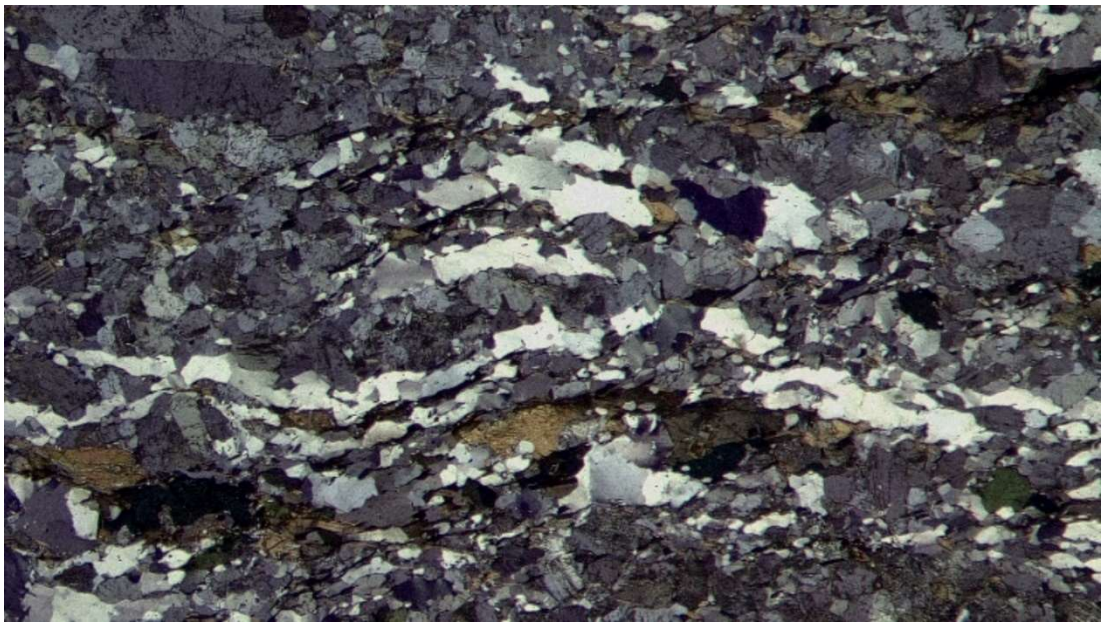

*Attachment figure 54. Xpl-image of Leevi18. Image size 5x8 mm.*

| **Sample** | **Leevi 19** |
|---|---|
| Coordinates (ETRS-TM35FIN): | N=6971800<br>E=394096 |
| Sample type: | Boulder |

| **Petrographical analysis** | | |
|---|---|---|
| Modal composition (Point count of 1000 observations) | Kfsp 44.8 %<br>Plg 9.0 %<br>**Qtz 26.2 %**<br>**Qtz (m) 1.0 %**<br>Bt 10.8 %<br>Hbl 7.8 %<br>Px 0.4 % | |
| Rock type | **Granite** | |
| Undulatory extinction angles (angle and size of measured grain) | 1. 4° 2.0 mm<br>2. 0° 1.5 mm<br>3. 12° 2.0 mm<br>4. 4° 1.5 mm<br>5. 3° 1.5 mm<br>**Average: 4.2° 1.75 mm** | 6. 5° 1.5 mm<br>7. 7° 2.0 mm<br>8. 2° 2.0 mm<br>9. 1° 1.5 mm<br>10. 4° 2.0 mm |
| Grain size | Medium to coarse (1.0-5.0 mm). Largest grains kfsp granophyres. | |
| Texture | Kfsp granophyres, myrmekites present, undeformed, minor feldspar (plg) alteration | |
| Quartz description | Mainly unstrained, euhedral and equigranular (1.0-2.0 mm) grains, individual microcrystals at grain boundaries | |

*Attachment figure 55. Picture of rock sample Leevi19. Width of the sample approximately 13 cm.*

*Attachment figure 56. Ppl-image of Leevi19. Image size 5x8 mm.*

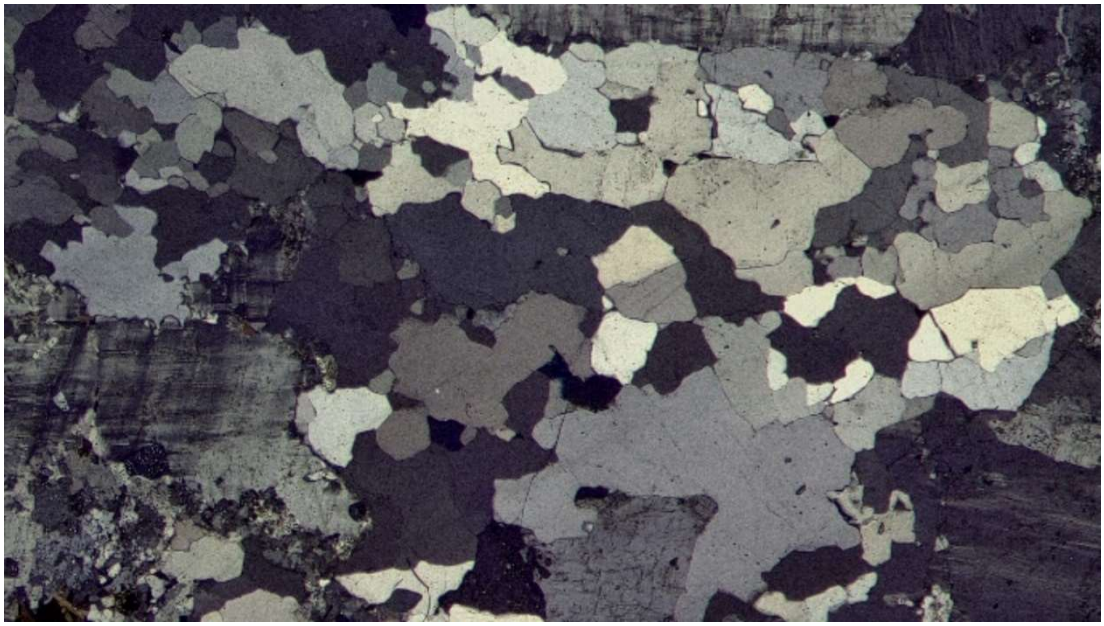

*Attachment figure 57. Xpl-image of Leevi19. Image size 5x8 mm.*